Microelectrochemical characterization of titanium biomaterials by scanning electrochemical microscopy

Doctoral thesis

Ph.D.

Author:
Abdelilah Asserghine

Doctoral School of Chemistry,
Department of General and Physical Chemistry

Doctoral supervisor:
Prof. Dr. Géza Nagy

Co-supervisor:
Dr. Lívia Nagy

Head of the Doctoral School:
Prof. Dr. Ferenc Kilár

University of Pécs, 2020.

Contents

Preface

The work presented in my dissertation is written based on the following publications:

[1] **A. Asserghine**, M. Medvidović-Kosanović, L. Nagy, G. Nagy, *In Situ Monitoring of the Transpassivation and Repassivation of the Passive Film on Nitinol Biomaterial by Scanning Electrochemical Microscopy*, ***Electrochemistry Communications*** 107 (2019), 106539.
(IF: 4.19, Q1)

[2] **A. Asserghine**, D. Filotás, B. Németh, L. Nagy, G. Nagy, *Potentiometric Scanning Electrochemical Microscopy for Monitoring the pH Distribution During the Self-Healing of Passive Titanium Dioxide Layer on Titanium Dental Root Implant Exposed to Physiological Buffered (PBS) Medium*, ***Electrochemistry Communications*** 95 (2018), 1-4.
(IF: 4.66, Q1)

[3] **A. Asserghine**, D. Filotás, L. Nagy, G. Nagy, *Scanning Electrochemical Microscopy Investigation of the Rate of Formation of a Passivating TiO_2 Layer on a Ti G4 Dental Implant*, ***Electrochemistry Communications*** 83 (2017) 33-35.
(IF: 4.56, Q1)

[4] **A. Asserghine**, M. Medvidović-Kosanović, A. Stanković, L. Nagy, R. M. Souto, G. Nagy, *Sensing the Localized Corrosion Reactions at Anodically Degradable Nitinol Biomaterial by Scanning Electrochemical Microscopy*, Under preparation.

[5] **A. Asserghine**, M. Medvidović-Kosanović, L. Nagy, R. M. Souto, G. Nagy, *Scanning Electrochemical Microscopy Investigation of the Cathodic Polarization Impact on the Electrochemical Behavior of Titanium Biomaterial*, Under preparation.

Conference presentations

Oral presentations:

[1] **A. Asserghine**, L. Nagy, G. Nagy, *Electrochemical Characterization of Titanium and its Alloys Assessed by Scanning Electrochemical Microscopy in Amperometric and Potentiometric Modes*, 10th Workshop on Scanning Electrochemical Microscopy (SECM-10), Paris, France, 2019.

[2] **A. Asserghine**, D. Filotás, M. L. Nagy, G. Nagy, *Electrochemical Characterization of Titanium Biomaterials Using Scanning Electrochemical Microscopy*, Analytical days, Balaton, Hungary, 2018. "Best oral presentation winner"

[3] **A. Asserghine**, D. Filotás, M. L. Nagy, G. Nagy, *Electrochemical Characterization of Titanium Biomaterials Using Scanning Electrochemical Microscopy*, 1st Cross-Border Seminar on Electroanalytical Chemistry, Furth in Wald, Germany, 2018.

[4] **A. Asserghine**, D. Filotás, L. Nagy, G. Nagy, *Scanning Electrochemical Microscopy Investigation of the Rate of Formation of a Passivating TiO_2 Layer on a Ti G4 Dental Implant*, 9th Workshop on Scanning Electrochemical Microscopy (SECM-9), Warsaw, Poland 2017.

Poster presentations:

[1] **A. Asserghine**, L. Nagy, G. Nagy, *In Situ Monitoring of the Transpassivation and Repassivation of the Passive Film on Nitinol Biomaterial by Scanning Electrochemical Microscopy*, International Conference on Chemical Sensors, Visegrád, Hungary, 2019.

[2] D. Filotás **A. Asserghine**, L. Nagy, G. Nagy, *Short-Term Influence of Interfering Ion Activity Change on Ion-Selective Micropipette Electrode Potential; Another Factor that can Affect the Time Needed for Imaging in Potentiometric SECM*, International Conference on Electrochemical Sensors, Visegrád, Hungary, 2017.

Acknowledgement

I would like to give sincerest gratitude to my supervisors, Prof. G. Nagy and Dr. Livia Nagy. They have given me the best opportunity to work on my subject and guided me to be a good scientist. I would never have finished my Ph.D. thesis without their help and support.

I also grab the opportunity to thank my best friend Dr. Filotás Daniel for his help and contribution in research. We really had a great time full with jokes and spectacular moment that we will remember forever. I wish him the best for his career and life.

I would like to thank Dr. M. Medvidović-Kosanović and Dr. A. Stanković for their welcome and hospitality I have received when I have been in their laboratory in Osijek, Croatia. I also thank them for their contribution in research.

I am thankful to Prof. R. M. Souto for his contribution in research and for his advices.

I am thankful to the head of our doctoral school Prof. F. Kilár for his guidance and support.

I am thankful to Stipendium Hungaricum program for funding my Ph.D. study.

Last but not least, I would never thank enough to my lovely family for always supporting me to achieve my goals.

Motivation

Prior I started my Ph.D. I did my master's degree at the University of Mohammed V in Morocco. My master thesis was about the investigation of the fretting corrosion impact on the corrosion of the materials used as orthodontic wires. As the methods for the evaluation of the corrosion resistance of the tested samples, potentiodynamic polarization, and electrochemical impedance spectroscopy were employed. After my master's degree, I moved to Hungary starting my Ph.D. at the University of Pécs under the supervision of Prof. Géza Nagy and Dr. Livia Nagy. When my supervisors introduced me to the research carried out in their group, I was very fascinated by the topics. Particularly, I was attracted by the scanning electrochemical microscopy technique. After learning the basics of the SECM, I realized that it is a powerful tool for understanding the performance of the surface of the material on the micrometer scale. Also, it can be used for studying the heterogeneous electron transfer between a metal surface and its surrounding environment. Besides, it can be employed to resolve the chemical reactions in the vicinity of the metal surface. That guide me to think about the work done in my master thesis, to apply the SECM for understanding in more detail the electrochemical properties of the biomaterials made from titanium.

Aims of the work

Titanium and its alloys are of great industrial interest due to their versatility. They have broad-scale applications especially in aeronautics, electrochemical industries, and orthodontia. Indeed, the titanium alloys have been widely used for clinical applications such as dental implants, stents, and orthopedic devices because of their biocompatibility and their outstanding mechanical properties such as low elastic modulus, high tensile strength, and low density. Also, they are known for their exceptional osseointegration character functioning in living tissue. Besides, they are well known for the formation of robust protective film on the surface. That provides a high corrosion resistance via inhibiting the release of metal cations from the surface and hinders the electron transfer reactions with the surrounding environment. However, the clinical problems of titanium and its alloys were broadly reported. Metal ions were detected in blood and urine also localized corrosion was observed in vitro and in vivo. In fact, the improvement of properties of titanium-based biomaterials required a deep comprehension of the electrochemical feature that take place on their surface.

The corrosion resistance of frequently used biomaterials made of pure titanium, and its alloys such as Nitinol, as well as its change upon different mechanical and physiological impacts is an extremely important character. Most of the corrosion studies of objects used as implanted medical supports were done with conventional methods. The reports appeared about the results of these experiments however, turned up some questions, or uncertainties. Application measurements with new ultramicroelectrodes combined with the conventional methods seemed very promising for obtaining fine details about the corrosion resistance and about its changes. It was specially so far using SECM with its different modes and measuring micro tips. In my research I planned to prepare different ultramicroelectrodes applicable in SECM measurement, work out selective SECM methods applicable for corrosion studies and use them in examination of the corrosion of biomaterial objects made of titanium and titanium alloys.

As generally known, the implanted biomaterials are highly susceptible to fretting corrosion. That is the result of the micromovement generated between the implant and the adjacent bone or metal surface. Numerous in vitro studies were carried out investigating the fretting corrosion of different titanium alloys. It was demonstrated that it enhances the corrosion of titanium. That was proved based on detecting the metal ion releases and observing the

localized corrosion occurrence. Those features are principally the result of the damage of the protective film on the titanium surface, while, if such a film after the damage required longer time to repassivate. The corrosive species in the electrolyte will enhance the corrosion of the metal. That leads to the occurrence of localized corrosion. Therefore, the study of the self-healing kinetics of the passive film on titanium biomaterial is crucial. However, there are only a few reports dealing with the self-healing of the surface film of biomaterials. Mostly it was investigated with conventional electrochemical testing that provide only information on a large scale. Whereas, the corrosion is a result of the heterogeneous electron transfer between the metal and its surrounding environment. This cannot be studied with the conventional electrochemical testing. I hoped that data about kinetic of the self-healing of the protective film formed on the titanium G4 implant surface could be obtained by SECM. Since that has been considered as the proper tool to gather quantitative information on the heterogeneous electron transfer at the metal surface.

Another issue concerning the fretting corrosion, that it affects the electrochemical potential of the materials. Numerous reports proved that during the fretting corrosion of titanium its electrochemical potential shifts to cathodic potentials that can go to a lower value as low as -1500 mV. Indeed, several studies proved that the cells around the implant decrease with the rise of the negative polarization. That highlights the importance of understanding the electrochemical properties of titanium under the cathodic polarization in situ. For that purpose, I employed the SECM to study the electrochemical behavior of cathodically polarized titanium.

As mentioned earlier that Nitinol which is an equiatomic alloy of titanium and nickel is regarded among the alloys frequently employed for making medical devices. However, several problems related to its clinical application were intensively reported. For instance, the release of hazardous nickel ions from Nitinol exposed to the neutral physiological medium was reported. That was suggested to be as a result of the nickel ions released from areas enriched with nickel on the Nitinol surface. Besides, titanium ions accompanied with a significant release of nickel were detected from Nitinol soaked to the acidic physiological medium. However, this feature was not fully investigated. For this reason, I proposed to employ the SECM operated in the feedback mode to examine the corrosion of Nitinol biomaterial in acidic medium. Another limitation of the medical application of Nitinol is the susceptibility to undergoing pitting corrosion. That was proved in vivo, also it was demonstrated by several electrochemical testing methods such as potentiodynamic polarization and SECM. However, no study was performed to monitor the corrosion products of the degradable Nitinol. Since the SECM

regarded as powerful tool for resolving the chemical reactions at the metal surfaces, I proposed using it to resolve the corrosion reactions evolve during the corrosion of Nitinol.

The results of my work are presented in 4 independent chapters in the III.1-4 sections.

Part I. Introduction

I.1. Biomaterials

Biomaterials are generally defined as substance engineered to interact with biological systems to treat, evaluate, and replace any tissue, organ or function of the body [1-3]. In the last few decades, large number of biomaterials have been developed for application in the field of healthcare. They mainly find use as drug delivery, orthopedics, dental care, tissue engineering of cardiovascular devices and skin, as shown in **Fig.** 1 [4,5]. While, before recognizing any new biomaterial to be used in the human body, several prerequisites recognized by the International Standards Organization (ISO) and The American Society for Testing and Materials (ASTM) must be fulfilled [6]. The biocompatibility is considered as the vital requirement for the suitable application of the biomaterials. Williams defined the biocompatibility as "*the ability of a biomaterial to perform its desired function with respect to a medical therapy, without eliciting any undesirable local or systemic effects in the recipient or beneficiary of that therapy, but generating the most appropriate beneficial cellular or tissue response to that specific situation, and optimizing the clinically relevant performance of that therapy*" [7]. This means the implanted biomaterials shouldn't generate any harmful reactions with the local surrounding environment. However, the implanted biomaterials are highly susceptible to corrosion because they are countered with severe corrosive environment, like blood and other kind of extracellular fluids containing chloride ions, proteins, and amino acids. This underlines that the implanted materials must provide a high corrosion resistance as claimed by the ISO and ASTM. The implanted object can also suffer from wearing out due to the micromovement generated between it and the adjacent metal or bone [8]. That yields in the formation of wear debris which can develop unwanted interactions with the living tissue. Therefore, the wear resistance and the osseointegration property regarded as a major of importance for the longevity of the implanted materials [9]. Nowadays, the biomaterials are made of metals and alloys, polymers, ceramics, and composites. In my Ph.D. thesis I examined the electrochemical properties of titanium and its alloys that are regarded as the most useful as medical devices.

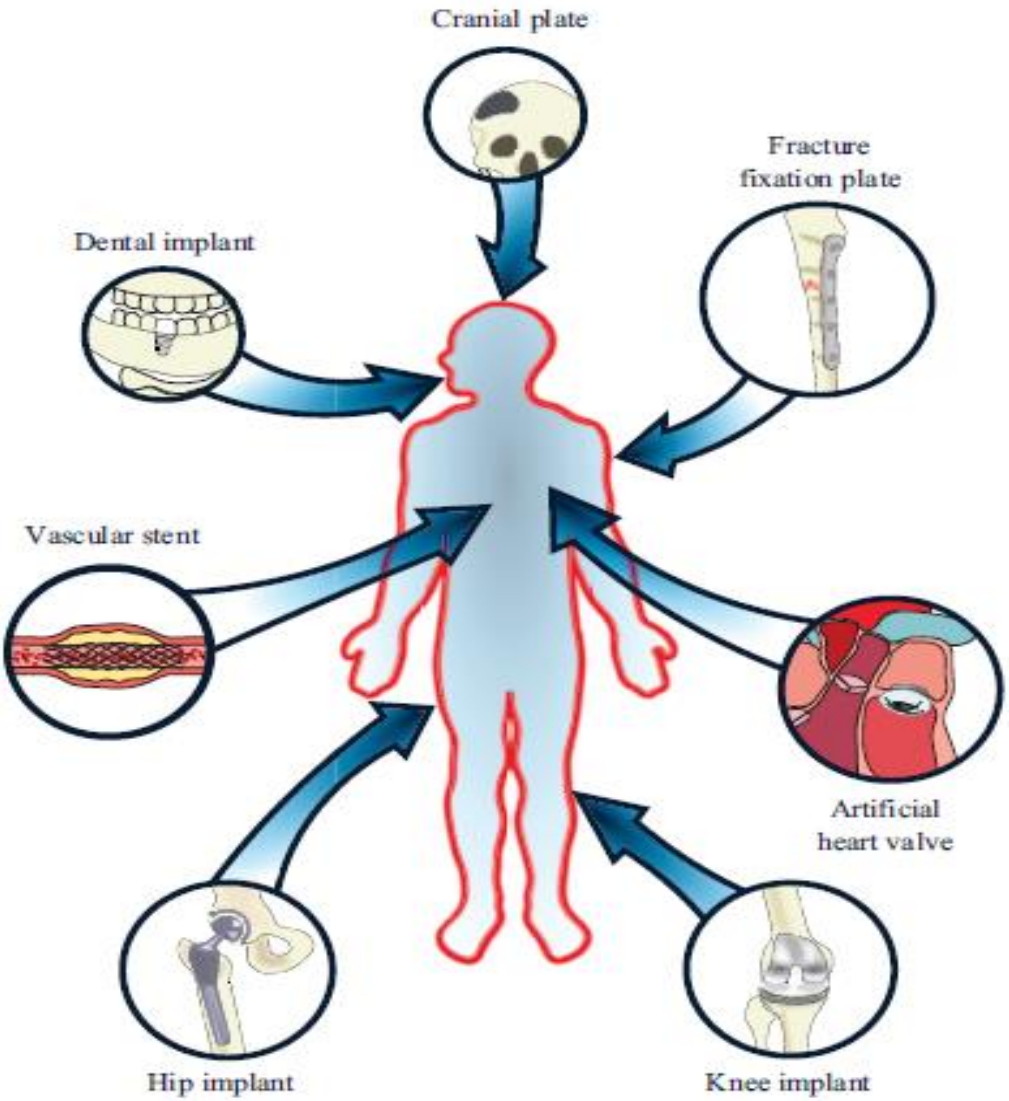

Figure 1: Applications of biomaterials in the human body [4].

I.2. Titanium and its alloys

Titanium as new element was discovered in 1790 by William Gregor but its name was given by Klaproth in 1795. It is considered as the ninth most abundant element in the earth. In recent decades, titanium and its alloys became very popular materials. They are widely applied in numerous fields. Health care is one of the fastest expanding application fields of them. So far titanium and titanium-based alloys are accepted to be the most suitable materials for biomedical applications, mostly as implants [3]. They have been used in manufacturing biomedical implants since the 1950s. It is reported that over 1000 tons of titanium are used in biomedical devices annually [10]. This is due to their biocompatibility and mechanical properties such as low elastic modulus, high tensile strength, and low density. Also, they are known for their exceptional osseointegration character functioning in living tissue after implantation. It is generally known that under atmospheric conditions, a robust protective film can develop spontaneously on the surface of titanium objects. Its thickness is in the range of nanometers. The protective oxide film is mainly composed of TiO_2 mixed with some of Ti_2O_3 and TiO. The TiO_2 has a semiconductive property with a wide bandgap of 3.2 eV [11], provides a high corrosion resistance through mitigating the release of the hazardous metal ions from the surface and inhibits the electron transfer reactions with the implanted environment. Once the titanium surface gets harmed, the titanium metal repassivates through the spontaneous formation of the passive titanium dioxide film [12]. Since the surface of the implantable materials makes the first contact with living tissue, thus the stability of the oxide film is a crucial factor for achieving successive treatment of the implantation. Different surface modification treatments are often performed to enhance the stability of the surface of the devices to be implanted. Numerous surface modification methods have already been developed such as plasma assisted physical vapor deposition (PVD), nanograined (NG) and thermal oxidation (TO), etc. [13-16]. The stability of passive oxide films can also be increased by employing properly selected amount of alloying metallic additives during metallurgic steps of preparation. Extensive research is still carried on for developing new titanium-based alloys with excellent mechanical and corrosion properties. Mostly Ta, and Zr are the alloying metallic elements. They are employed on one hand because of their nontoxic nature [17]. In addition, they facilitate the formation of a very stable oxides films. However, in certain conditions, the protective film developed on titanium and its based alloys is not entirely stable. Localized corrosion has been observed on a large microscopic scale [18-20]. Beside metal ions released from implanted titanium biomaterials were detected in blood and urine, Table 1 illustrates the most released

metals from the medical devices and their effect [21,22]. It has been reported that the release of metal cations harmfully affects the healing of bone and surrounding tissue wounds [23]. Extensive wastage of material from an implanted device can change its mechanical properties, can wakening it that could lead to losing its supporting function [24-26]. While, the occurrence of the localized corrosion and the release of metal cations are mostly the result of the damage of the protective film on titanium metal surface due to the combined effect of chemical, electrochemical, and mechanical processes as summarized in the next section. However, if such a film after the damage required longer time to be completely healed. The corrosive species in the electrolyte will enhance the corrosion of the metal. That leads to the occurrence of localized corrosion. Hence, the self-healing of the passive film on titanium biomaterial regarded critical to study.

Metal	Effects	Reference
Nickel (Ni)	- The main source of allergic contact dermatitis. - Harmful to bone in tissue cultures.	[27] [28] [29]
Molybdenum (Mo)	- Toxic in large doses.	[30]
Vanadium (V)	- Toxic in elementary state.	[31]
Aluminum (Al)	- Can cause epileptic effects. - Al is a considered as source of Alzheimer's disease.	[32] [33]

Table 1: Illustrates the effect of corrosion in human body due to various biomaterials.

I.2.1. Corrosion of titanium and its alloys in physiologic environments

The Ti based biomaterial devices implanted in living human tissue can suffer from corrosion through the following type of corrosion processes:

- **Pitting corrosion**, it is a corrosion that proceeds in a very limited area. It often takes place on the surface of passive alloys [34], yielding the formation of small area cavities on the metal surface in form of numerous individual pits. That can happen principally in the presence of halogen ionic species such as chloride, and fluoride ions being in the corrosive medium contacting the metal surface. The pitting corrosion often generates a local, more aggressive environment and enhances the corrosion. In our days extensive research is carried out examining the corrosion of titanium and its alloys in a different physiological environment containing chloride and fluoride at different concentrations. Titanium-nickel based alloys are the most susceptible to the pitting corrosion that was proved under in vitro and in vivo conditions [35].
- **Galvanic corrosion**, it is a typical type of corrosion that takes place when two different metals exposed to a common electrolyte and electrically in contact with each other [23]. When two metals are galvanically coupled, the more active metal acts as an anode that releases the metal cations, while the more noble metal behaves as cathode reduces the oxidants present in the electrolyte. Numerous reports examined this effect. J.P. Collier et al. [36] investigated the corrosion behavior of coupled cobalt-chromium alloy with Ti6Al4V which are the major elements of hip joint replacements. In their investigation the occurrence of localized corrosion on the cobalt alloy surface could be identified. It was attributed to the galvanic corrosion phenomena. Another experiments, also for studying corrosion of implanted titanium alloys were performed by P. Hou and co-workers [37]. They co-implanted magnesium and titanium objects into experimental rats and observed the corrosion rate. It could be proved that titanium accelerates the corrosion of the magnesium implant.
- **Crevice corrosion**, it is a severe form of high localized corrosion that is usually takes place at the region of contact between metal/metal or metal/nonmetal parts [38]. This is typically happening when a metal surface is partially isolated from the environment. The anodic reactions preferentially occur in the crevice owing to the difference in the aeration with the bulk environment. This type of corrosion was reported in the case of implant devices made of certain kinds of steel [39]. However, only a few reports

appeared about cases of clinical problems with titanium implants caused by the crevice corrosion. Waller et al. [40] reported the occurrence of the crevice corrosion on implanted femoral support osteotomy components made of Ti6Al4V and Ti6Al7Nb when they were fixed with bone cement.

- **Fretting corrosion**, it is a phenomenon which takes place when two materials are submitted to friction under a slight relative motion. The implanted biomaterials are highly susceptible to this type of corrosion [41]. Kawalec et al. [42] investigated the effect of fretting corrosion on Ti6Al4V exposed to aerated aqueous 0.9% NaCl solution and to 10% calf serum containing isotonic electrolytes. It was proved that the wear accelerates the corrosion of the testing samples. In addition, F. Contu et al. [43]. testified that the mechanical abrasion of commercial pure titanium (cpTi) and Ti6Al4V results in a shift of the open circuit potential (OCP) toward cathodic potentials. That can get to a value as low as –1500 mV vs. SCE depending on the pH of the testing electrolyte. Lately similar potential change has been shown with titanium niobium (Ti-Nb) and titanium molybdenum (Ti-Mo) alloys [44]. Recently, J. L. Gilbert and co-workers [45] examined the impact of the combination between the fretting corrosion and the cathodic polarization on the viability of biological cells cultured on Ti-6Al-4V surface. It was demonstrated that the viability of the cells decreases during the fretting corrosion and with the increase of the negative polarization.

As clearly shown in a certain conditions, titanium and its alloys can affect the surrounding biological cells, also they are highly susceptible to the localized corrosion. Therefore, the improve of titanium and its alloys properties required a deep understanding of the electrochemical surface features present on their surfaces. However, the titanium biomaterials were mostly examined using conventional electrochemical testing. That provide only information on a large scale. Hence, understanding the electrochemical properties under in situ condition regarded as critical. In my dissertation scanning electrochemical microscopy that is considered as powerful in situ tool was employed in the examination of titanium alloy surfaces in different physiological conditions.

I.3. Scanning electrochemical microscopy

Scanning electrochemical microscopy (SECM) is a version of scanning probe microscopy technique introduced by Bard and Enstrom [46]. Since then, the SECM became a very powerful tool for investigation of fine details of chemical reactions at the solid/liquid and liquid/liquid interfaces. It is broadly applied in different fields such as energy production and storage, experimental life-, materials-, corrosion sciences, etc. [47]. The constituent of the SECM apparatus can be seen in **Fig.** 2. It is composed of an ultramicroelectrode that is hooked up to a three-axis (X, Y, and Z) high precision positioning system. Its important part is the electrochemical measuring unit employed as electrochemical interface. That contains bipotentiostat, and a high impedance. In SECM measurements the ultramicroelectrode (UME) measuring tip is positioned in the close vicinity of the area to be investigated. It gathers chemical information about the sample area such as surface topography, nature and concentration of different species at micro areas. The positioning of the measuring tip, the data acquisition and evaluation/image formation are carried out by a computer. The data field composed of 3D tip location coordinates and corresponding electrochemical signals can be well used for characterizing the chemical nature of the studied area with high resolution. Heterogeneous chemical reactions taking place at electrolyte/metal interfaces – as ones proceed during corrosion- can be studied.

The SECM methods most often employed amperometric detection. Potentiometric detection mode with ion selective microelectrode tip is also used.

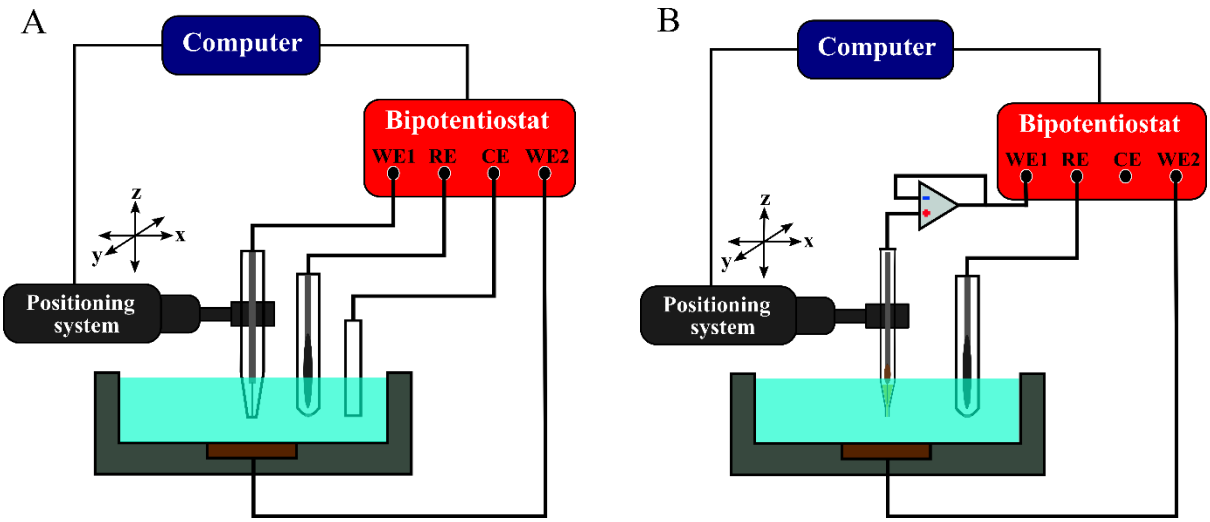

Figure 2: Illustrates the schemes of the operation of the SECM in amperometric mode (A) and potentiometric mode (B).

I.3.1. Different modes of SECM

I.3.1.1. Feedback modes

The feedback mode has been broadly applied for studying the heterogeneous electron transfer kinetics [48]. In my dissertation the feedback mode was used to gather quantitative information on the electron transfer reaction at the titanium surface under the effect of different conditions such as mechanical, cathodic polarization and acidic medium effects.

In the case of the feedback measurement, a quasi-reversible mediator is added to the background electrolyte. While, if we considered that the reduced species R are added to the background electrolyte, and the UME is polarized to sufficient potential to oxidize the R to its oxidizing (O) form (**Eq.** 1).

$$R \rightarrow O + ne^- \quad (1)$$

When the UME is in the bulk of the electrolyte, a steady Faradaic current is recorded ($i_{T\infty}$) given according to the following reaction [46].

$$i_{T\infty} = nFDca \quad (2)$$

Where *F*, is the Faraday constant; *a*, the microelectrode radius; D, the diffusion coefficient of the mediator; and, c, is its concentration.

While as the UME vertically approaches to an insulating surface, the current decreases due to the hindered mass transport of the mediator toward the microelectrode surface as it is illustrated in **Fig.** 4 (black line). This is called as negative feedback as shown in **Fig.** 3 b. During the negative feedback phenomena, the tip current variation follows the following equation [46]:

$$\frac{i}{i_\infty} = \frac{1}{0.292 + 1.515\frac{a}{d} + 0.6553exp\left(-2.4035\frac{a}{d}\right)} \quad (3)$$

Where *d* is the distance from the surface *i* and i_∞ are the current at *d* distance and at "infinite" long distance where the surface does not have influence on the amperometric current, respectively. The *a/d* generally marked as *L*. It has to be noted that the constants in (**Eq.** 3) would be different if the RG (ratio between the diameter of the platinum micro disc and the surrounding glass) value was different from 10.

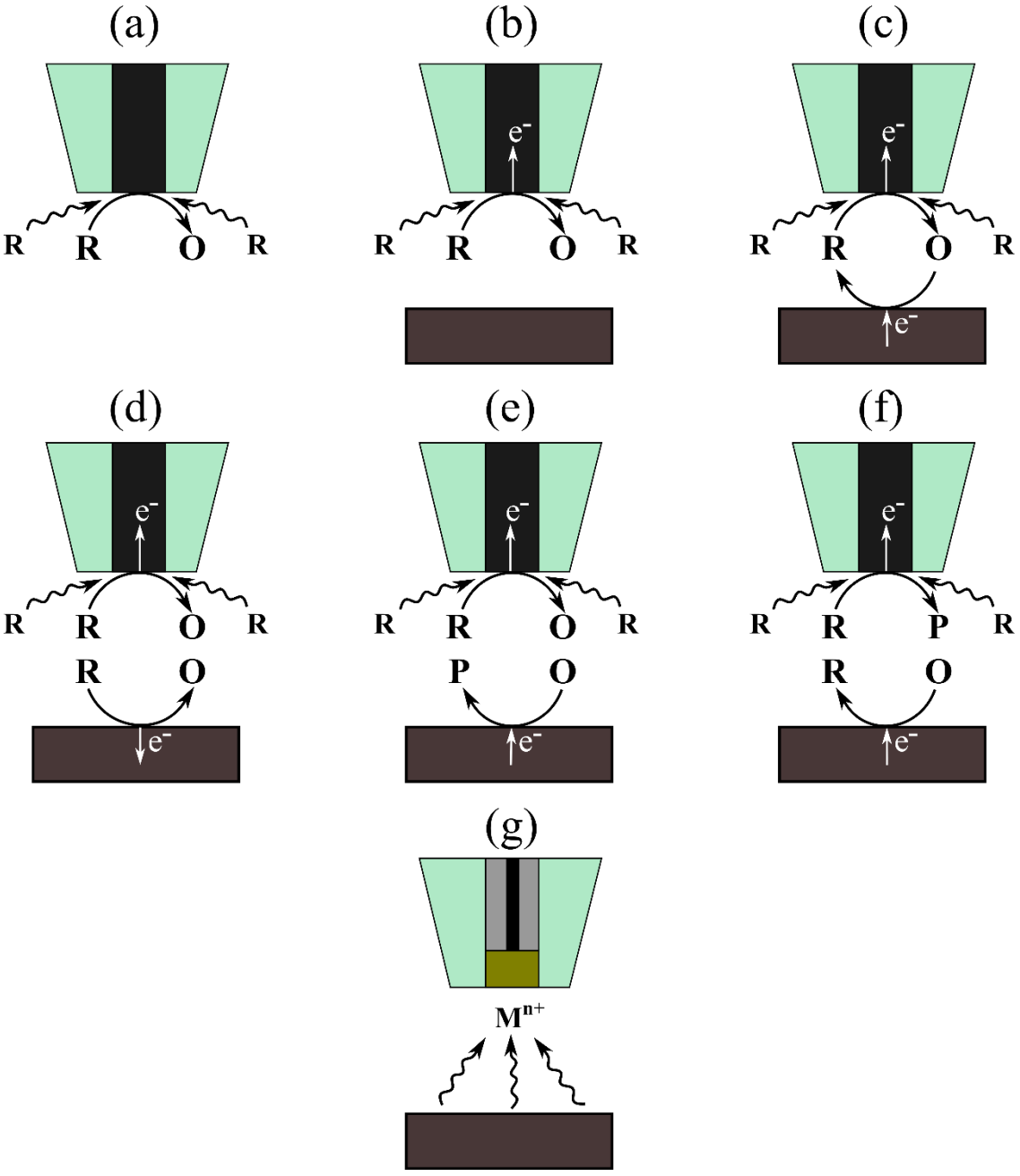

Figure 3: Illustration different modes of the SECM. (a)- Microelectrode in the bulk (b)- negative feedback (c) positive feedback (d)- redox competition mode (e) tip generation substrate collection mode (f) substrate generation tip collection mode (g) potentiometric mode.

On the other hand, if amperometric SECM tip is approaching to a conductive surface, then part of the oxidized form of the mediator produced on the microelectrode reaches the sample surface. It takes part in an electrochemical reduction. Therefore, the concentration of the *R* species at tip surface increases, consequently the tip current increases as it can be seen in **Fig.** 4 (red line). This kind of tip-sample interaction shown in **Fig.** 3 c, is named positive feedback. The normalized current – distance dependence is in acceptable agreement with the following equation [46]:

$$\frac{i}{i_\infty} = 0.68 + 0.78377\frac{a}{d} + 0.3315\exp\left(-1.0672\frac{a}{d}\right) \quad (4)$$

While, in cases when the mediator regenerating reaction is slower, then the approach curves recorded can be situated between the theoretical negative and positive approach curves, as shown in **Fig.** 4. It has been expected, that experimental approach curves can be used for estimating of the rate coefficients of mediator regenerating reactions. Along this line several groups developed numeric forms for estimation of the effect of mediator regeneration rate (k_{eff}) on the experimental approach curves. For instance, Wittstock and coworker proposed a model which is the following [48].

$$I_T\ (L) = [\ I_T^{ins}(\mathrm{L}) + I_S\ (\mathrm{L})(1 - \frac{I_T^{ins}(\mathrm{L})}{I_T^{con}(\mathrm{L})})] \quad (5)$$

Where $I_T(L)$ is the current at L distance, $I_T^{con}(L)$ and $I_T^{ins}(L)$ represent the tip currents for conductive and insulating substrates, respectively. $I_T^{con}(L)$ and $I_T^{ins}(L)$ can be described by the (**Eq.** 3) and (**Eq.** 4) for an RG ≈ 10 amperometric tip.

$$I_T^{con}(\mathrm{L}) = 0.7449932 + \frac{0.7582943}{L} + 0.2353042 \cdot e^{-\frac{1.683087}{L}} \quad (6)$$

$$I_T^{ins}(\mathrm{L}) = \frac{1}{0.4571825 + \frac{1.4604238}{L} + 0.4312735 \cdot e^{-\frac{2.350667}{L}}} + \frac{-0.145437.L}{5.5768952 + L} \quad (7)$$

I_S is the kinetically controlled substrate current which can be expressed in terms of normalized first order rate constant *k*. It is described by the following (**Eq.** 8):

$$I_S\ (\mathrm{L,k}) = \frac{0.78377}{L(1+\frac{1}{kL})} + \frac{0.68 + 0.3315\ e^{\frac{-1.0672}{L}}}{1 + (\frac{\frac{11}{kL} + 7.3}{110 - 40L})} \quad (8)$$

While the theoretical approach curves can be generated by inserting the values of a normalized distance (L) and a chosen value of the normalized rate constant *(k)* into equation (**Eq.** 8). The k_{eff} (**Eq.** 9) can be determined by knowing the diffusion coefficient of the mediator (*D*), the radius of the microelectrode (*a*), and the normalized rate constant *k* which is derived from experimental approach curve.

$$k_{eff} = k \cdot \frac{D}{a}$$

However, the model proposed by Wittstock and coworker is only valid for a probe that has an RG ≈ 10 and for a normalized distance situated between 0.1 and 1.6. A further expression has been proposed by Cornut and Lefrou [49], (**Eq.** 10):

$$I_T = I_T^{Con}.(L + k^{-1}) + \frac{I_T^{Ins} - 1}{(1 + 2.47.RG^{0,31}L.k).(1 + L^{0,006.RG+0,113}.k^{-0,0236.RG+0,91})}$$

This new model can be applied for SECM probes that has an *RG* values less than 20 and for normalized distance (*L*) higher than 0.1.

The equation developed by Cornut and Lefrou was frequently used in my dissertation to simulate the Z-approach curves performed over titanium surface.

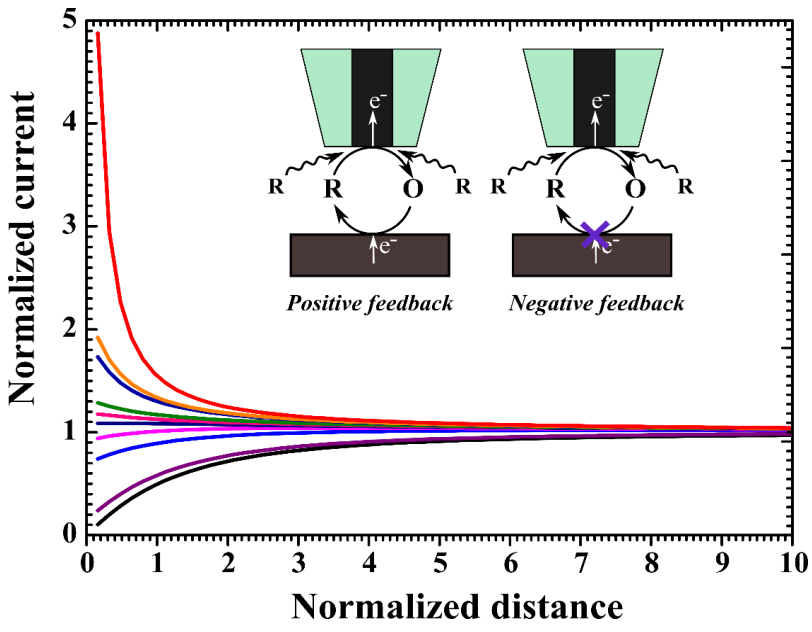

Figure 4: Theoretical approach curves, where the red and the black line are the pure positive and negative feedback approach curves, respectively.

I.3.1.2. Redox competition mode

The redox competition mode of the SECM (RC-SECM) was first introduced by Schumann and coworkers [50]. In the RC-SECM mode, the tip and the conductive substrate are activated to consume the same redox species, as it is shown in **Fig.** 3 d. When the SECM probe is far from the substrate, a steady tip current is measured. However, as the tip-sample gap gets smaller, then the mass flow to the tip of the reacting species is decreased by competing action of the approaching sample surface. Therefore, the amperometric tip current decreases. This mode is broadly employed for detecting and mapping surface activity of metal- or organic protector film coated metal object [51].

I.3.1.3. Tip generation substrate collection mode (TG-SC)

In TG-SC mode, the polarized tip generates a species that can react on active spots of the sample surface leading the formation of a product P, see the illustration in **Fig.** 3 e. While the generated P species doesn't react at the microelectrode, thus preventing the feedback loop. The TG-SC mode was generally employed for the pitting corrosion studies. It was commonly used for producing the chloride ions at the microelectrodes for creating the pits at the metal surface [52].

I.3.1.4. Substrate generation tip collection (SG-TC) mode

In this mode, the SECM tip is employed for collecting the species generated at the substrate as seen in **Fig.** 3 f. High tip signal indicates that high amount of reaction product is released from the sample surface spot being close to tip location. This mode is widely applied for corrosion studies because from active corroding spots of metal surfaces usually detectable species are released. Several reports appeared about using SECM measurements in SG-TC mode for detecting released ions (M^{n+}) like Fe^{2+} [53], Ni^{2+} [54], Cu^{2+} [55], and Cr^{2+} [56]. The locally evolved hydrogen gas was also mapped using SG-TC mode. It was done in the case of investigation the corrosion of magnesium and iron systems [57,58]. In my thesis the hydrogen gas was monitored at the cathodic spots on titanium biomaterial. That is considered as the first study to detect hydrogen gas on titanium, it will be discussed in details in the result and discussion (chapter 3).

I.3.1.5. SECM with potentiometric detection

As it was told earlier potentiometric detection has been frequently used in practice of SECM. This version of probe microscopy sometimes called the scanning ion-selective electrode technique (SIET). The SECM with potentiometric detection actually is a version of the SG-TC mode SECM. Its important advantage that no redox mediator is needed for these measurements. Whereas, the potential at the microelectrode depends on the activity of the ion of interest as shown in **Fig.** 3 g. In the last decades, numerous ISME's were developed mostly for corrosion applications. They were used for mapping the concentration distribution of different ions such as Cu^{2+}, Mg^{2+}, and Zn^{2+} [59-61]. The pH microsensors were also developed such as antimony and iridium microelectrodes [62,63]. In my work I used antimony microelectrode because of its simple preparation also it can be used for amperometric detection to set the tip-sample distance. Using antimony as SECM probe the pH at the vicinity of mechanically damaged titanium biomaterial was monitored as will be discussed in details in the result and discussion chapter 1. In addition, the antimony microprobe was also employed to monitor the pH produced during the anodic degradation of the Nitinol biomaterial, this will be the topic of chapter 3 in the results and discussion.

I.3.2. Microelectrochemical characterization of titanium and its alloys by SECM

SECM has already been employed for the characterization of titanium and titanium-based alloy surfaces [64]. The first results obtained with the technique was reported by Basame and White [65]. They examined the behavior of the passive titanium dioxide film on titanium materials (Ti/TiO_2) employing different reagent such as Br^-, I^-, $SO_4^{2-}$and $Fe(CN)_6^{4-}$. It was found that the titanium dioxide film was more susceptible to the localized corrosion in the presence of Br^- ions. In the work of Casillas et al. [66] it was suggested for explanation that bromide ions form a bond with titanium and that leads to the dissolution of the oxide film. In a further study of the same authors [67] active spots on titanium surface with a diameter in the range of 10 μm to 50 μm could be identified using the SECM in the feedback mode. That was attributed to pitting precursor sites formation. Garfias-Mesias et al. [68] suggested that the pitting precursor sites observed might be formed because of presence of Al and Si inclusions in the titanium alloy. They proved their hypothesis by combining the SECM with the energy-dispersive x-ray spectroscopy (EDX). In those experiment high concentration of Al and Si was identified in the active sites.

Another study was done by Fushimi et al. [69] for testing that how far the heterogeneity of the oxide film follows the pattern of underlying grain boundaries. The relationship was demonstrated by mapping the activity of oxide film grown on a polycrystalline titanium electrode in a deaerated borate solution. It was shown that the heterogeneity rises with the increase of the anodic polarization. A similar study was carried out by Zhu et al. [70,71]. They examined the electrochemical reactivity of the native oxide film on Ti grade 2 and Ti grade 7 surfaces. They demonstrated that the presence of impurities plays a significant role in enhancing the rate of localized corrosion. It was confirmed by detecting the reactive spots and the grain boundaries. SEM/EDX experiments supported the concept that the formation of reactive spots could be to the presence of the impurity such as Fe. A further study has been performed by G. Wittstock and co-workers. They have investigated the electrochemical behavior of the oxide film on the Ti6Al4V alloy which is composed of α and β phases [72,73]. The kinetics of the electron transfer at the Ti6Al4V surface was tested by employing different mediators. They demonstrated that the electron transfer kinetics on the α phase strongly depends on the redox potential of the mediator. Also, a difference in the electronic conductivity of α and β phases was observed, while the β phase showed the higher reactivity.

R.M. Souto and co-workers believed that the electrochemical properties of the passive oxide film on titanium surface significantly depend on the ways of the alloy fabrication. They tested the fabrication procedure's impact on the corrosion resistance of TiMo alloys [74]. It was shown that the alloys prepared by crucible levitation melting (CCLM) produced a compact film with high corrosion resistance. In contrast, the alloys made by the powder sintering (PS) method showed a porous structure and weaker corrosion. Besides, they studied the effect of niobium content on the corrosion resistance of TiMo alloys [75]. It was proved, the presence of niobium in the range of 8 to 16% can enhance significantly the corrosion resistance of TiMo.

Corrosion resistance character of Nitinol that is an equiatomic alloy of titanium and nickel, was also examined with the SECM. The Nitinol is frequently employed for making implantable biomedical devices. Schulte and coworkers [76] reported about the susceptibility of Nitinol to undergo to pitting corrosion. It was confirmed by visualizing the pits on Nitinol surface using alternating current scanning electrochemical microscopy (AC-SECM). The same authors examined the corrosion of NiTi/steel joints. In their work, the Ni^{2+} ions evolved from Nitinol were detected using SECM operated in stripping mode [77]. Furthermore, they reported a series of experiment to improve the corrosion resistance of Nitinol by using electropolishing procedure. Recently, Izquierdo, et al. [78] examined the properties of the passive film on Nitinol under polarization. It was illustrated that the electron transfer reaction on Nitinol significantly depends on the applied polarization. As well, they showed the susceptibility of Nitinol to the pitting corrosion under the anodic polarization. Because of the nickel toxicity, widespread research has been carried out to substitute the nickel with non-toxic metals keeping the same mechanical and corrosion resistance properties as Nitinol has. In most cases nickel is substituted by Zr and Ta. Bolat and co-workers [79] studied the electrochemical behavior of three different ZrTi alloys which are the following. Zr5Ti, Zr25Ti, and Zr45Ti. Their behavior was compared with that of the pure titanium. Via using the SECM, it was demonstrated that the increase of titanium content increased the corrosion resistance of Zr. That was proved based on quantifying the rates of electron transfer reaction on the surface of the alloys.

So far, no systematic study with SECM was performed to study the kinetic and the corrosion mechanisms of the self-healing of the protective film on titanium biomaterial. Also, the cathodic polarization effect on the electron transfer reaction at titanium was not fully investigated. In addition, no study was carried out to monitor the corrosion products on the Nitinol surface. In my dissertation those issues were studied in details.

Part II. Materials and methods

II.1. Materials

The phosphate buffer saline solution (PBS) that has pH of 7.2 was prepared using 8 g/L NaCl, 0.2 g/L KCl, 1.44 g/L Na_2HPO_4, and 0.24 g/L KH_2PO_4. All the chemicals were supplied by Sigma Aldrich. For acidifying, high purity HCl (Aristar) was used. In SECM measurements ferrocene methonol (FcMeOH) supplied by Sigma Aldrich was used as redox mediator. All the solutions were made using ultrapure water (Millipore water system, specific conductivity $\kappa = 6 \times 10^{-6}$ S/cm; Merck Millipore, Billerica, MS, USA).

Antimony microelectrode was made using antimony powder purchased from Aldrich (Saint Louis, MO, USA). Pt disk microelectrodes (ME) was made from 25 μm diameter Pt wire (Goodfellow, Cambridge, UK). Borosilicate capillaries (outer dia. Ø = 1.5 mm, inner dia. Ø = 1.0 mm) were bought from Hilgenberg GmbH (Germany). Nitinol wire (55% Ni and 45% Ti, Ø = 0.8 mm) and pure titanium sheet (99.99%) were supplied by (Goodfellow, Cambridge, UK). Titanium G4 implant (99.5% Ti and 0.5% Fe) was supplied by Dr. B. Németh. The targets were prepared using epoxy resin purchased from Struers (Denmark), employed for embedding the metal samples.

II.2. Targets preparation technique

All the tested metal samples investigated in my thesis were embedded in the epoxy resin. They were prepared by mounting the testing samples in a cylindrical mold, then filling the cylindrical mold by 3ML liquid that was made by mixing the resin and Epofix hardener by a mass ratio of 8 to 1. Afterward, it was left for 12 hours at room temperature for drying. The top area of the target was grounded with SiC paper to establish a flat surface, then it was wet polished sequentially with 1, 0.3, 0.05 μm grain size alumina slurries. The electrochemical cell was created by wrapping around the cylindrical plastic body a sellotape. Copper wire was soldered on the metal sample piece. It was extended over the plastic on the back side that allowed connecting the sample to the potentiostat when polarized sample were studied.

II.3. Electrode preparation methods

Homemade microelectrodes were used as SECM measuring tips in these studies. Procedures taken from literature were slightly modified in preparing them.

II.3.1. Platinum microelectrode

The platinum microelectrode used in the SECM experiments was prepared by following the procedure reported in [80]. First, a borosilicate capillary was rinsed with acetone and double distilled water then one end of the capillary was closed using the oxidizing flame of the Bunsen burner. Afterward, a platinum microfiber of diameter of 25 μm and 1-2 cm length was introduced into the lumen of capillary all the way down to the sealed end. The open end of the capillary was connected to a vacuum pump for preventing formation of air bubbles around the Pt wire during sealing in step. Then the capillary was positioned vertically in center, slightly above of an electric heating coil made from kanthal. Employing sufficient electric power about half of the fiber was sealed inside melted glass moving the capillary slowly down. Actually, as a first step a cleaning phase with lower power was performed. In the lumen of the capillary a copper wire was soldered to the extending Pt wire to provide electric contact. The sealed part of the capillary was taken off by sand paper as long as a Pt micro disk appeared up in the center. The small end plate was carefully polished using abrasive papers and pads (Buehler Ltd., Bluff, IL) coated with alumina having diameters of 1.0 μm, 0.3 μm and 0.05 μm, respectively. After it a pointy end was carefully prepared checking periodically the progress with an optic microscope. In this way micro disk type electrode with RG ≈ 10 value was fabricated and used in my SECM measurements.

II.3.2. Antimony microelectrode

The antimony microelectrode was prepared by following the procedure reported in [63]. As a first step about 10 g of antimony powder was melted in as small ceramic crucible using Bunsen flame. The molten antimony was sucked into the lumen of a thick walled glass capillary using a large (250 mL) syringe. Afterward the capillary with the solidified antimony fiber inside was pulled manually with standard glass blowing technique. In this way a glass capillary of about 0.2 mm diameter with antimony fiber diameter of a few μm inside was obtained. Under surveillance of optical microscopy, a 5-10 mm long section of it with continuous metal fiber

was selected and cut. Then, it was glued inside a capillary body with sticking out the antimony containing sensor part in one side (3-5 mm) and the copper wire in the other one.

II.4. Conventional electrochemical measurements

The conventional electrochemical measurement such as electrochemical impedance spectroscopy, potentiodynamic polarization, and cyclic voltammetry were performed using CHI604E type electrochemical workstation build by CH Instruments. As reference and counter electrodes, Ag/AgCl/KCl (3M) and platinum were used, respectively.

II.5. Scanning electrochemical microscopy apparatus

The experiments were performed with three different microscopes, two were homemade and the other was a commercial one. This later was a 370-model supplied by Uniscan Instruments. It is composed of a high precision, three-dimension tip positioning unit based on three stepper motors. These linear motors provide quite long tip travel distance of 75 mm in all XYZ directions with 8 nm resolution. The second part used as electrochemical interface of the SECM was the bipotentiostat model 59580R type supplied by Uniscan Instruments.

The positioning unit of one of the homemade SECM used in my work were based on three stepper motors model UE166PP (Newport, Irvine, CA, TypeMMFN25PP). Their step size resolution is 75 nm and they can provide 25 mm travel range. EF437 bipotentiostat supplied by (Elektroflex Ltd., Szeged, Hungary) is employed as measuring unite. The program controlling the tip positioning, data acquisition and evaluation were written on Microsoft Visual Basic 6.

The construction of the second homemade microscope used in my experiments is described in [81]. In brief, it is composed of three stepper motors controlled by a SD4DX USB Controller (Peter Norberg Consulting, Inc. 117 South Clay Ave. Ferguson, MO, USA), and driven by a Gecko step-and-direction driver board (Geckodrive, Inc. 14662 Franklin Ave, Santa Ana, CA.). The controlling of the positioning was performed by a software written in Java installed in a personal computer.

II.6. Energy dispersive x-ray spectroscopy (EDX)

An elemental analysis of cp titanium and nitinol surface was carried out using EDX (Ametek, USA) scanning an area 250 μm × 250 μm. The accelerating potential was 25 KV.

II.7. Atomic absorption spectroscopy (AAS)

The release of nickel and titanium from nitinol were examined using the atomic absorption spectroscopy (PerkinElmer PinAAcle 900T). High purity NaCl (Roth) and HCl (Aristar) were used for the solution preparation. The nickel standard solutions (Merck) were prepared in the range of 0-600 and 0-200ppb for titanium (Merck), employing the matrix modifier (5µg Pd + 3µg $Mg(No_3)_2$). Where the calibration curve for Nickel and titanium are: y = 0.00963x, R^2=0.9906 and y=0.00008x, R^2=0.962 respectively. The AAS experiments were done through preparing 9 plastic vials of 1mL volume, one filled with 0.1M NaCl (pH=7) and the others (8 plastic vials) with acidified NaCl (pH=3). First, as-received Nitinol wire that has a surface area of 0.2 cm^2 was exposed for 10 min in the neutral NaCl then was immersed for 10 min at every single vial filled with the acidified NaCl (ordered from 2 to 9). Subsequently, nickel and titanium were measured at each vial employing the graphite furnace.

Part III. Results and discussions

Chapter 1 – Monitoring the self-healing of the native passive film on titanium biomaterial after mechanical removal.

III.1.1. Resume

Titanium and titanium-based alloys considered among the most used materials as implantable biomaterials because of their high corrosion resistance provided by the protective passive film formed on the titanium surface. However, numerous reports showed the failure cases of titanium implants, due to the fact of the damage of the protective film [18,20]. That would happen via mechanical, chemical, and biological impacts [82]. While if such protective film takes time to be healed, it would enhance the corrosion of the implant. That eventually leads to the failure of the implant. Therefore, understanding of the kinetic and the mechanism of the repassivation process of titanium and its alloys regarded critical. However, there are only a few reports dealing with the self-healing of the biomaterials. For instance, F. Contu et al. [43]. examined the repassivation of mechanically damaged surface of pure titanium and Ti-6Al-4V immersed in inorganic buffer solutions. In their work, the repassivation kinetics was carried out through measuring the open circuit potential of the testing samples before and after the mechanical damaged. Moreover, J.L. Wang et al. [83]. They investigated the self-healing of different titanium alloys using in situ scratching, whereas the repassivation rate was controlled by the chronoamperometry. In their experiments, the test samples were polarized to 0.1 V for 600 s. Afterward, they scratched the surface. They considered the time needed for the current after scratching to reach the same current value of the undamaged surface, as the time of the self-healing. They demonstrated that the time need for the self-healing of the tested titanium alloys varies between 10 and 150 s, depending on the composition of the alloy. However, the method used is not adequate for estimating the self-healing rate because protective surface film of the tested samples was prepared by electrochemical polarization which enhances the formation of the protective film. Besides, the kinetic of the self-healing will be controlled by the imposed polarization. Thus, in situ tool is required for studying the self-healing of the passive metals. For that purpose, I proposed the scanning electrochemical microscopy for this task as an in situ tool. In this chapter, I examined the kinetics of the self-healing of titanium dioxide formed on titanium G4 implant surface using SECM operated in amperometric and potentiometric modes.

III.1.2. Investigation of the electron transfer at titanium biomaterial after removal of the native passive film, using SECM operated in the feedback mode

III.1.2.1. SECM approach curves measurements

In our SECM experiments, 25 µm diameter Pt microelectrode (ME) used as SECM probe. About 3ML of PBS physiological background solution containing FcMeOH in 1.2 mM concentration was introduced into the small cylindrical cell created over the embedded sample. 0.6 V vs. Ag/AgCl/KCl (3M) electrode potential was employed and the amperometric current was recorded at different tip positions. The sample metal that in this case was an implantable dental root matter was cut by diamante saw perpendicularly to its stem. After embedding it with the circular surface up, the Ti G4 sample surface was freshly polished. The tip was positioned over the center of the sample 100 µm vertical (Z) distance from it. Afterward the electrolyte was introduced into the cell, and current – distance dependence was recorded without connecting polarization potential onto the sample. The tip was moving vertically down with 10 µm/s speed. Before touching the surface, the tip was detracted back to 100 µm. After certain times approach curves were recorded similarly.

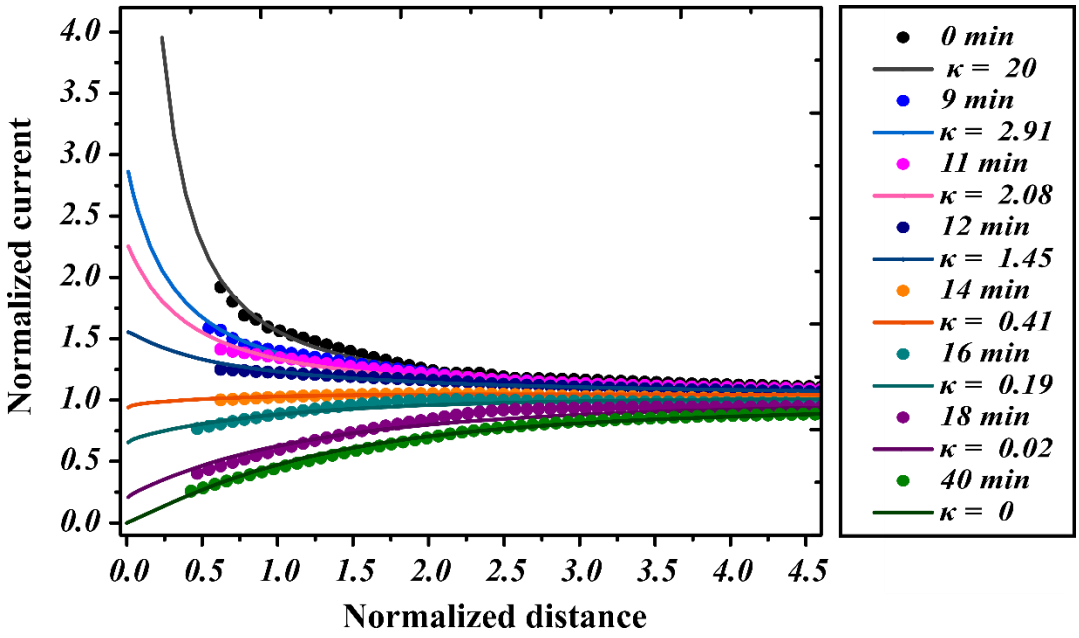

Figure 5: Z-approach curves measured using 25 µm platinum microelectrode over titanium G4 immersed in PBS mixed with 1.2 mM *FcMeOH. The tip potential was 0.6 V vs. Ag/AgCl/KCl (3M) and scan rate of 10 µm/s was employed. The symbols and the solid line represent the experimental and the theoretical data, respectively. The times shown in the inset correspond to the elapsed time between introducing the PBS electrolyte and recording the approach curve.*

The curves recorded at different times are presented as dotted lines in **Fig.** 5. The abscissa values of the curves mark the normalized distance L ($L=d/a$ where d is the gap distance and a is the radius of the tip, in this case 12.5 µm) while the ordinate values show the so called normalized current $I_r = I_d/I_\infty$ where I_d is the measured tip current at d gap size and I_∞ is the current measured in the bulk, far from the sample surface.

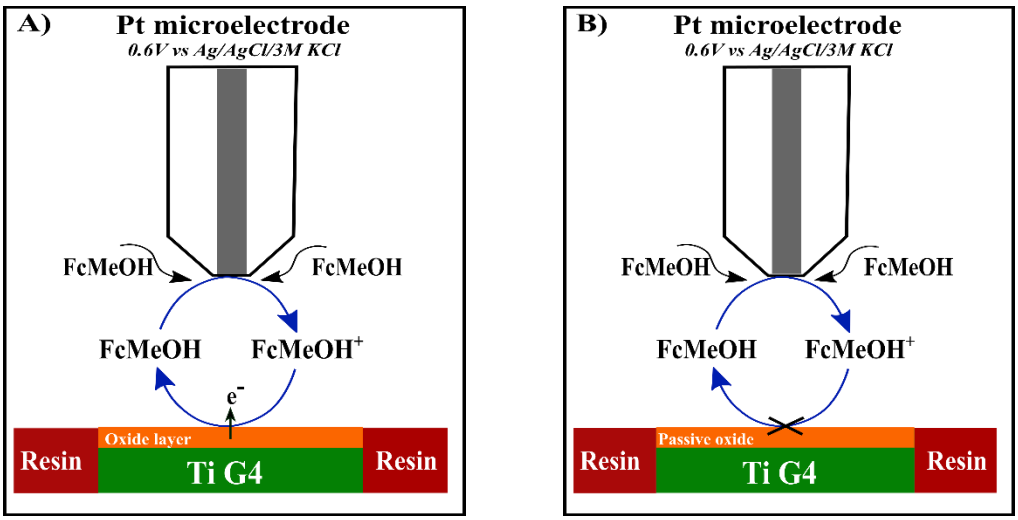

Figure 6: Electrochemical responses observed for the tip current as a function of time during amperometric SECM operation over titanium G4 surface. (A) Positive feedback effect recorded at the first period of immersion; (B) negative feedback effect recorded after 40 min of immersion due the total passivation of titanium G4 surface.

Negative feedback effect is expected above the freshly polished titanium G4 surface if formation of protective TiO_2 is an instantaneously fast reaction. Observing the dotted lines shown in **Fig.** 5, it can be seen that as long as the tip is far from the sample surface the normalized current does not depend on the normalized distance. Its value is constant and does not depend on the sample soaking time either. On the other hand, as the normalized distance starts decreasing below 3 that correspond to three times tip radius ($3a$) the normalized current values start to change. While, the approach curve recorded immediately after exposing the freshly polished titanium G4 surface to the electrolyte shows an intensive positive feedback effect (black dots), due to the reactivity of the titanium G4 surface (see **Fig**. 6 A). As the time of sample electrolyte interaction goes on, the extent of the contribution of the positive feedback is gradually decreasing. This indicates that the rate of the mediator reduction reaction is decreasing by the immersion time. The reason might be the formation of the passivation layer. Most likely titanium oxide is building up on the sample surface that hinders the regeneration of the mediator (see **Fig.** 6 B). After 14 minutes of immersion time no more positive feedback

shows up (yellow curve). This shows that the concentration of the FcMeOH will not be higher at the tip surface than it is in the bulk. As the time goes on, the approach curves show gradually more and more extensive negative feedback character. This indicates that the further decelerated chemical reaction less and less can compensate the diffusion transport hindering effect of the approaching surface. After 40 min of immersion a pure negative feedback character could be observed (see **Fig.** 5) indicating that the passive titanium oxide layer formed completely blocks the reduction of $FcMeOH^+$ as shown in **Fig.** 6 B.

As it is well known, the shape of amperometric approach curve recorded over conductive sample surfaces with SECM and employing appropriate mediator species will be determined by the competition of the mediator regenerating reaction and the diffusion transport hindering. Therefore, knowing the diffusion coefficient of the mediator, the rate coefficient of mediator regenerating reaction can be estimated. The equation developed by Cornut and Lefrou can be effectively used for this task [49].

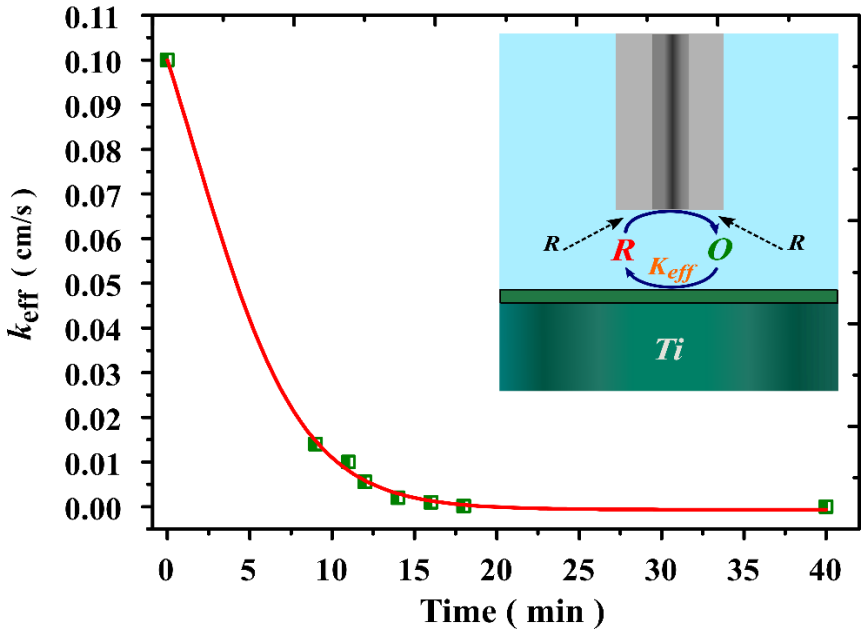

Figure 7: Variation of the calculated effective rate coefficient as a function of immersion time.

In this way, the dependence of k_{eff} values on the time period between time exposing the renewed Ti G4 surface to the electrolyte and time of approach curve taking (Δt) could be obtained. **Fig.** 7 shows the k_{eff} – (Δt) dependence obtained in this way. It can be accepted that the decrease of the k_{eff} value in time indicates the rate of the self-healing process.

As it can be seen in the initial period, the k_{eff} values decrease rapidly. After about 12 minutes exposition time a section with moderate decrease follows reaching all the way to the k_{eff} = 0.

At the initial moment of immersion, the freshly cleaned sample surface is conductive. On the contrary, with time, the effective rate coefficient decreases progressively indicating the more moderate regeneration of the FcMeOH caused by the fewer electrons on the titanium G4 surface. The k_{eff} value achieved the zero value after 25 min of immersion due to the formation of insulator oxide layer on the titanium alloy.

The approach curves obtained in our experiment show that the formation of the passivation TiO_2 film on the Ti G4 surface is not an instantaneous process. About 25 minutes time is the needed for getting entirely formed.

III.1.3. pH monitoring on titanium biomaterial after removal of the native passive film, using SECM in the potentiometric mode

Heterogeneous redox reactions are often involving local pH changes in the vicinity of the surface taking part in the process. Therefore, it was obvious to investigate the changes of local pH values over the dental implant sample during healing of the protective surface film.

III.1.3.1. SECM line scans measurements

The above discussed experiments with SECM operated in amperometric mode prove that the formation of the titanium dioxide on titanium G4 is a time-dependent process. That indicates that electrochemical processes are taking place on titanium G4 surface, most likely they are anodic and cathodic processes. In my further experiments, SECM operated in potentiometric mode was used for monitoring the pH in the vicinity of the titanium G4 surface. Sb/Sb_2O_3Microelectrode as SECM probe was used and measurements were done in different times after mechanically damaging of the protective surface layer of titanium G4 by polishing.

In the actual SECM experiments, first, the Ti G4 sample embedded in the epoxy resin was freshly polished, then about 3ML PBS physiological background solution was added into the electrochemical cell. The distance between the Sb/Sb_2O_3Microelectrode probe and the target was set to 30 µm adjusted by lowering the SECM probe carefully over the epoxy surface and the potential jump at “touch down” was noticed and accepted as zero distance. Afterward the tip was retracted from the surface by 30 µm. The setup of the experiment is shown in **Fig.** 8

The potential was measured at the tip versus Ag/AgCl/KCl (3M) reference electrode. Subsequently a series of consecutive horizontal line scans were carried out across the center of freshly polished titanium G4 at different periods of time.

Fig. 9 show the line scans recorded. They are showing local pH values measured at different exposition times as the tip traveled horizontally across the surface containing of titanium G4 sample. As it can be seen, the pH above the epoxy resin is almost the same as in the bulk (pH ≈ 7.3). However, an acidification could be detected at the close vicinity of the freshly polished titanium G4. After 3Min of immersion of the freshly polished titanium G4 in PBS solution, a pH value of 6.5 was measured. This indicates that chemical reaction taking place right after the interaction of the mechanically polished titanium surface with the PBS solution. Nevertheless, the pH increases progressively with time, indicates the slowing down of the chemical processes. Whereas about 15 min the pH is almost identical to the one measured above the epoxy resin. This implies the cessation of the chemical reaction at close vicinity of the titanium sample.

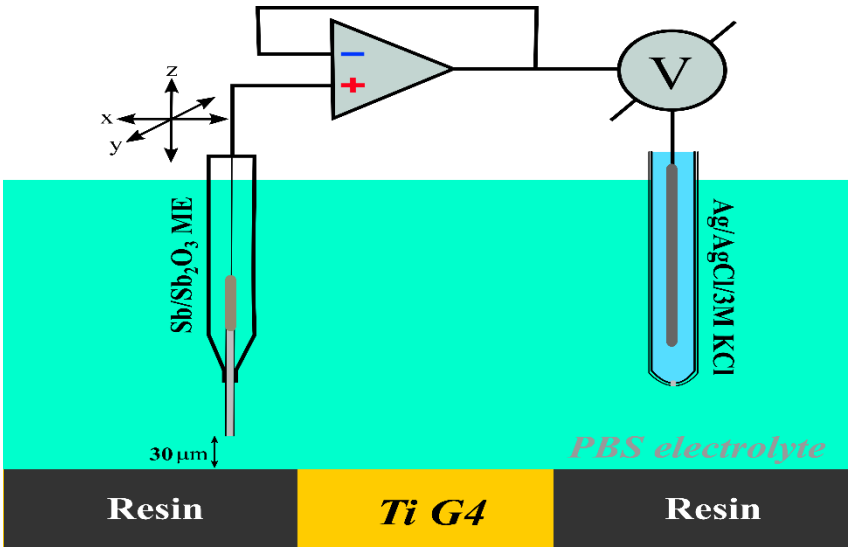

Figure 8: Scheme represents the setup used for the SECM potentiometric measurement where antimony microelectrode used as SECM probe and PBS solution as background electrolyte were applied. The potential was measured versus Ag/AgCl/ 3M KCl using a homemade voltage follower based on 10^{12} Ω *input impedance operational amplifier.*

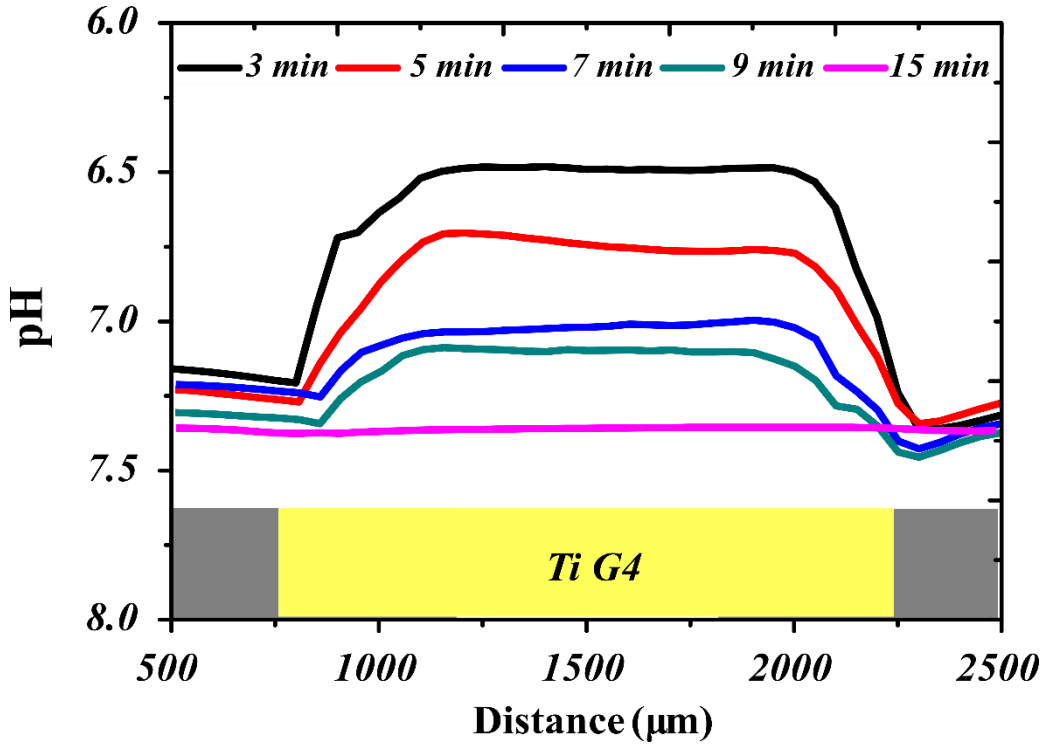

Figure 9: Line scans recorded over freshly polished titanium G4 surface immersed in PBS solution using antimony microprobe. The vertical tip-sample distance was 30 µm and a scan rate of 50 µm/s was used. The time values shown in the color code represent the elapsed between introducing the PBS solution and recording of the individual line scan.

In corrosion mechanisms, the acidification is ordinarily attributed to the hydrolysis of the hydrated metal [84]. Therefore, the local pH change observed can be explained by considering the released of the metal cations from the anodic areas. This implies the oxidation of titanium metal is required for forming the Ti^{4+} (**Eq.** 11). While the electrons yield from the oxidation reaction must be consumed by the oxidant present in the electrolyte, mostly likely by water or /and oxygen since their reactions are thermodynamically possible with titanium [85].

Whereas, in aqueous phase the Ti^{4+}cation is not steady, the hydrolysis reaction take place forming the titanium hydroxides through the following reactions (**Eqs.** 12-14):

$$Ti \rightarrow Ti^{4+} + 4e^- \quad (11)$$

$$Ti^{4+} + 2H_2O \rightarrow Ti(OH)_2^{2+} + 2H^+ \quad (12)$$

$$Ti(OH)_2^{2+} + H_2O \rightarrow Ti(OH)_3^{+} + H^+ \quad (13)$$

$$Ti(OH)_3^{+} + H_2O \rightarrow Ti(OH)_4 + H^+ \quad (14)$$

Therefore, it can be accepted that the local acidification that occurs in the vicinity of the polished titanium G4 shown in **Fig.** 9 is the result of the hydrogen ions yielded from the hydrolysis reactions of Ti^{4+} ions.

Y. Fovet et al. [86] examined the stability of Ti^{4+} in Ringer solution at different pH values. It was proved that at pH 7.3 the titanium tetra hydroxide $Ti(OH)_4$ is the dominant form which will dehydrate forming the TiO_2 insulating layer, as follows:

$$Ti(OH)_4 \rightarrow TiO_2 + 2H_2O \quad (15)$$

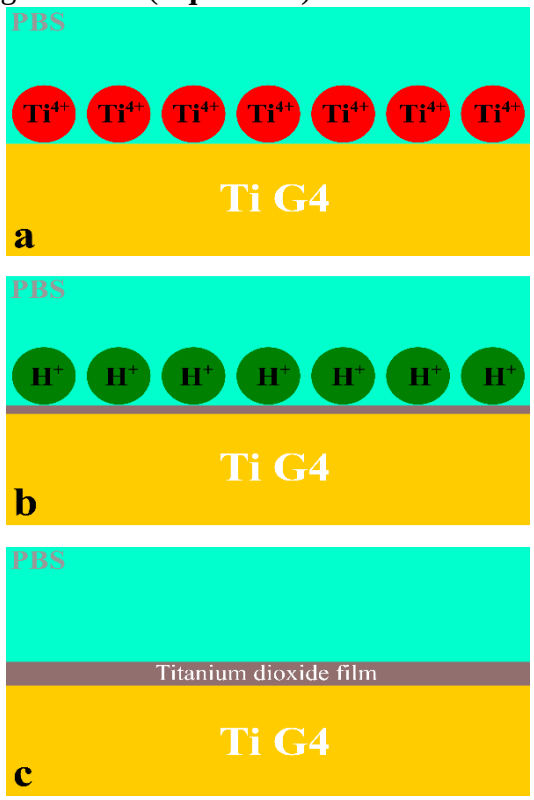

Figure 10: Represent the corrosion mechanisms of the self-healing of the titanium dioxide on titanium G4. A- the oxidation of titanium B- hydrolysis reaction C- dehydration reaction.

The local pH change observed by potentiometric SECM experiments clearly revealed that the above-mentioned chemical reactions can occur on freshly polished titanium G4 and take part in the formation of TiO_2 insulating layer on the metal surface. **Fig.** 10 summarizes the different process of the self-healing.

III.1.4. Investigation of the corrosion resistance of titanium biomaterial after removal of the native passive film, using EIS.

In conventional corrosion studies the impedance spectroscopy is frequently employed for investigations of the processes. In order to gather information on the impact of the immersion time on the corrosion resistance of the passive film developed on the titanium G4 surface, electrochemical impedance spectroscopy was employed. In this experiment the passive surface film was removed by mechanical polishing. Then PBS solution was introduced into the electrochemical cell. Afterward, the EIS spectra were recorded at every 5 min applying a range of frequency of 100 kHz – 0.1 Hz and sinusoidal voltage of 10 mV. The impedance spectra registered are illustrated in **Fig.** 11 in the form of Bode and Nyquist plots. As clearly can be seen, the Bode diagrams presented in the **Fig.** 11 A can be partitioned into three segments. The first section located at the high frequency range of 10^3-10^5 Hz. It displays a stable value of log $|Z|$ that doesn't depend on the immersion time, whereas the phase angle is approaches to a value of zero. This is ordinarily attributed to the resistance of the electrolyte between the tested sample and the reference electrode. The second region that is situated at intermediate frequencies, the phase angle diagrams shows almost a stable angle own a value close to 80°, while the log $|Z|$ vs. log f spectrum reveals a linear slope with a value adjacent to -1; as generally known is the typical performance of the compact passive film [87]. The last section is taking place at low frequencies, while the phase angle spectrum exhibited a variation of the phase angle from 36° to 57 ° as the time of immersion raises. That suggested the development of the protective oxide film on titanium G4 surface [88]. Besides, the Nyquist plots presented in **Fig.** 11 B, exhibit different single depressed capacitive like-semicircles that is correlated to the passive oxide layer on titanium G4 surface that acts as a barrier layer at all periods of immersion [88]. Therefore, the increase of the diameter of the capacitive like-semicircles indicates the development of the passive film on the titanium G4 surface with lengthening of exposure time.

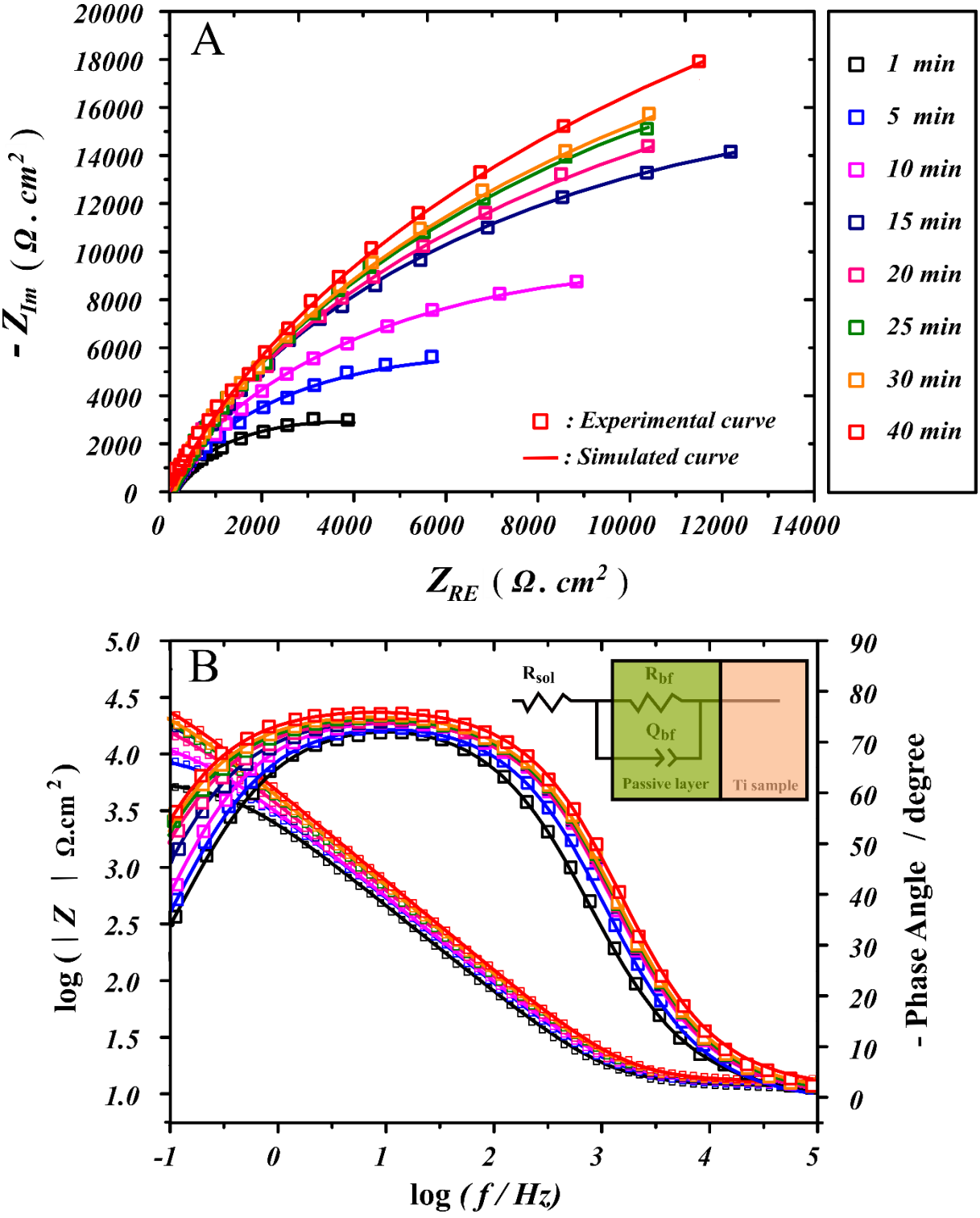

Figure 11: Electrochemical impedance spectra recorded on freshly polished titanium G4 exposed to PBS solution. (A) Nyquist plot (B) Bode diagram. The experiment was carried out in a frequency range of 100 kHz – 0.1 Hz and sinusoidal voltage of 10 mV was applied. The inset in Figure 11 A represent the electric circuit used for fitting the experimental data. The experiments were done at the open circuit potential condition.

Based on the Bode plots, that displays a single peak. This suggested the simulation of the impedance spectra using the equivalent circuit composed by one RC element as shown in **Fig.** 11 B. Where R_s and R_{bf} represent the resistances of the electrolyte and the native barrier oxide film, respectively. Q_{bf} define the constant phase element of the native barrier oxide film. Similar equivalent circuit has been proposed to model EIS spectra of different titanium and titanium-based alloys such as pure titanium [89], titanium grade 2 that has almost a similar composition compare to titanium grade 4 [90-92] and other titanium alloys such as Ti35Nb10Ta-xFe and TiNbZr [93,94]. The EIS parameters were gathered by simulating the EIS spectra using the Ec-Lab software, whereas the quality of the fittings was evaluated based on the Chi-squared values. **Fig.** 11 shows the fitted curve (solid lines) manifests a very good correlation with experimental data (discrete points).

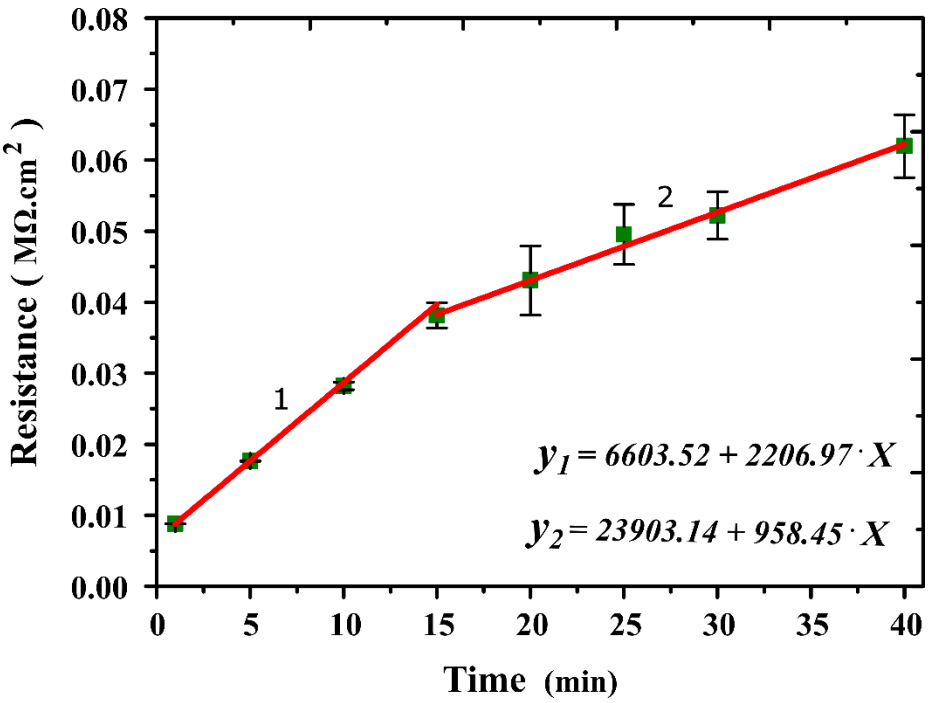

Figure 12: Variation of the oxide film resistance as function of self-healing time.

Fig. 12 displays the variation of the resistance of the barrier oxide film as a function of time. As can be seen, the resistance raises with the increase of the exposure time. It indicates the protection of the titanium G4 surface with a compact film after the interaction with PBS solution. At the first period of immersion up to 15 min, the resistance increases with a rate of 2206 MΩ·cm^2/min, nevertheless after 15 min the resistance rate declines to 958 MΩ·cm^2/min. This suggests that the chemical reactions occurring at the vicinity of titanium surface for

forming the passive film became less favored after 15 min of exposure. This is in a close correlation with results of potentiometric and amperometric SECM experiments.

These experiments clearly show that the self-healing of the titanium dioxide on titanium metal is a process that takes well measurable time for completion. Several minutes were needed for the formation of compact passive film. That was proved by the occurrence of the electron transfer reactions between the titanium and the local environment. Also, it was demonstrated by the low pH detected during the repassivation process which indicates the discharge of titanium cations from titanium surface. This underlines that during self-healing unwanted release of cations can happen. This is a crucial factor which must be taken into consideration in the biomaterial application.

Chapter 2 – Impact of cathodic polarization on the electrochemical reactivity of titanium biomaterial

III.2.1. Resume

The anticorrosion property is one of the main factors providing suitable biocompatibility. In the case of titanium biomaterials, the anticorrosion property is principally conferred by the passive titanium dioxide protective layer which inhibits the release of hazardous metal cations from the surface, and hinders the electron transfer reactions with the surrounding tissue. Numerous papers have been published on evaluating the anticorrosion property of titanium metal. In those works, different physiological electrolytes, surface treatments, and anodic polarization were employed, and their effects were compared [95,96]. To our knowledge, however, a very limited number of studies dealt with the investigation of the cathodic polarization impact so far. While the implanted materials can suffer from the cathodic polarization during the fretting corrosion. F. Contu et al. [43] showed that during the mechanical abrasion of commercial pure titanium (cp Ti) and Ti6Al4V their open circuit potential can drop to a value as low as –1500 mV vs. SCE. Similarly, was revealed in the case of titanium niobium (Ti-Nb) and titanium molybdenum (Ti-Mo) alloys [44]. Moreover, the cathodic polarization can occur during the galvanic corrosion most likely when titanium is coupled with a dissimilar material. Recently, in vivo studies carried out by P. Hou and co-workers [37] the corrosion rate of magnesium co-implanted with titanium object was examined. It was demonstrated that titanium accelerated the corrosion of the magnesium implant. Furthermore, studies testing the influence of catholic polarization on viability of cells in tissues surrounding polarized titanium implants, that it decreased with the increase of the negative polarization [97,99]. Further study performed by Brooks et al. showed that under the cathodic polarization the corrosion resistance of titanium declined and it accompanied by intensive release of metal cations [100]. Therefore, understanding the electrochemical behavior of negatively polarized titanium in situ is recognized as critical character. In this chapter, the electrochemical behavior of commercial pure titanium sample was investigated under cathodic polarization using scanning electrochemical microscopy in the amperometric mode.

III.2.2. Chronoamperometric measurement on freshly polished cp titanium

In order to ensure the formation of the passive titanium dioxide film on the cp titanium surface (99.99 % Ti), chronoamperometric measurement was carried out on freshly polished embedded titanium sample. The experiment was conducted in 0.1 M NaCl at room temperature. Freshly polished titanium sample was kept at 2 V vs. Ag/AgCl/KCl (3M) polarizing potential for 60 s, meanwhile the current-time dependence was recorded. The recorded curve is shown in **Fig.** 13. As it can be seen the current decays by the time. In the first stage a fast decrease of it shows up afterward the current remains almost stable. That indicates the development of a protective film on the cp titanium surface. Most likely the passive film is composed of titanium dioxide which can be formed through the following reaction.

$$Ti + 2H_2O \rightarrow TiO_2 + 4H^+ + 4e^- \qquad [16]$$

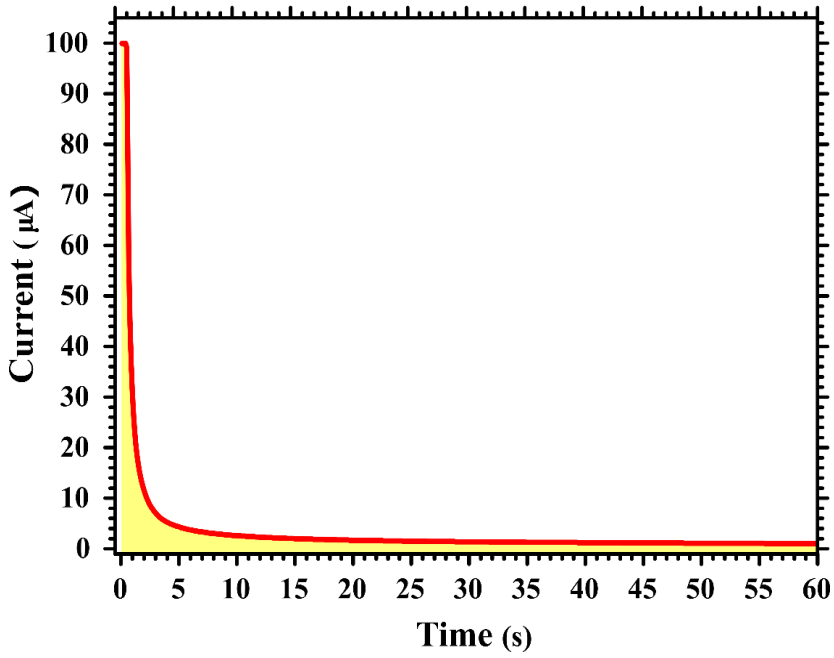

Figure 13: Chronoamperometric curve recorded on freshly polished pure titanium soaked in 0.1 M *NaCl. The titanium sample was polarized to 2 V vs. Ag/AgCl/ 3M KCl for 60.*

III.2.3. Titanium surface characterization by energy dispersive x-ray spectroscopy

The percentages of different atoms in the surface film formed upon oxidative polarization could be estimated using EDX spectroscopy. As a result of that study **Fig.** 14 shows the elemental composition of the surface layer of Ti sample after electrode polarization to 2 V vs. Ag/AgCl/KCl (3M) for 60 s. It can be seen that oxygen and titanium elements were detected. The estimated weight percentage of oxygen and titanium were found to be 27.5% and 72.5%, respectively. The presence of oxygen affirms the creation of the passive titanium dioxide film on the surface in agreement with the observations reported in [101].

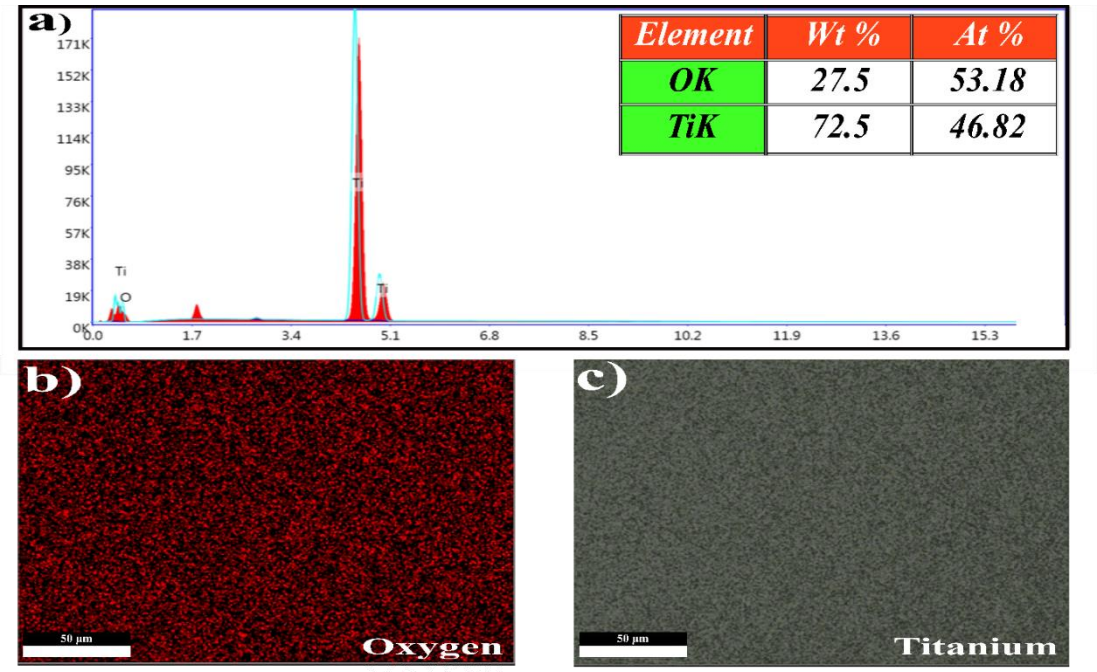

Figure 14: EDX done after polarizing titanium for 2 V *vs. Ag/AgCl/KCl (3M) for 60 s. (a) represent the EDX spectra (b) and (c) correspond to the oxygen and titanium distribution on titanium surface, respectively. The table shown in the inset shows the weight and atomic percentage of oxygen and titanium on the surface.*

III.2.4. Electrochemical characterization of commercial pure titanium using cyclic voltammetry

Cyclic voltammograms were carried out on freshly polished pure titanium (99.99% Ti) electrode immersed in deaerated 0.1M NaCl solution, as shown in **Fig.** 15. As it can be seen, in the first CV swept anodically starting from -0.5V vs. Ag/AgCl/KCl (3M), a very fast increase of current shows up. It is the result of the TiO_2 layer formation on the metal surface [102].
As the electrode potential proceeds to negative direction, an increasing reduction current shows up starting at about -100 mV. As suggested by Ohtsuka et al. [103] we can assume that the electro-reduction of anodically formed titanium dioxide takes part in this cathodic polarization range. The electrochemically reduced protons ($H^+_{aq} + e^- \rightarrow H_{ad}$) get absorbed. This leads to the transformation of titanium dioxide to titanium hydroperoxo species, described by the following reaction [103]:

$$TiO_2 + ne^- + xH^+_{aq} \rightarrow TiO_{2-x}(OH)_x \qquad [17]$$

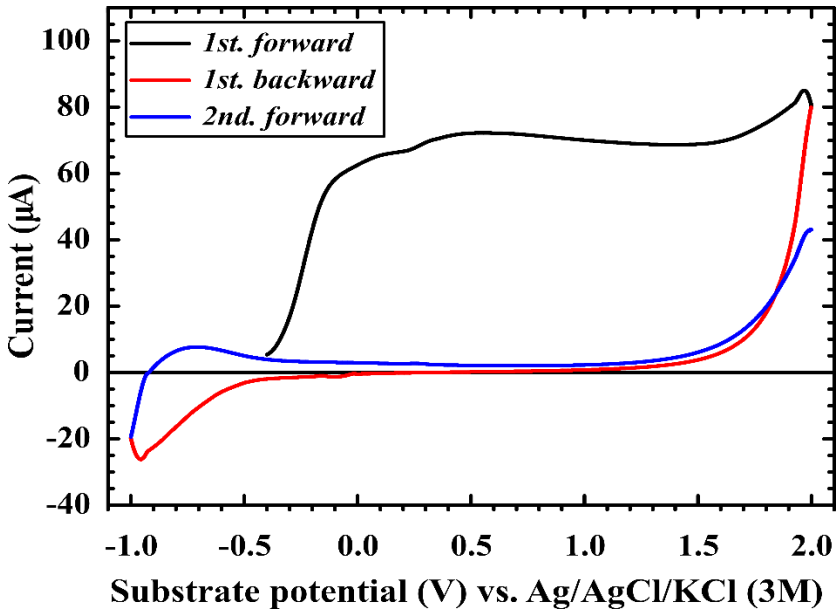

Figure 15: Cyclic voltammograms recorded on freshly polished titanium electrode in 0.1M *NaCl. The first scan began from* -0.5 V *up to* 2 V *(black line). The second line (red line) and the third line (blue line) were performed at the range of potential of* -1 V – 2 V *vs. Ag/AgCl/KCl (3M). A scan rate of 1 mV/s was employed.*

III.2.5. SECM investigation of the reactivity of titanium surface

III.2.5.1. SECM approach curves measurements

Further electrochemical characterization of the thin titanium oxide layer formed on a pure titanium surface has been done with SECM. For investigating the dependence of the electrochemical reactivity of the titanium sample surface on the cathodic polarization potential, consecutive approach curves were recorded over the surface of embedded titanium sample surface. Platinum disk as amperometric SECM tip that has a diameter of 25 µm was employed. For these experiments 0.1M NaCl background solution containing 5mM FcMeOH was introduced into the cell and tip potential of 0.5 V vs. Ag/AgCl/KCl (3M) was imposed. The tip was positioned over the center of the sample for 500 µm vertical (Z) distance from it. Then after steady amperometric current could be observed the tip was moving vertically down with 1 µm/s speed meanwhile the current – distance dependence was recorded. First, the Z-approach was done at open circuit sample potential (OCP) with disconnected titanium surface. Afterward the sample was connected to the potentiostat and similar approach curves have been recorded consecutively employing different negative polarizing potentials, starting from -100 mV vs. Ag/AgCl/KCl (3M).

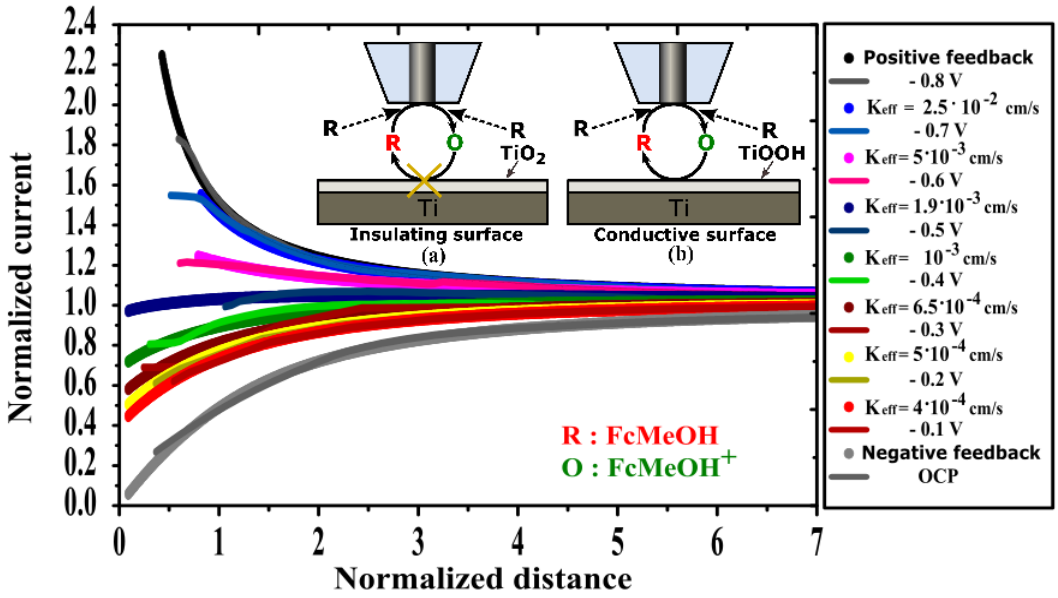

Figure 16: Z-approach curves recorded over titanium at different *electric polarization potentials. The experiments were performed in* 0.1M *NaCl mixed with* 5mM *FcMeOH. Platinum micro-disk electrode of 25 µm diameter was used as SECM probe moving with scan rate of 10 µm/s. The inset shows the calculated effective rate coefficients corresponding to each polarizing potential value applied to titanium sample.*

The curves recorded are presented as lines in **Fig.** 16. The abscissa values of the curves mark the normalized distance L ($L=d/a$ where d is the gap distance and a is the radius of the tip) while the ordinate values show the so-called normalized current $I = I_d/I_\infty$ where I_d is the measured tip current at d gap size and I_∞ is the current measured in the bulk, far from the sample surface. As can be seen, the Z-approach curve recorded at OCP showed pure theoretical negative feedback character. It proves that the thin layer formed anodically passivates the titanium sample surface, which avoids the regeneration of the mediator (**Fig.** 16 a). However, as titanium sample biased to cathodic polarization, the Z-approach curves became gradually separated from the theoretical approach curve relating to insulating surface. As the negative polarizing potential gradually increases the shape of the approach curve gradually changes, showing more and more extent of mediator regeneration. As it can be seen for the approach curves recorded in the potential range between -100 and -400 mV the negative feedback character is the dominant whereas a mixed positive-negative feedback effect shows up at the potential of -500 mV. Besides, positive feedback occurs at more negative potential than -500 mV. This is due to the electro-reduction of $FcMeOH^+$ that causes the increase of FcMeOH concentration in the vicinity of titanium surface. That results in a positive feedback as the applied potential increases (**Fig.** 16 b). Since the titanium sample was polarized negatively, molecular hydrogen might be produced and could interfere with the oxidation of FcMeOH at the platinum tip. To clarify this point, cyclic voltammograms were recorded over titanium surface using platinum microprobe held at 10 µm constant distance from the center of the titanium sample surface as shown in **Fig.** 17. The **Fig.** 17 A depicts several cyclic voltammograms recorded from 0 to 500 mV vs. Ag/AgCl/KCl (3M) with the tip immersed in 0.1M NaCl solution containing 5mM FcMeOH. The substrate was held at constant potential during CV recording. These polarizing constant potential values kept on the sample for different CV taking were varied from -100 to -800 mV by step size of 100 mV. As it can be seen, the higher is the negative potential applied on titanium the greater limiting currents are observed at the platinum tip. This affirms the regeneration of FcMeOH mediator on the sample surface, as well as the dependence of the rate of regeneration reaction on the applied polarizing potential. These findings are in accordance with the Z-approach curves seen in **Fig.** 16.

The platinum micro-tip positioned over the Ti sample surface can also detect the hydrogen if it evolves from the sample upon negative polarization. In order to examine the hydrogen evolution on titanium, several CV-s were recorded with the platinum probe, scanning in potential range of -0.4 V to 0.5 V. In those experiments 0.1M NaCl background solution (without mediator)

with tip-sample distance of 10 μm was applied. The obtained CV-s are shown in **Fig.** 17 B. As it can be seen the CVs recorded at different sample polarization potential in close vicinity of the sample surface in absence of mediator do not show significant increase of the tip current. This proves that the current measured during the feedback experiments seen in **Fig.** 16 and **Fig.** 17 A is resulted predominantly by the oxidation of FcMeOH at the probe.

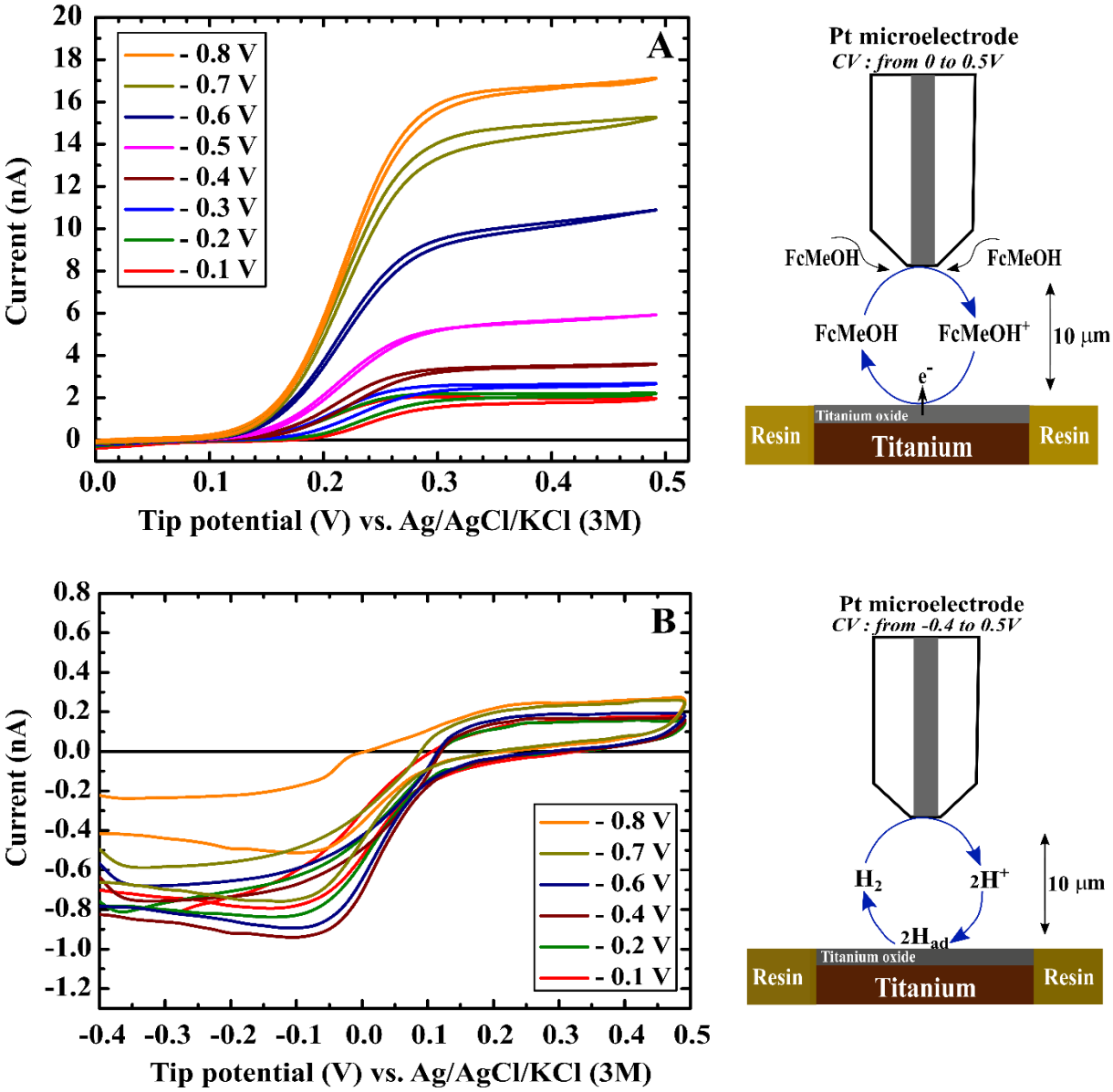

Figure 17: Cyclic voltammograms recorded on 25 μm platinum microelectrode over titanium polarized to different electric polarization. (A) - CVs recorded on titanium exposed to 0.1M *NaCl solution containing* 5mM *FcMeOH mediator. (B) CVs recorded on titanium exposed to* 0.1M *NaCl solution (no mediator). The tip-sample was 10 μm and scan rate of 25 mV/s was employed.*

The effective rate coefficient (k_{eff}) of mediator regenerating electrode process can give quantitative information about surface condition of sample surfaces. The equation developed by Cornut and Lefrou [49] was used for characterization of sample properties and for checking their changes upon negative polarization. As can be seen, the theoretical curves in **Fig.** 16 indicated by circle symbols show very good fit to the experimental curves. The obtained k_{eff} coefficient values are in the range of $4 \cdot 10^{-4}$ cm/s to $2.5 \cdot 10^{-2}$ cm/s when titanium sample biased cathodically between -100 mV and -700 mV as illustrated in **Fig.** 16 The k_{eff} – polarizing potential dependence clearly denotes that the increase of the applied negative potential facilitates the electron transfer at the titanium oxide layer.

III.2.5.2. 2D maps of electrochemical reactivity recorded with SECM over embedded titanium metal sample

In order to image the electrochemical reactivity of the protective oxide formed on pure titanium and make a comparative study with the approach curve experiments, 2D SECM images were recorded over titanium surface immersed in deaerated 0.1M NaCl solution mixed with 5 mM FcMeOH mediator. The 25 µm measuring tip of the SECM was set to 0.5 V vs. Ag/AgCl/KCl (3M). Constant height (Z direction) of 20 µm from the target was set and amperometric 2D scans over selected area of 2000 µm × 1600 µm area with a scan rate of 20 µm/s were carried out. First, the SECM map was made over titanium maintained to its OCP and then a sequence of 2D images were recorded setting different fixed negative substrate polarization potentials. The recorded SECM images are presented as normalized current values (I_d/I_∞), given in **Fig.** 18.

The map recorded at the OCP shows a similar distribution of the normalized current of 0.63 over the whole scanned area. It can be seen that the current values are the same over the embedding epoxy resin and over the metal. The whole area acts as insulator with clear negative feedback. This agrees with the Z-approach curve (grey color) in **Fig.**16. Current values higher than the current above the insulating resin are clearly visible over titanium sample in images recorded employing appropriate cathodic bias potential. The applied sample polarizing potentials of -0.4 V, -0.6 V and -0.8 V resulted in normalized current values of 0.92, 1.08 and 1.35, respectively. This feature is caused by the electron transfer donation at titanium oxide to the ferrocenium species, results in positive feedback as proven by the approach curve experiment depicted in **Fig.** 16. Obviously, the SECM images showed a uniform negative and positive feedback in cases of the maps recorded at OCP and at application of polarizing negative

potentials, respectively. This indicates the super homogeneity of titanium surface which obviously is the result of the high purity of the titanium sample.

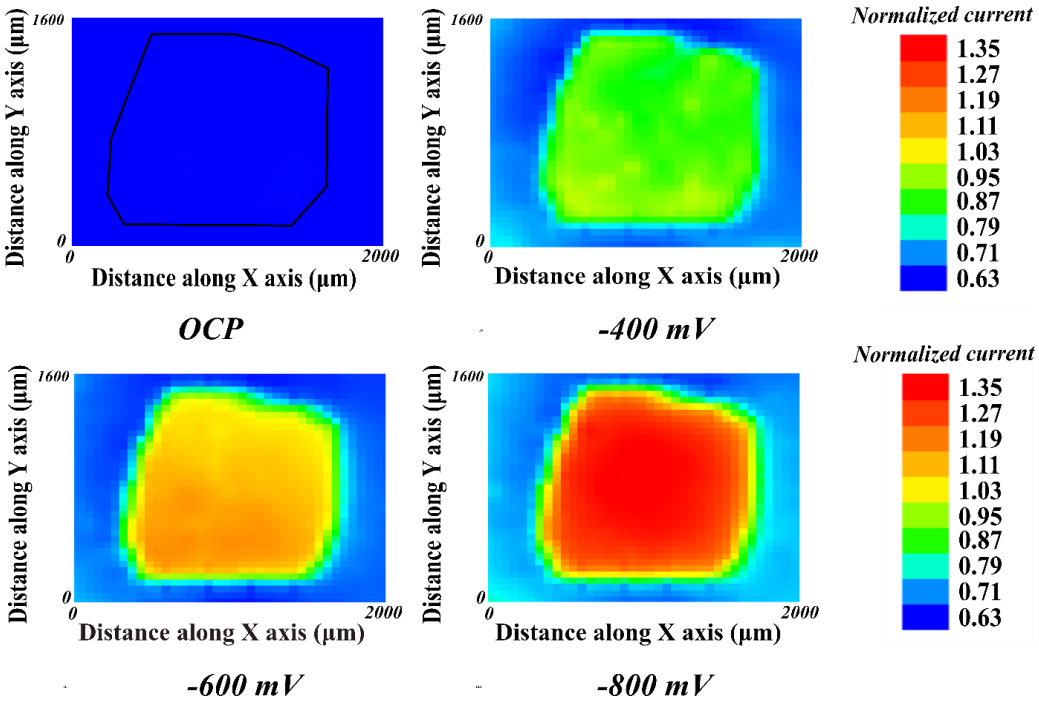

Figure 18: 2D images recorded over titanium at the OCP and under cathodic polarization of -400 mV, -600 mV *and -800 mV. The images were recorded at scanned area of 2000 µm × 1600 µm in* 0.1M *NaCl solution with* 5mM *FcMeOH mediator concentration, carried out with platinum micro-disk electrode (diameter25 µm) moved with a scan rate of 10 µm/s, while the vertical tip-sample distance was 20 µm.*

This is in good agreement with EDX mapping seen in **Fig.** 14. The SECM images, as well as approach curves obtained in the experiments, indicate in close agreement that the negative polarizing potential increases the conductivity of titanium oxide. The positive feedback appearance under cathodic polarization seen in the approach curve experiments and SECM images can be explained by the change of the surface film from a passive insulating character to a more conductive oxide structure. The CV shown in **Fig.** 15 is in agreement with electrochemical reduction of titanium dioxide (**Eq.** 17) accompanied by the absorption of hydrogen. When higher cathodic polarization potential was applied, more hydrogen was absorbed in the oxide film [103]. Since titanium dioxide has a semi conductive property, the mentioned processes result in the incorporation of additional states within the band gap of titanium oxide. This increases its conductivity with an extent that depends on the applied polarizing potential [104], reaching a limit of conductivity at -0.8 V vs. Ag/AgCl/KCl (3M)

(3M) as shown in **Fig.** 16. Hence, the increase of surface conductivity and the facilitated electron transfer at titanium oxide film can be understood.

III.2.5.3. Hydrogen absorption monitoring using SECM

In order to monitor the hydrogen concentration over biased titanium at different cathodic polarization, SECM measurements were carried out. In these experiments 6000 µm long horizontal line scans were rerecorded over the center of titanium sample embedded in epoxy resin. The Ti potential was set to different constant values and deaerated 0.1M NaCl background solution was used. -0.6 V vs. Ag/AgCl/KCl (3M) platinum tip potential, typically used for hydrogen ion detection [105], was set and it was moved (in X direction) with a scan rate of 10 µm/s. The vertical distance between the SECM probe and the sample surface was set to 20 µm. It was done via making Z-approach curves over the resin surface (pure negative feedback has been observed) in 0.1M NaCl solution mixed with 5mM FcMeOH mediator, then the tip was retracted by 20 µm. Subsequently the solution was replaced by deaerated 0.1M NaCl testing electrolyte. **Fig.** 19 shows selected plots obtained at various substrate polarizations. They are current – distance values recorded as the tip travels at horizontal line across the metal sample 20 µm above it.

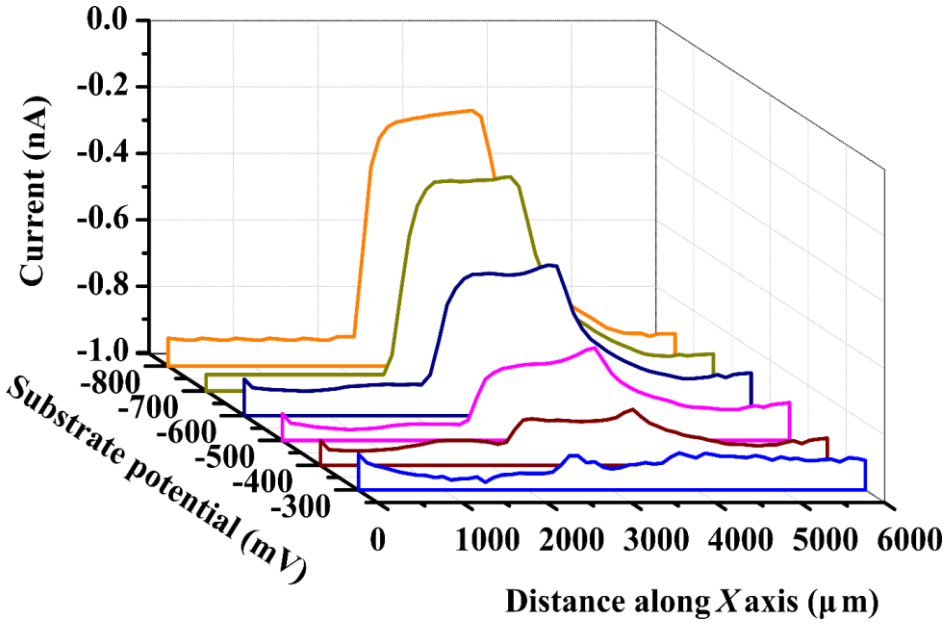

Figure 19: Line scans recorded with platinum micro-disk electrode of 12.5 µm tip radius in deaerated 0.1M *NaCl solution above embedded titanium sample polarized negatively from* -300 *to* -800 *mV with an increment of* 100 *mV. The tip sample distance was set to* 20 *µm and scan rate of 20µm/s was employed.*

As it can be seen above the insulating resin a constant current value shows up. On the other hand, over the Ti surface the current value depends on the applied polarizing potential. Higher negative potential goes along with smaller tip currents resulted by the competitive effect as illustrated in **Fig.** 20. If sufficient cathodic polarization potential is applied on the Ti sample surface, then the reduction reaction (**Eq.** 17) competes with the tip reaction, thus the concentration of hydrogen ions decreases in the vicinity of titanium, therefore the tip current decreases.

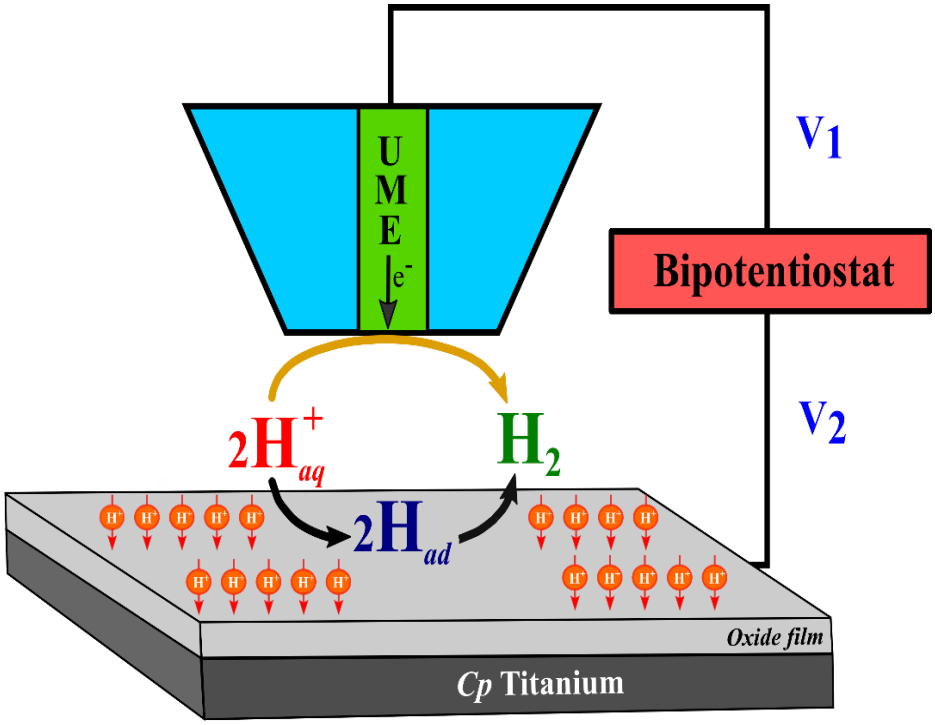

Figure 20: Scheme representing the redox competition between tip and sample for hydrogen ion reduction when titanium sample is negatively polarized.

As readily seen, only a moderate competitive effect showed up when the applied potential was -300 mV and -400 mV. It ensured that the rate of electrochemical reduction is slow in the vicinity of titanium. Conversely, at a negative potential higher than -500 mV, an intense competitive effect could be seen owing to the significant reduction of protons. This finding is in good agreement with CV measurements seen in **Fig.** 15, which showed a remarkable current increase at the potential more negative than -500 mV. At that polarization range hydrogen is significantly absorbed in the surface (**Eq**. 17), in accordance that was reported in [103]. In

correlation with these findings, the approach curve experiments demonstrate that titanium gets more conductive at potentials more negative than -500 mV.

Generally, the hydrogen gas takes place at the reduced passive oxide films when it gets completely activated. For that purpose, the hydrogen gas was monitored above the cathodically polarized titanium using the SG-TC mode. In these experiments the platinum probe was polarized at 0 V vs. Ag/AgCl/KCl (3M) and the titanium sample was biased to different cathodic polarization at the range of -0.1 V and -1.4 V. The platinum tip was positioned 20 µm from the surface. It was set by recording a Z-approach curve above the insulating resin using 5 mM FcMeOH dissolved in 0.1M NaCl solution, the negative feedback was observed, and the tip position was determined by fitting the measured approach curve to the theoretical one, then the tip was positioned for 20 µm vertical distance from the sample surface. Afterward the solution was replaced with deareated 0.1M NaCl solution. Line scans were recorded. They are shown in **Fig.** 21. As could be seen, a steady current of close to 0 nA was recorded above titanium sample when the applied polarizing potentials were between -0.1 V and -1.2 V. That indicated no hydrogen gas evolution on the surface. It implies that the reduction of the oxide film is the dominant electrochemical process taking place at the potential below -1.2 V vs. Ag/AgCl/KCl (3M). That is in agreement with the findings reported by Y. Zeng et al. [106]. On the other hand, a significant current was recorded at applied potential of -1.4 V that proved the hydrogen gas evolution from the titanium surface Interestingly the current showing the concentration of evolved hydrogen was very high at the edges of the titanium sample.

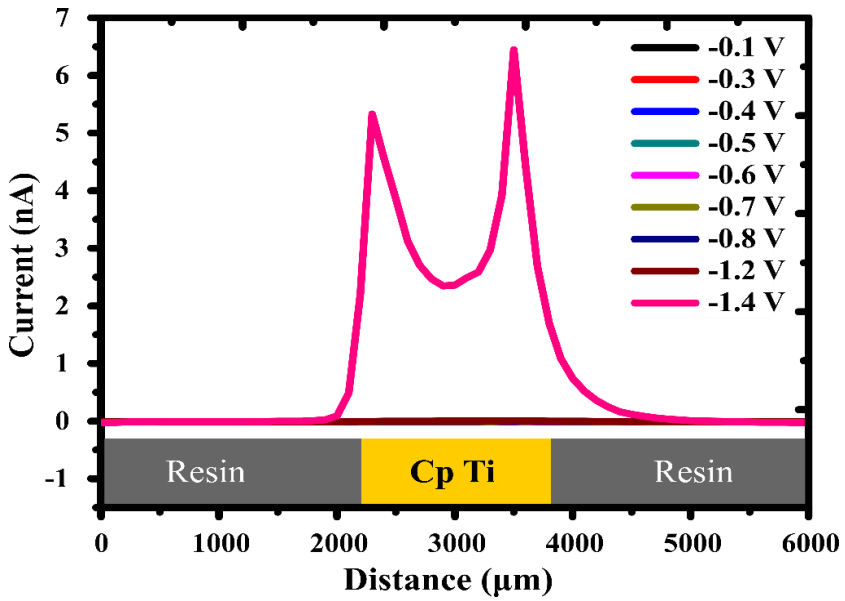

Figure 21: Line scans indicating the hydrogen concentration above epoxy resin implanted titanium sample polarized to different negative polarizations. The recordings were taken with 25 µm size platinum tip polarized to 0 V vs. Ag/AgCl/3M KCl. The tip-sample distance was 20 µm and scan rate of 20 µm/s was employed. Deaerated 0.1 M NaCl solution was used as background electrolyte.

III.2.6. Examination of the cathodic polarization impact on the corrosion resistance of titanium using EIS.

It was important to investigate how and what extent the cathodic polarization affects the corrosion resistance of titanium. In my work electrochemical impedance spectroscopy was employed for these studies. In the sample preparation step oxide layer was formed anodically on titanium surface. In the next step EIS spectrum was recorded on it without employing polarization, that is at open circuit potential (-50 mV vs. Ag/AgCl/KCl (3M)). Afterward, electrochemical impedance spectra were recorded applying different constant polarization potential values on titanium from -100 mV to -800 mV. **Fig.** 22 shows the impedance spectra at the form of Nyquist and Bode plots.

As it is shown, the size of the Bode spectra decreases with the increase of the cathodic polarization potential. At low frequencies, a phase angle value of 63.71° was obtained when the Bode diagram was recorded at the OCP. While a progressive decrease of the phase angle with the increase of the cathodic polarization potential is observed that reached a value as low as 50.85° at the polarization potential of -0.8 V vs. Ag/AgCl/KCl (3M). Similar trend was observed with log $|Z|$ vs. log f. The Nyquist plots depicted in **Fig.** 22 A reveal different depressed semi-semicircles. Their radius decreases with the increase of the cathodic polarization potential. This implies the decrease of the corrosion resistance of the titanium sample with the increase of the degree of cathodic polarization employed.

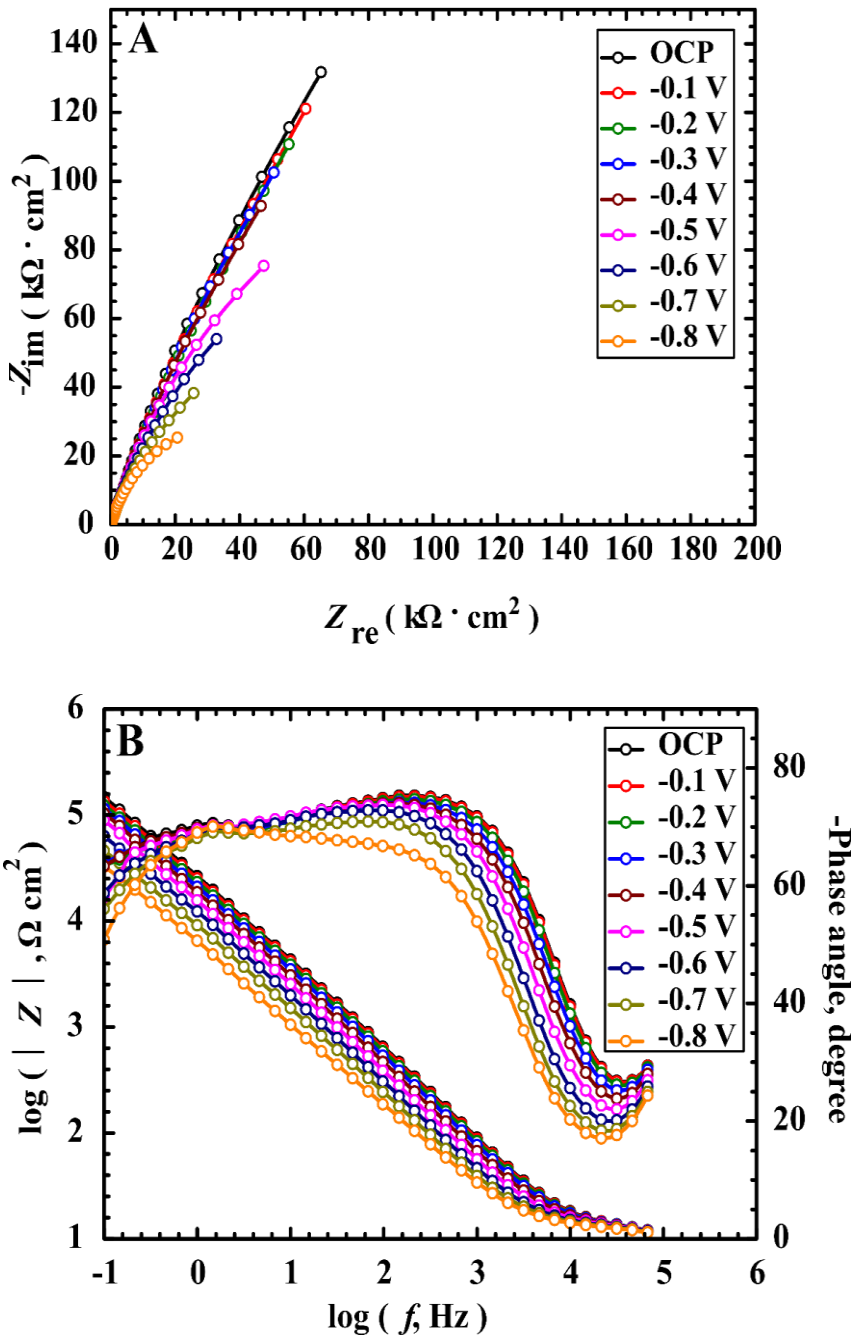

Figure 22: Electrochemical impedance spectroscopic plots obtained with titanium polarized to different negative potentials from – 100 mV to -800 mV with 100 mV increment. Figures A and B represent the EIS spectra in the form of Nyquist and Bode plots, respectively. The EIS spectra were recorded at the frequency range of 100 kHz - 0.1 Hz and using an alternating sinusoidal potential with an amplitude of 10 mV.

Quantitative information was gathered via simulating the impedance spectra using the equivalent electric circuit (EEC) shown in **Fig.** 23. That was chosen based on the Bode plots which displayed two-time constants. The EEC is composed of the electrolyte resistance *R*s in series with two parallel RQ elements.

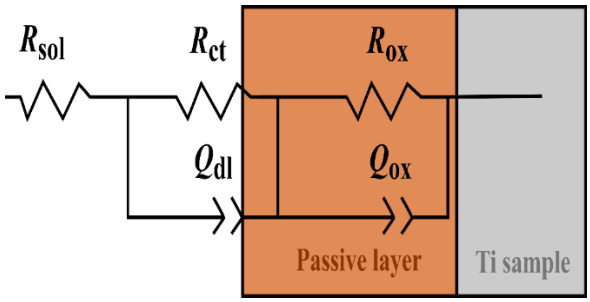

Figure 23: Equivalent electric circuit used to simulate the experimental data

Where R_{ct} and Q_{dl} are the resistance and the capacitance, relating to the reactions proceeding on the titanium oxide layer/electrolyte interface. Whereas R_{ox} and Q_{ox} stand for the resistance and capacitance of the titanium oxide, respectively [101]. **Fig.** 24 shows the dependence of the resistance and capacitance of the titanium oxide on the applied potential. As it can be seen, under -0.4 V polarizing potential only a slight change of the R_{ox} and Q_{ox} shows up. However, at more cathodic potentials than -0.4 V, those properties significantly change. The capacitance increases considerable and the resistance significantly decreases. These finding are in tight correlation with results of SECM experiments. They show significant increase of the surface conductivity at cathodic potentials higher than -0.4 V vs. Ag/AgCl/KCl (3M).

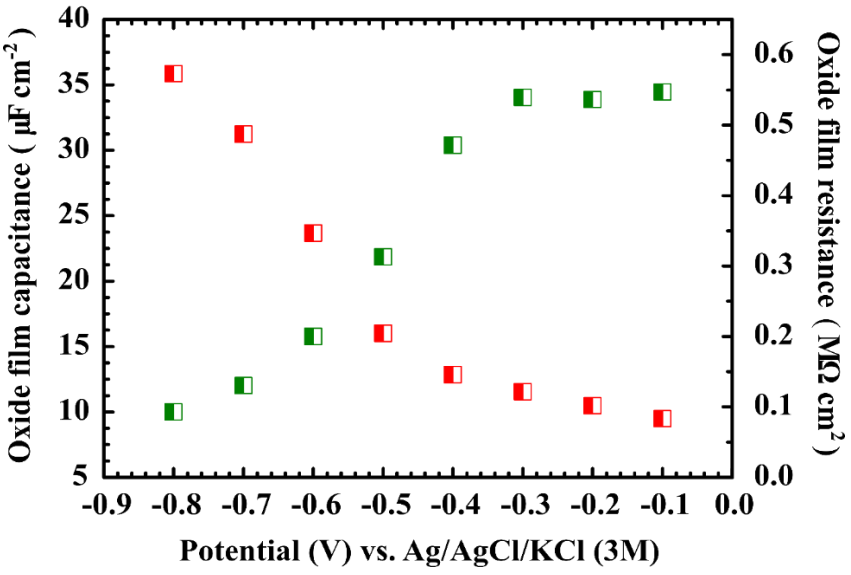

Figure 24: Variation of the resistance and CPE parameter of the oxide film as a function of polarization.

The experiments proved that application of cathodic polarizing potential lower than -0.4 V increased the conductivity and the occurrence of the electron transfer reactions between the metal and the surrounding electrolyte. That is titanium biomaterial loses anticorrosion property under the cathodic polarization. That would affect the viability of the biological cells surrounding the implanted titanium.

Chapter 3 – Anodic polarization impact on the electrochemical behavior of Nitinol biomaterial using SECM

III.3.1. Resume

Nitinol is a nearly equiatomic alloy of nickel and titanium [107]. It is considered amongst the alloys widely used for medical applications due to its biocompatibility, shape memory, superelasticity, and high corrosion resistance. Nitinol is largely applied as orthodontic wires, stents, dental implants, and orthopedic devices [27,29]. However, in the literature problems related to the uses of Nitinol are quite frequently have been mentioned and discussed [108]. For instance, its susceptibility to the pitting corrosion under in vitro and in vivo conditions was demonstrated [109], as well as the discharge of Ni^{2+} ions from Nitinol soaked in neutral, physiological environment [29]. Also, Nitinol biomaterial was examined in acidic physiological environment. Since the pH of the extracellular fluid of human body can drop to significantly lower value at certain location in extreme physiologic conditions like in inflamed muscle or joint tissues. It was proved that the pH can drop to a value as low as 3 [110]. A significant release of nickel ions from NiTi exposed to an acidic environment was also found [111]. However, up to now, this feature was not fully investigated. Commonly known that nickel is a toxic species and numerous studies attest nickel as a source of allergic reactions [28,112]. That highlights the importance of the investigation of the corrosion process in situ and understanding the nature of the reactions happening on the surface of the biomedical objects.

Nitinol biomaterial was generally characterized by employing conventional electrochemical testing such as electrochemical impedance spectroscopy (EIS) and potentiodynamic polarization tests. Those methods are confined to test the steadiness of the passive films and to gather quantitate information on a large scale. In my experiments, SECM was used for obtaining fine details about behavior of Nitinol. To the best of our knowledge, no systematic study was performed to survey the electrochemical properties of Nitinol in the acidic medium using SECM. Also, the anodic and the cathodic spots on the active areas where the chemical reactions proceed have not been visualized. In this chapter, the electrochemical behavior of Nitinol biomaterial was carried out under anodic treatment performed with scanning electrochemical microscopy.

III.3.2. Characterization of Nitinol surface using the energy dispersive x-ray spectroscopy

The elemental surface analysis of Nitinol sample was performed using energy dispersive x-ray spectroscopy. Through scanning a surface area of 250 µm × 250 µm of the Nitinol sample titanium, nickel and oxygen were detected as shown in **Fig.** 25 B, C and D. The table revealed as inset in **Fig.** 25, summarizes the obtained percentages of the three detected elements in weight and atomic number percentages. As it is indicated, estimated weight percentages of 43.14, 48.38 and 8.48 were obtained for Ti, Ni and O, respectively. The existence of oxygen confirms the creation formation of passive oxide layer on the Nitinol surface. Most likely the oxygen is in TiO_2 and NiO forms as it was demonstrated earlier by XPS measurements reported in [113]. In the bulk of Nitinol, the Ti/Ni ratio is 0.82, whereas in the surface film of it is about 0.9. This suggests that the titanium slightly accumulates on the surface due to the favored state of titanium dioxide formation. That might be explained by considering the formation Gibbs energy (ΔG) of titanium dioxide that is -889 $kJ.mol^{-1}$ (298 K), whereas the nickel oxide owns a moderate ΔG (298 K) of -211.7 $kJ.mol^{-1}$ [114].

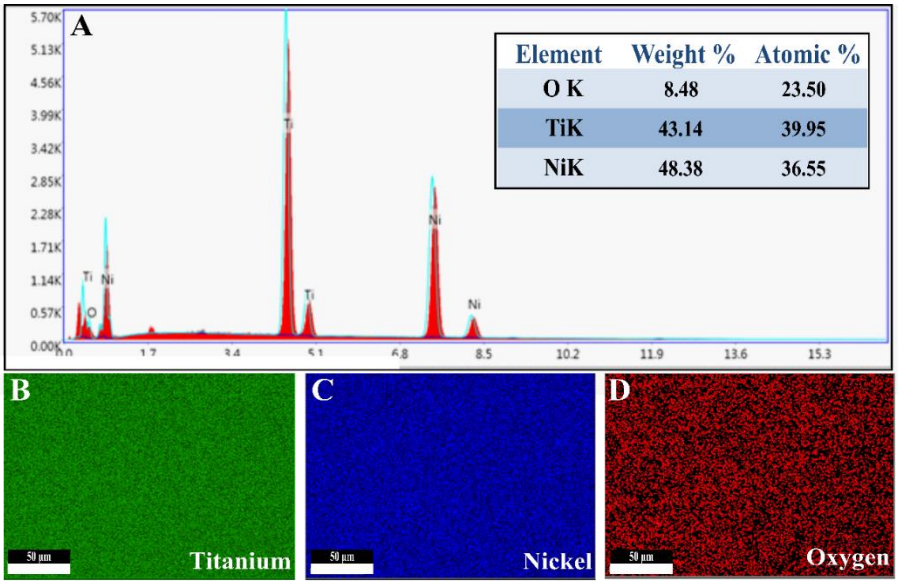

Figure 25: Results of EDX experiments done over Nitinol surface. A displays the EDX diagram while B, C and D shows the distribution of titanium, nickel, and oxygen, respectively. The table shown in the inset indicates the ratios of O, Ti, and Ni in weight and atomic percentage.

III.3.3. Electrochemical characterization of Nitinol using potentiodynamic polarization

The potentiodynamic polarization measurements were done on embedded Nitinol sample that was exposed to 0.1M NaCl solution for 1.5 hours. The obtained curve is shown in **Fig.** 26. As can be seen, a short passivation plateau appears extending up to 0.48 V vs. Ag/AgCl/KCl (3M). It indicates that a stable passive oxide layer is formed on the Nitinol surface. However, a swift of current reveals at 0.48 V in agreement with the previous reports [115]. This means that over 0.48 V the integrity of the passive oxide film ceases. That can result in the initiation of the pitting corrosion [78].

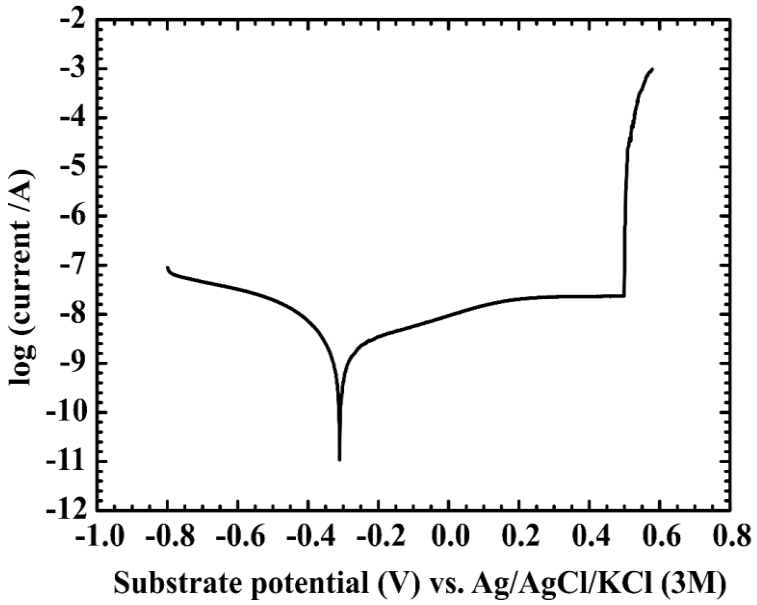

Figure 26: Tafel polarization curve of Nitinol recorded on Nitinol sample in 0.1 M NaCl. It was carried out in a potential range of -0.8 V – 0.6 V vs. Ag/AgCl/KCl (3M), and scan rate of 1 mV/s.

III.3.4. Electrochemical characterization of Nitinol surface before and after anodic treatment using EIS

The electrochemical impedance spectroscopy (EIS) was performed in order to characterize the Nitinol surface before and after the anodic polarization. The impedance spectra were carried out in 0.1M NaCl solution. First it was done on Nitinol exposed to 0.1M NaCl solution for 1.5 hours (unbiased Nitinol). Afterward, the EIS was performed on Nitinol polarized to 1 V vs. Ag/AgCl/KCl (3M) for 15 min (biased Nitinol). The measured spectra are shown in **Fig.** 27, displayed in the form of the Bode diagram. Comparing the two plots (before and after polarization), it is obvious that the behavior of the Nitinol surface considerably changes in consequence of the anodic polarization.

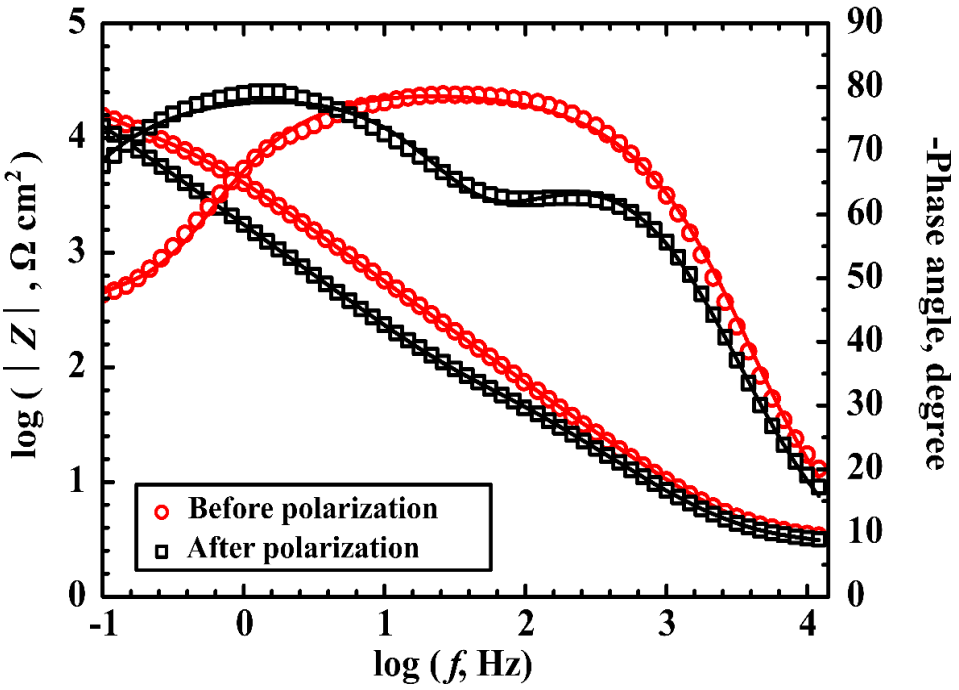

Figure 27: Electrochemical impedance spectroscopy spectra of Nitinol sample in a form of Bode plot. The Bode plot with red symbols was recorded on Nitinol sample immersed for 90 min in 0.1M *NaCl, while the one with black symbols was carried after polarizing the Nitinol sample for 1 V vs. Ag/AgCl/KCl (3M) for 15 min. The solid lines represent the fitted data. The experiments were performed at the frequency of 100 kHz - 0.1 Hz and an alternating sinusoidal potential with an amplitude of 10 mV was applied.*

The Bode diagram obtained before polarization displays two time constant, one at high frequencies and the other one at low frequencies. At the high-frequency range, the Bode modulus plot shows a short range of the constant log |Z| with a phase angle close to 0° due to the electrolyte resistance between the reference electrode and the testing sample, similarly seen with anodically polarized Nitinol. In the middle frequencies, the Bode diagram related to unbiased Nitinol shows a linear slope of about -1 and a phase angle of 80°. As generally known, it is a typical response of a capacitive behavior of the passive films [88]. It implies that nickel and titanium passive oxides were developed on the Nitinol surface.

The Bode diagram of the biased Nitinol shows two-time constants, clearly manifested by the incidence of two waves. One at a frequency in the range of 10^{4} -$10^{1.5}$ Hz, while the other wave appears between $10^{1.5}$ - 10^{-1} Hz. However, it doesn't show a linear slope in the middle frequency range. This behavior could be the result of the bilayer oxide structure [74], or the localized corrosion occurring on the metal surface [116,117]. Since the Nitinol sample was polarized at 1 V. The applied potential belongs to the transpassivation region as seen in the Tafel plot shown in **Fig.** 26, this will result in a breakdown of the Nitinol surface. This highly suggests that the localized corrosion is causing of the behavior presented in the Bode diagram.

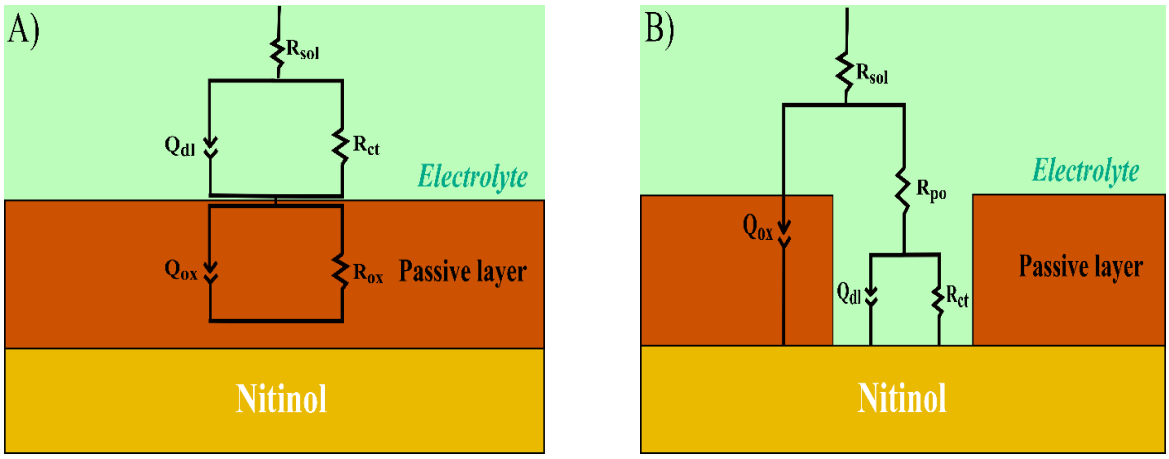

Figure 28: The equivalent electric circuit (EEC) used for simulating the experimental data. (A) The EEC used to simulate the EIS registered after exposing Nitinol for 90 min in 0.1M *NaCl. (B) The EEC employed to simulate the EIS after polarizing the Nitinol sample for 2 V vs Ag/AgCl/KCl (3M).*

In the sake to model the corrosion processes at the Nitinol/electrolyte interface, two EEC were proposed based on the above results, as shown in **Fig.** 28 A. As could be seen a very good correlation was obtained between the simulated data and the experimental impedance spectra. The Bode diagram of unbiased Nitinol was simulated using the EEC shown in **Fig.** 28 A. Composed of the electrolyte resistance R_{sol} in series with two parallel RQ elements. The high frequency, R_{ct} and Q_{dl} describe the properties of the reactions at Nitinol passive oxide/electrolyte interface, respectively the charge transfer resistance and the double layer capacitance [101]. Whereas, at low frequency, R_{ox} and Q_{ox} define the properties of the passive Nitinol oxide layer correspondingly to the resistance and capacitance of the barrier native oxide film [101].

The EEC displayed in **Fig.** 28 B, was used to simulate the Bode diagram of anodically polarized Nitinol. It is considered the most often employed circuit for analyzing the heterogeneity and the localized corrosion of materials involved. The first-time constant observed at high frequency, composed of the resistance of the electrolyte in the pores of the oxide film (R_{po}) and the capacitance of the passive area (intact) Q_{ox}. Whereas, the second time constant at low frequency takes into account the corrosion reaction at the Nitinol substrate. It is characterized by the charge transfer resistance (R_{ct}) and the electrical double layer capacitance (Q_{dl}) at passive film pores [117].

III.3.5. SECM investigation of the reactivity of Nitinol surface before and after anodic treatment

The electrochemical reactivity of the Nitinol surface before and after the anodic polarization was investigated using SECM. In these experiments, the SECM was operated in the feedback mode, employing platinum microelectrode (disk diameter 15 µm) as SECM probe. Ferrocenemethanol 2mM FcMeOH applied as reversible electrochemical mediator added to 0.1M NaCl electrolyte background. Where, the platinum probe monitored the current arising from the oxidation of FcMeOH. The tip was biased to 0.6 V vs. Ag/AgCl/KCl (3M) to ensure the diffusion control, as commonly practiced in amperometric feedback SECM experiments [64].

First, SECM was done on unbiased Nitinol. Via making the 2D image using meander mode data collecting pattern. Selected area of 2000 µm × 2000 µm with a scan rate of 20 µm/s was scanned. The tip-sample distance was set to 10 µm, established through making a Z-approach curve above the insulating resin. Fitting the measured negative feedback plot to

theoretical one helped to determine distance and to set the needed 10 µm value. Subsequently, the probe moved in an XY plane parallel to the sample. **Fig.** 29 A illustrates the recorded feedback current map across the unbiased Nitinol surface.

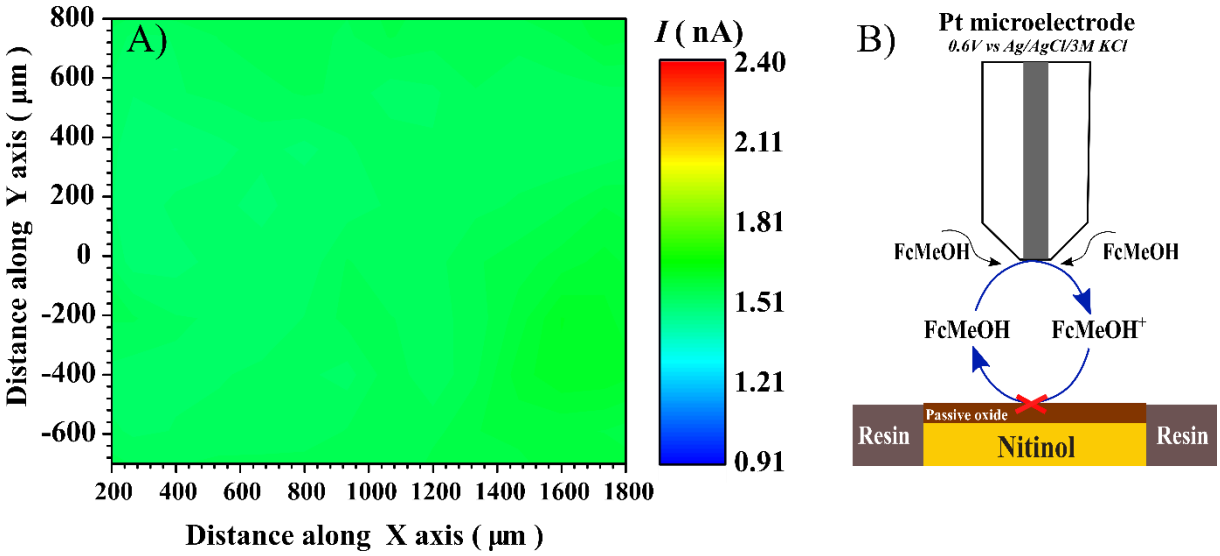

Figure 29: A - Image generated by SECM of Nitinol sample immersed for 90 min in 0.1M *NaCl solution mixed with* 2mM *FcMeOH. Tip potential: 0.6 V vs. Ag/AgCl/KCl (*3M*); scan rate: 20 µm/s; tip radius: 7.5 µm. Selected area of 2000 µm × 2000 µm was scanned. B - Negative feedback effect scheme.*

The obtained image shows a homogenous current distribution over the Nitinol sample and the surrounding resin. It implies the total sampled area exhibits negative feedback character, due to the passive oxide layer grown at the NiTi surface. The close vicinity of the sample surface hinders the diffusion of the mediator to the measuring tip that results in smaller current that is in negative feedback as shown in **Fig.** 29 B. However, when a single SECM line scan was recorded over the same vertical distance from the surface of the biased Nitinol, significant change of the current by the tip location could be seen, as it is illustrated in **Fig.** 30. It depicts various current regions. Ones have higher current than the negative feedback value monitored above the insulating resin (>1.8 nA), at one spot a moderate current value close to 1 nA have been recorded.

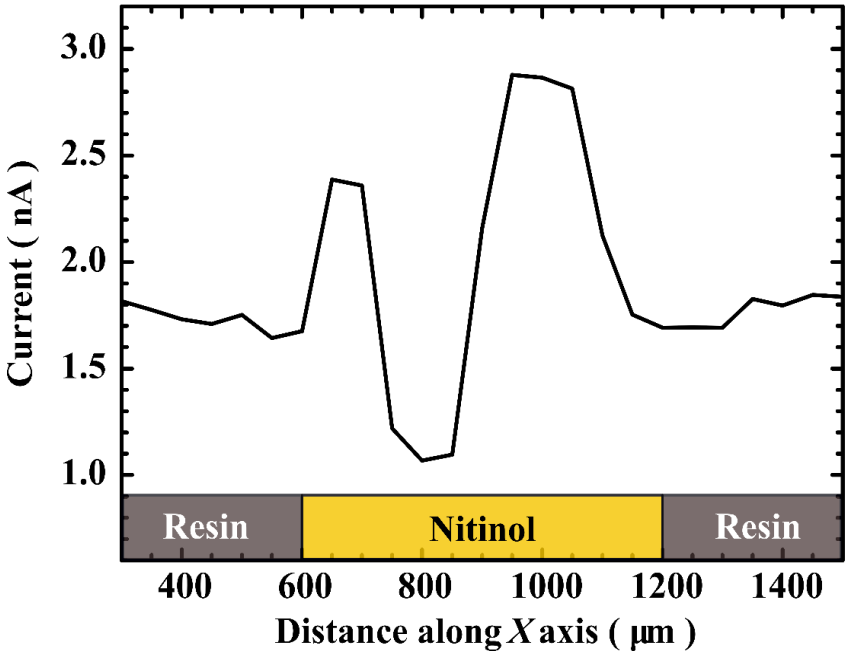

Figure 30: Line scan recorded above anodically treated Nitinol (polarized for 15 min) in 0.1M *NaCl* + 2mM *FcMeOH. Tip potential: 0.6 V vs Ag/AgCl/KCl (3M); scan rate: 20 µm /s; tip radius: 7.5 µm.*

In the sake of having a closer view, 2D image was recorded over the biased Nitinol. It is presented in **Fig.** 31. As it can be seen, a heterogeneous image has been obtained. At regions over the edges of Nitinol, the current values are mostly higher than 1.8 nA. Whereas, spot showing current values smaller than the areas over the insulating resin (negative feedback) appeared over the central regions of the Nitinol sample surface. Based on the SECM measurements we can say that 1V vs. Ag/AgCl/KCl (3M) polarization (for 15min) brakes down the integrity of the passive surface layer, and the originally homogenous Nitinol surface brakes down to regions of different activities. Some area produces positive feedback, but some show current smaller than the expected negative feedback value. These activity differences are the consequence of the localized corrosion on the Nitinol surface. Hence, anodic and cathodic spots take place on the NiTi surface.

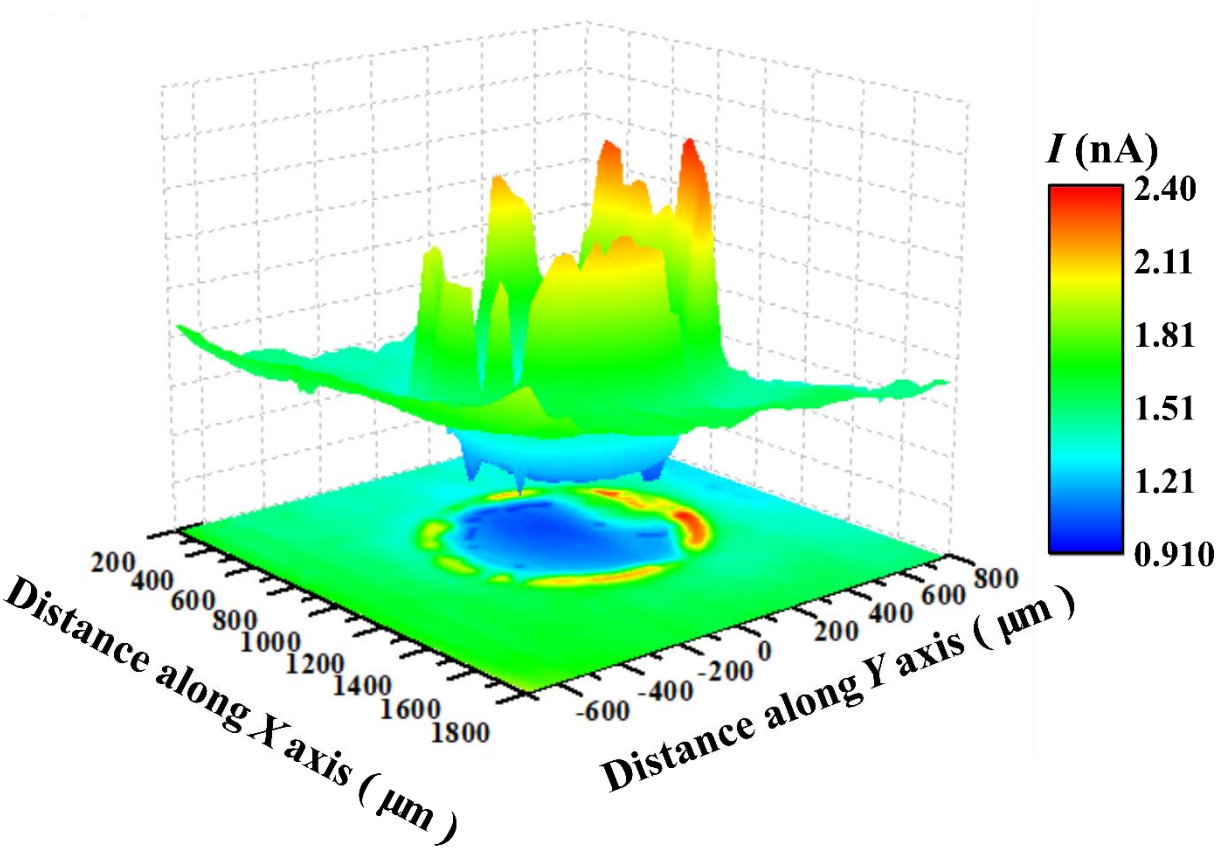

Figure 31: 2D image generated by SECM of biased Nitinol sample in 0.1M *NaCl solution mixed with* 2mM *FcMeOH. Tip potential: 0.6 V vs. Ag/AgCl/KCl (3M); scan rate: 20 µm /s; tip radius: 7.5 µm. Selected area of 2000 µm × 2000 µm was scanned.*

As seen in **Fig.** 30 and **Fig.** 31, current values smaller than the ones measured above the resin show up over certain areas of the sample surface. The negative feedback effect cannot be responsible for obtaining these small currents, since we know that over the resin complete negative feedback conditions dominate. Growing of the thickness of the passive oxide layer on the concerned metal surface can arise as a straight forward explanation [118,119]. The growth of thickness decreases the sample – tip distance gap, in this way increases the shielding that hinders the diffusion transport of mediator to the tip. However, the significant extent of growth of the oxide film thickness in micrometer scale is not the case with biased NiTi. The oxide layer thickness on surface of titanium and its alloys, would not extend over a very few nanometers, not even when it was formed by anodic polarization [120]. The possible change of its thickness comparing to the 10 µm gap won't affect noticeably the tip current. The action of so called redox-competition between the sample and the tip gives a more acceptable explanation for obtaining that small current over center of the Nitinol sample. We can assume that it is resulted by the oxidation of the FcMeOH mediator at active spots of the sample surface acting as an

anode, as it is illustrated in **Fig.** 32. The concentration of reduced form of the mediator is smaller in center sample regions because of the competition. At the sample sides the spherical diffusion carries more mediators to the tip. Obviously at the sides the competition can have less effect on the tip current than at the center. The redox competition mode often observed in SECM measurements [64].

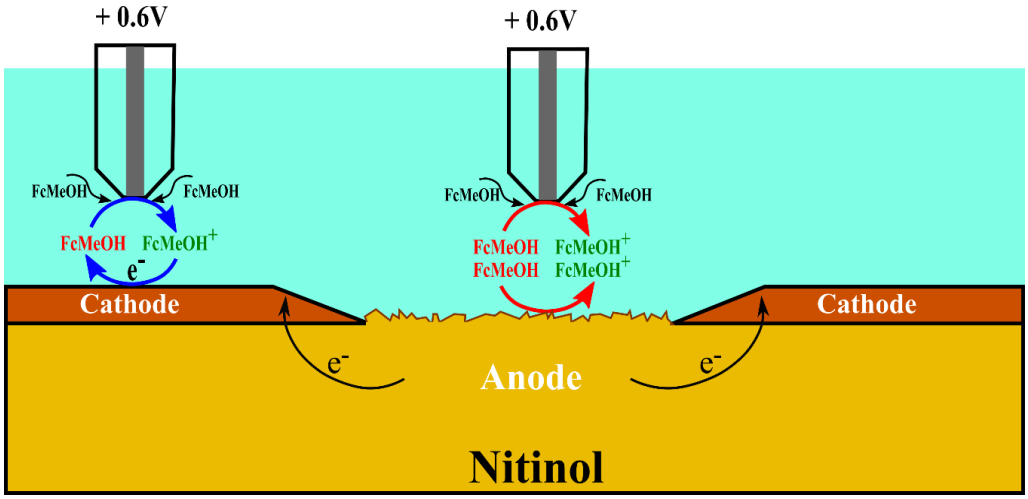

Figure 32: Scheme of the feedback phenomena occurring on the biased Nitinol. Positive feedback effect recorded above the intact area (edges of the Nitinol sample), while a redox competitive effect recorded at center where the localized corrosion is happening.

The high current values detected at the edges of the Nitinol sample displayed by the line scan **Fig.** 30 and 2D image **Fig.** 31, could be explained by the regeneration of the mediator. The electrons yielded from the anodic spots (center of Nitinol) will be consumed by the passivated area of the Nitinol sample (intact) which will act as the cathode. Therefore, the $FcMeOH^+$ generated at the tip will be reduced due to the electron donation by the passive area (intact). This is the well-known as a positive feedback effect, as illustrated in **Fig.** 33.

The experiments performed with the SECM operated in the feedback mode clearly showed that the Nitinol sample before anodic polarization maintained a homogeneous passive surface. After anodic polarization however, heterogeneous surface was obtained. Appearance of the spots with different activity, at the center and at the edges of the Nitinol sample could be seen. On these base chemical reactions, most likely corrosion processes would take place at the vicinity of Nitinol sample. At the anodic spots, the formation of the metallic cations, mostly Ti^{4+} and Ni^{2+} (**Eq.** 18 and 19) is happening. In parallel, oxygen and water reduction take place, most likely it happens typically at cathodic spots of the surface (**Eq.** 20 and 21):

$$Ti \rightleftharpoons Ti^{4+} + 4e^- \quad (18)$$

$$Ni \rightleftharpoons Ni^{2+} + 2e^- \quad (19)$$

$$2H_2O + 2e^- \rightleftharpoons \quad 2OH^- + \uparrow H_2 \quad (20)$$

$$O_2 + 2H_2O + 4e^- \rightleftharpoons \quad 4OH^- \quad (21)$$

As generally known, the SECM is a very promising in situ tool for investigation the chemical reactions above the corroding materials [64]. SECM measurements can be adopted for monitoring the hydrogen which might be evolved over the biased Nitinol (**Eq.** 20). In this approach, platinum microprobe set to 0 V vs. Ag/AgCl/KCl (3M) for amperometric detection of hydrogen is usually employed. This is known as substrate generation tip collection (SG-TC) mode of the SECM [46]. It has been broadly applied in various model systems such as the corrosion of iron and magnesium [57,58]. In my experiments local hydrogen concentration was mapped over embedded Nitinol sample soaked in 0.1M NaCl solution. The tip sample-distance established through monitoring the oxygen with a 15 µm platinum probe set to -0.6 V. Recording Z-approach curve over the insulating resin, negative feedback was observed. Afterward, the probe was set to 10 µm vertical distance from the surface then biased to 0.0 V vs. Ag/AgCl/KCl (3M). Subsequently, the tip moves parallel to the surface crossing the surface of the biased Nitinol. The SECM map recorded is presented in **Fig.** 33. As it can be seen it displays small steady current over the epoxy resin. However, above the biased Nitinol, heterogeneously distributed high current values could be detected. Over the side region the current reached a value as high as 80 pA that indicates considerable rate of hydrogen evolution. (**Eq.** 20). This finding being in tight correlation with results of feedback mode experiments revealed the presence of cathodic areas merely at the sides of the biased Nitinol.

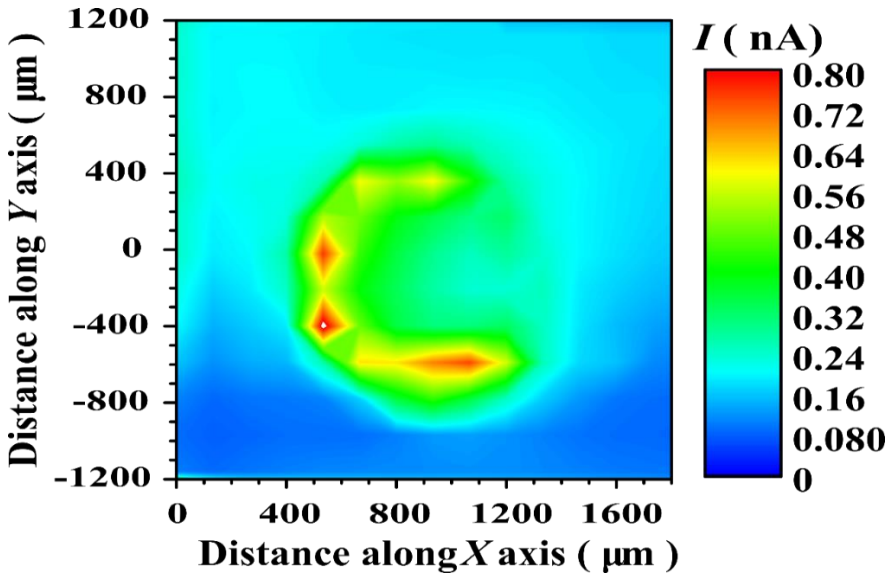

*Figure 33: Image generated by SECM of biased Nitinol sample in 0.1 M NaCl containing 2 mM FcMeOH. Tip potential: 0 V vs. Ag/AgCl/KCl (*3M*); scan rate: 20 µm /s; tip radius: 7.5 µm. Selected area of 2000 µm × 2000µm was scanned.*

Other experiment using SECM operating in potentiometric mode was carried out. Antimony microelectrode was employed as SECM probe for monitoring the pH distribution in the solution adjacent to the biased Nitinol surface. In this work line scans were recorded along 4000 µm long tip travel distance crossing the surface of the biased Nitinol sample exposed to 0.1M NaCl solution. The tip-sample distance was set to 20 µm. It was adjusted by recording a Z-approach curve above the resin by operating the Sb microprobe in amperometric mode. The Sb probe was polarized to -0.6 V vs. Ag/AgCl/KCl (3M) in this way detecting the local concentration of the oxygen dissolved in the electrolyte. Negative feedback was observed, then the tip was retracted by 20 µm from the surface. In recording the pH – distance line scan, the Sb probe crossed the center of the biased Nitinol with 10 µm/s scan rate, measuring the potential versus Ag/AgCl/KCl (3M) reference electrode. **Fig.** 34, presents a pH – distance plot obtained in performing the line scan. Similar to the pH of the bulk solution a pH value of 6.5 was sensed over the insulating resin, while a value as low as 5.7 was detected at the vicinity of Nitinol. On the other hand, a slight alkalization could be observed at the edge of the Nitinol as it is shown at by the inset (**Fig.** 34). That is resulted from the hydroxide ions yielded from the cathodic reactions (**Eqs.** 20-21).

The acidification observed at the vicinity of Nitinol can be explained by considering that from anodic areas of the corroding sample surface cations are released. The hydrolysis of them, shown by (**Eq.** 22) generates the decrease of local pH observed [84]:

$$M^{n+} + xH_2O \rightleftharpoons M(OH)_x^{(n-x)+} + xH^+ \quad (22)$$

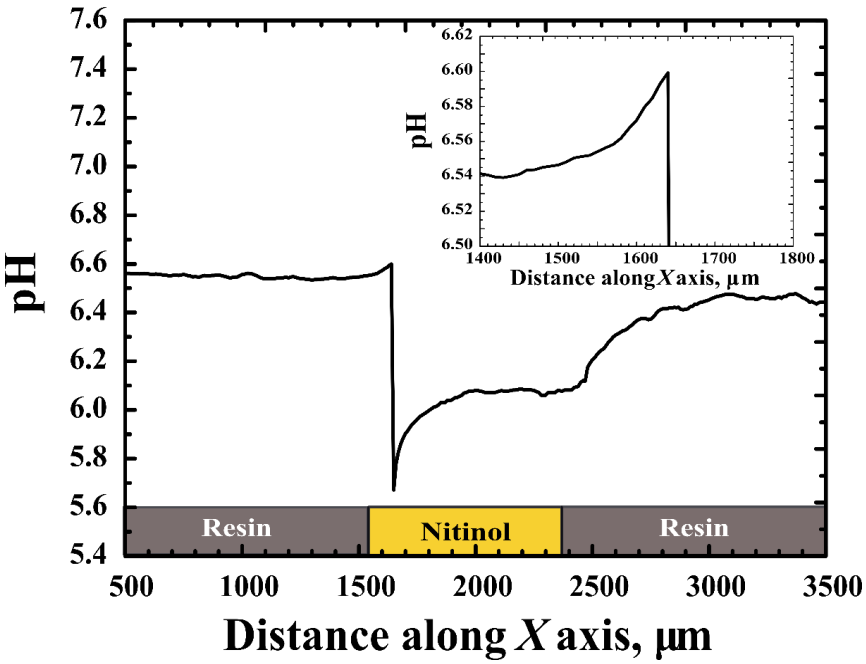

Figure 34: Line scan recorded along 4000 µm tip travel distance above the biased Nitinol in 0.1M *NaCl solution using antimony microprobe. Scan rate: 10 µm /s; tip radius: 15 µm.*

Distinctly, the acidification detected at the vicinity of Nitinol was resulted by the hydrolysis reaction of released cations. As it has been mentioned previously, Ni^{2+} and Ti^{4+} are assumed being the cations released from the metal surface. Accordingly $Ni(OH)_2$ and $Ti(OH)_4$ can be regarded as the stable metal hydroxides involved [86,121]. Comparing their solubility products (K_{sp}) in aqueous solution that for $Ni(OH)_2$ and $Ti(OH)_4$ are $5.7 \cdot 10^{-16}$ and $7.24 \cdot 10^{-30}$, respectively [86,122], we can say that the titanium hydroxide has quite small K_{sp} compare to that of the nickel. This is in agreement with the previous reports that indicated Ni^{2+} ions are the species favorably released from the corroding Nitinol surfaces [35]. Ruhlig et al. [54] came to the same conclusion evaluating their experimental finding in which they detected the release of Ni^{2+} ions from activated NiTi using stripping mode SECM. A remarkable transient peak discerned clearly above the anodic area, appeared immediately right after the probe crossed the cathodic spot (Nitinol edge). The pH reached a value of 5.6 afterward it fast risen to 6.1. This relatively large

change at a small distance could be resulted by the high dissolution rate of the metal since the anodic and cathodic spots were adjacent to each other. Similar phenomena have been observed with Mg/steel galvanic couple [123].

Eventually, **Fig.** 35 illustrates a sketch of the corrosion mechanisms of the degradable Nitinol, via considering the findings obtained with EIS and SECM in amperometric and potentiometric mode.

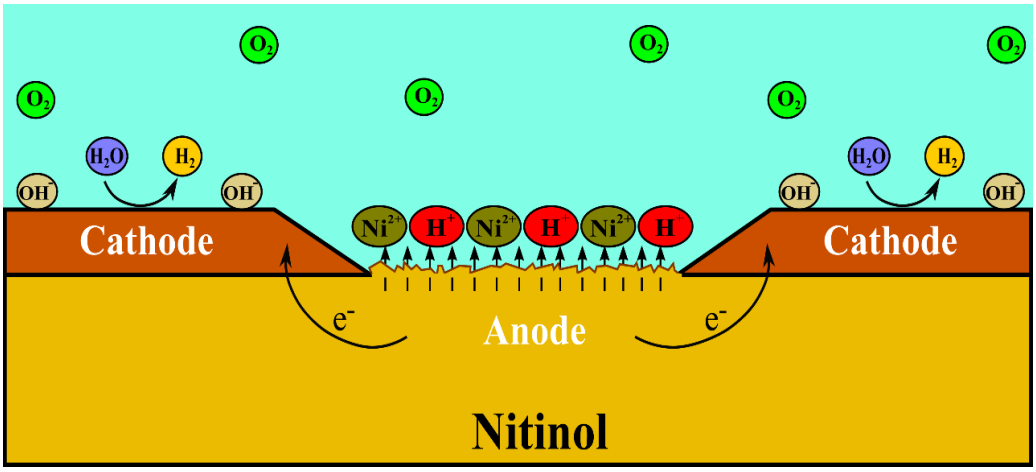

Figure 35: Scheme summarizes the corrosion reactions on corroded Nitinol surface.

Chapter 4 - Acidic medium effect on the electrochemical behavior of the Nitinol biomaterial

III.4.1. Resume

As it was mentioned earlier in some conditions the pH in certain areas of the human body can be as low as 3. In the surroundings of dental root implants this can be expected to happen. Therefore, the effect of acidic media on corrosion resistance of implantable devices made of Nitinol is of great importance. In my experimental work EIS, SECM, and AAS techniques were used for investigation this practically important feature.

III.4.2. Examination of the acidic medium impact on the corrosion resistance of Nitinol using EIS

The electrochemical impedance spectroscopy (EIS) well can be employed for measuring the resistance or studying its change upon different effects. The change of resistance can be considered as character showing the change of corrosion resistance. In EIS experiments the behavior of Nitinol sample in neutral and acidic media was compared.

First, the impedance spectrum was measured expositing the Nitinol to neutral 0.1M NaCl solution. Subsequently, it was recorded right after replacing the neutral NaCl with the acidic one. **Fig.** 36 shows the impedance spectra recorded in the form of Nyquist and Bode diagrams. All the EIS spectra were done under open circuit potential conditions.

EIS spectra on the Bode form is shown in **Fig.** 36 B. As it can be seen at high frequencies (10^4 to 10^5 Hz), the impedance is almost independent of the frequency. This is typical response character that corresponds to the resistance of the electrolyte. Due to the difference of the conductivity of the testing electrolytes a phase angle of 9 and 4° were recorded in neutral and in acidic NaCl solutions, respectively. In the medium frequency region (from 1 to $10^{3.5}$ Hz), the plot has a linear section with a slope of about -1, and phase angle of near to 80°. This is commonly attributed to the capacitive behavior of the passive oxide films [88]. Similarly, it was also observed for other titanium alloys [87]. Whereas at low frequency range ($1/s \geq 10^{-1}$Hz), the plot manifests a difference of the phase angles which are 46 and 39° recorded in the neutral and acidic medium, respectively. It implies the superior protection of the passive film formed on Nitinol in the neutral NaCl. The recorded Bode phase plots, clearly manifest two-time constants, one in the high-frequency- and the other one in the low-frequency range. In the high-

frequency range, the time constant indicates the charge transfer reaction occurring in the film-electrolyte interface while in the low-frequency it reflects the properties of the passive layer.

As it is clearly shown in **Fig.** 36 A, all the Nyquist plots can be characterized by a wide depressed queasy semicircle. The diameter of Nyquist plot decreases after interchanging the neutral electrolyte with the acidic one. It indicates a noble electrochemical behavior of the passive oxide layer on Nitinol exposed to neutral NaCl solution.

Based on the above results, the experimental impedance spectra were analyzed using the equivalent circuit seen in the inset in **Fig.** 36 A. The parameter R_{ct} and Q_{dl} represent the properties of the reactions at Nitinol passive oxide/electrolyte interface, the charge transfer resistance and the double layer capacitance, respectively. Whereas, R_{ox} and Q_{ox} stand for the properties of the passive Nitinol oxide layer, namely for the resistance and for the capacitance of the native, barrier oxide film [101]. In the sake of fitting the impedance spectra, the ideal pure capacitance was replaced by the constant phase angle element (CPE) to account the non-ideal behavior which is related to a non-equilibrium current distribution due to surface roughness and surface inhomogeneity [79]. When Nitinol was soaked in neutral NaCl solution, the passive film resistance was 36.04 $k\Omega \cdot cm^2$. Whereas a drop of the oxide film resistance to 28.24 $k\Omega \cdot cm^2$ could be observed right after the immersion of Nitinol to acidic NaCl solution. This intimates the partial dissolution of the passive film.

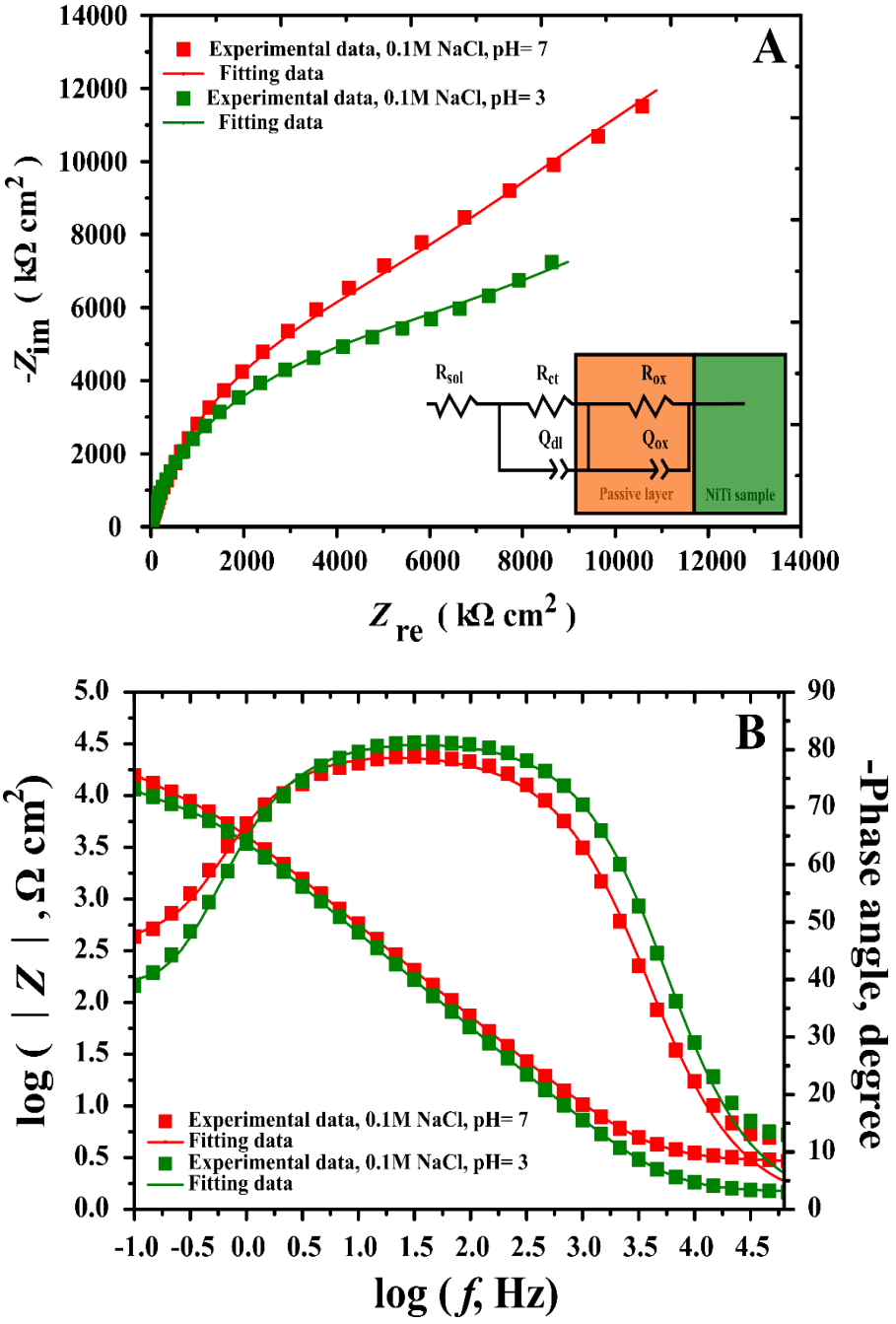

Figure 36: Electrochemical impedance spectra of Nitinol sample in Nyquist (A) and in Bode plots (B). The red symbol corresponds to the EIS measured after exposing the Nitinol sample to 0.1M *NaCl for 90 min, while the one with dark green color was taken immediately right after replacing the neutral* 0.1M *NaCl with acidic one (pH=3). The inset shows the EEC used for fitting the experimental data. The experiments were performed at the frequency of 100 kHz - 0.1 Hz and an alternating sinusoidal potential, with amplitude of 10 mV was applied.*

III.4.3. Examination of the acidic medium impact on the reactivity of Nitinol using SECM

III.4.3.1. SECM approach curves measurement

In the sake of examining the stability of the passive film on the Nitinol biomaterial, SECM operated in the feedback mode was used. In this task consecutives Z-approach curves were recorded after different periods of time. Platinum UME was used as SECM probe and 2mM FcMeOH was employed as redox mediator. The Pt UME was set to a constant potential of 0.6 V vs. Ag/AgCl/KCl (3M) to ensure the diffusion-controlled amperometric oxidation of the FcMeOH. Before staring the SECM measurements the embedded Nitinol sample surface was freshly polished, and immersed in 0.1 M NaCl for 90 min. During this time the formation of the native oxide film was expected. First approach curve was recorded over the Nitinol sample in the neutral solution. After the neutral 0.1M NaCl solution was replaced with the acidic one (pH = 3), and then a series of Z-approach curves were recorded rigorously controlling the length of time between the solution change and the individual approach curve recording time In order to take the approach curves, the platinum probe was located 300 µm above the center of the Nitinol. Then moved vertically down with scan rate of 10 µm/s, meanwhile the current–distance dependence was recorded

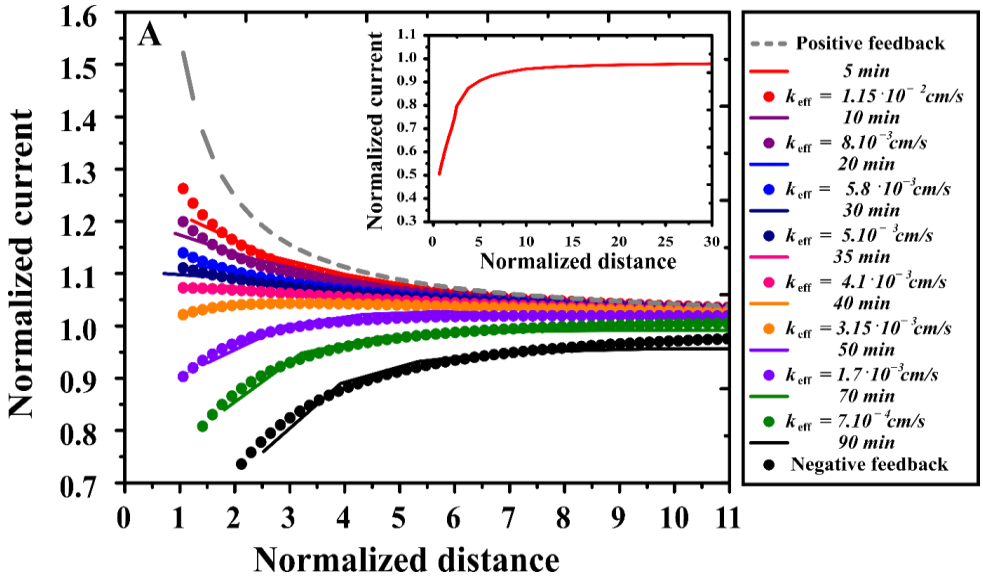

Figure 37: Z-approach curves recorded over Nitinol sample in neutral 0.1M *NaCl (shown in the inset) and in acidic (pH=3.0)* 0.1M *NaCl solution. The inset shows the different different length of times between the time of introducing the acidic solution and the time of recording the individual Z -approach curve. Tip potential 0.6 V vs. Ag/AgCl/KCl (3M), scan rate 10 µm/s.*

The inset in **Fig.** 37 shows the recorded Z-approach curve over the Nitinol sample surface that was immersed in neutral 0.1M NaCl electrolyte. It displays intensive negative feedback character. This implies that the Nitinol surface is protected with a passive oxide film that hinders the reduction of the $FcMeOH^+$ species generated at Pt UME (**Fig.** 38 A). Nevertheless, after replacing the neutral testing electrolyte with the acidic one, the recorded Z-approach curves at different periods show a dramatic change in the feedback character, as shown in **Fig.** 37 (solid lines). As it can be seen, when the SECM tip is a long way from the Nitinol surface, the current depends neither on the soaking time nor on the distance. However, a significant change could be seen at normalized distances below 3. After 5 min of exposure of the Nitinol surface in the acidic 0.1M NaCl intensive positive feedback character could be observed (red solid line).

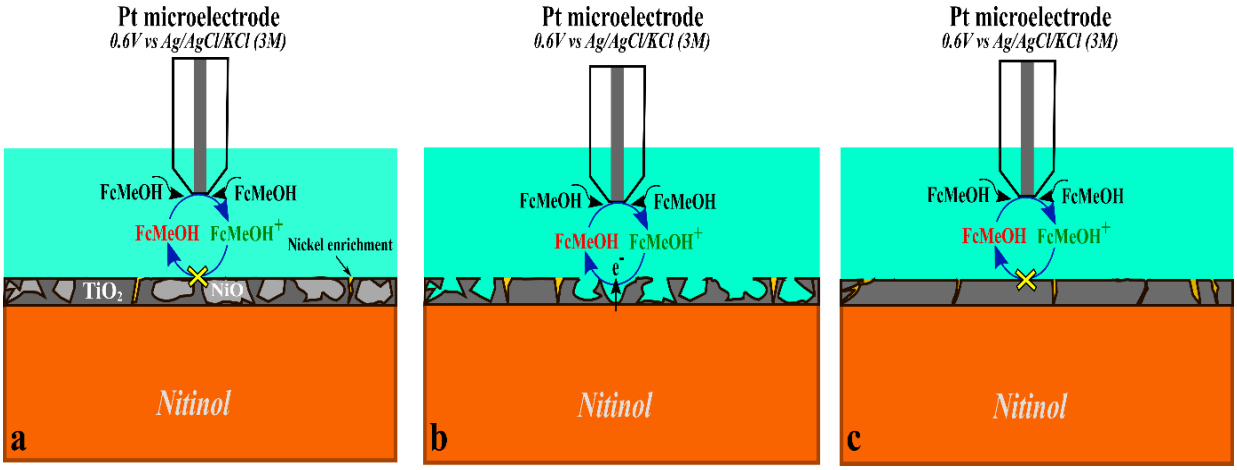

Figure 38: Schemes showing the phenomena occurring on Nitinol surface in different times and conditions. A - negative feedback recorded over Nitinol sample soaked in neutral 0.1M *NaCl, B - positive feedback recorded at the early immersion of Nitinol to acidic* 0.1M *NaCl. C - negative feedback recorded after a longer immersion time in the acidic* 0.1M *NaCl electrolyte.*

The shape of the approach curve recorded for Nitinol sample after short time exposition to acidic media is close to the theoretical approach curve calculated for a pure conductive surface (dashed grey line). This indicated the regeneration of the FcMeOH (**Fig.** 38 B). Nevertheless, the positive feedback character is gradually decreasing as the time of interaction of the Nitinol surface with the acidic medium prolonged. It implies that the regeneration of the mediator gets slower with increase of exposure time, that might be due to thickening of a newly formed of passive oxide layer that hinders the regeneration of the FcMeOH. A pure negative feedback character could be seen after 90 min of immersion. It indicates that the regeneration of the FcMeOH completely blocked by the newly developed passive oxide layer (**Fig.** 38 C). These occurrences could be explained by considering the following; the Nitinol surface is protected

by a spontaneously formed passive film composed of TiO_2 and NiO, as it was stated previously in [113]. Lately, Ding et al. [124]. investigated the Pourbaix diagrams of NiTi. It showed that in cases pH > 6, TiO_2 and NiO are stable. At pH = 3.0, however, the NiO dissolves and Ni^{2+} ions are discharged, whereas the titanium dioxide resides steadily [124]. This results in the transpassivation of the passive surface film with the formation of small pits [125]. Which will generate the electron transfer reaction between the Nitinol and the mediator. This would explain the positive feedback observed earlier. Since titanium is one of the main elements of the Nitinol material that has a very negative standard redox potential ($E^{\circ}_{Ti^{2+}/Ti}$= -1.63 V/SHE). It will lead to the formation of the passive titanium dioxide by its reaction with water or oxygen present in the surrounding environment [85]. Hence, the transformation in the feedback from positive to negative observed when Nitinol was exposed in the acidic media is the outcome of the repassivation process via the development of the passive titanium dioxide film on the pits.

In the aim to have a closer view on the action of the passive surface layer at the Nitinol surface, the effective heterogeneous rate constant (k_{eff}) of the mediator regenerating reaction was quantified employing the method demonstrated by Cornut and Lefrou [49]. In this way, the relationship between the values of the effective heterogeneous rate constant and the time interval from the time of introducing the acidic 0.1 M NaCl to the electrochemical cell and the time of recording the Z-approach curve (Δt) can be obtained. **Fig.** 39 illustrates the relationship between the k_{eff} and time (Δt). It can be supposed that the decay of k_{eff} with time signifies the rate of the growth of the passive layer on the Nitinol surface. At the initial moment of the immersion, the k_{eff} declines swiftly, while after about 50 min of exposure time a moderate decline of the k_{eff} is seen that eventually leads to k_{eff} = 0 at 90 min.

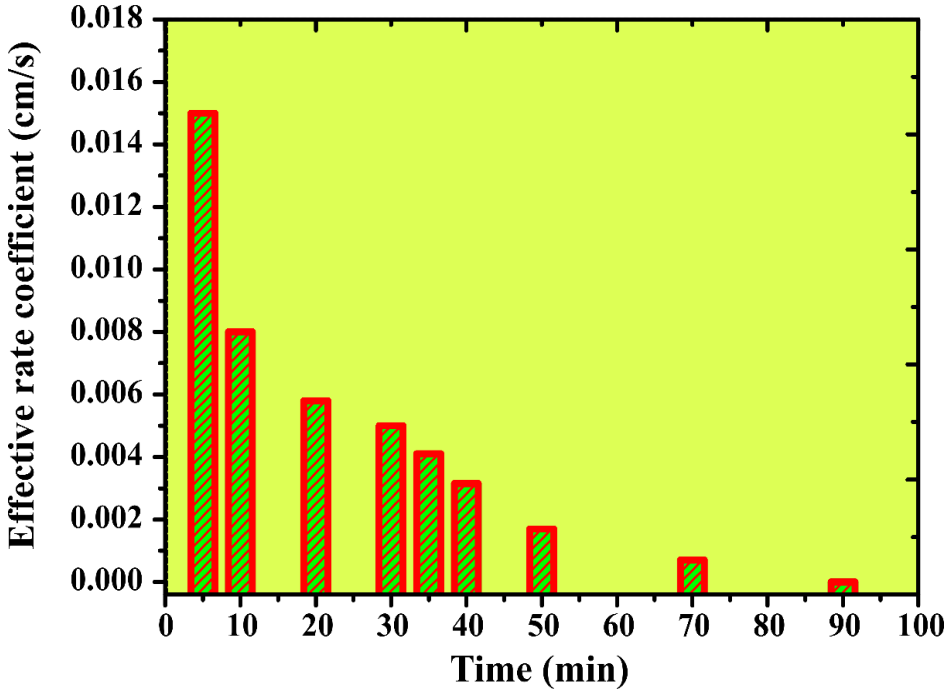

Figure 39: Variation of the calculated effective rate coefficient with time.

The findings with the experimental Z-approach curves showed that the passive oxide film on Nitinol biomaterial breaks up shortly after its interaction with acidic 0.1M NaCl, while as the Nitinol soaked in the acidic medium for a long period it repassivates by forming a new compact passive film.

III.4.3.2. Cyclic voltammetry measurements

Fig. 40 illustrates the CVs obtained after various periods. It can be seen that the CV recorded in neutral 0.1M NaCl shows a small limiting tip current value that is about 4.08 (CV is shown in red). While the first CV recorded immediately after replacing the neutral solution with the acidic one shows a leap in the tip current up to 6.5 nA (CV shown in black). This implies the increases in the concentration of FcMeOH at the vicinity of the Nitinol surface. This experimental finding is also in agreement with the Z-approach curve experiment showing that the surface of the Nitinol gets activated right after its interaction with the acidic medium. That leads to the reduction of the $FcMeOH^+$ generated at the UME to FcMeOH due to electron donation from the adjacent active Nitinol surface, as it is shown in the inset in **Fig.** 40.

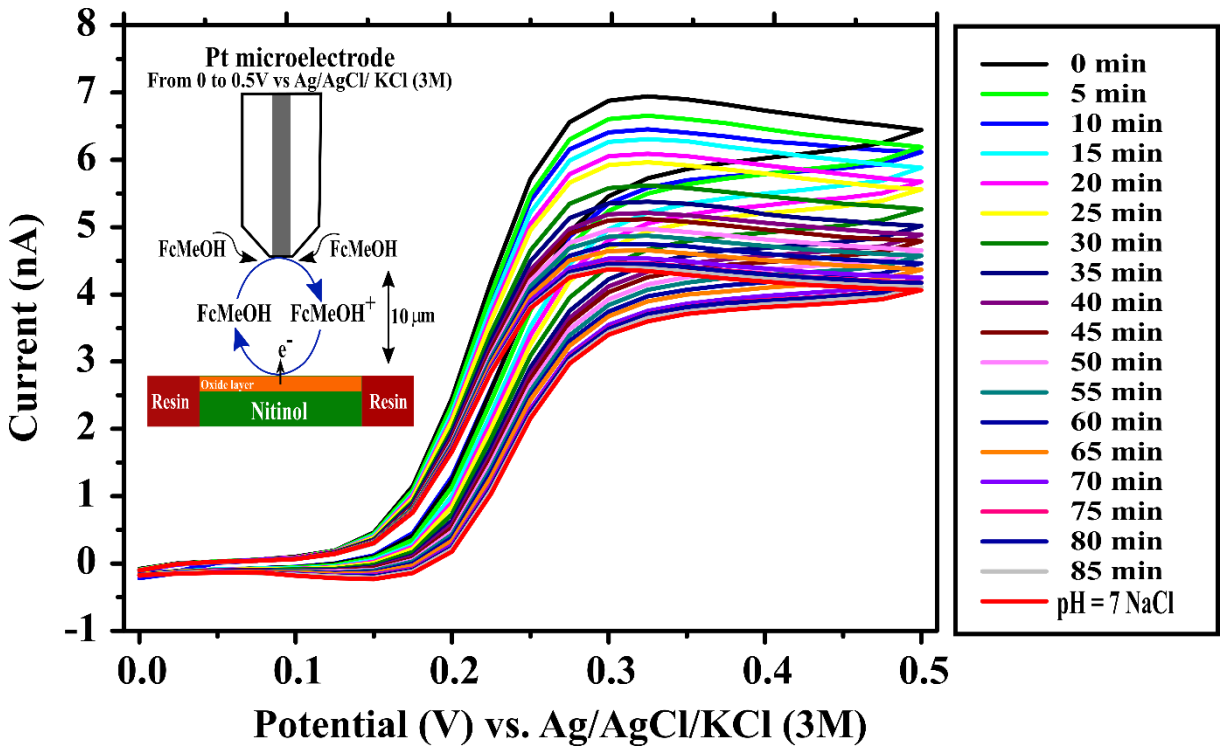

Figure 40: Cyclic voltammograms recorded on platinum micro disk electrode above the Nitinol sample. The tip potential 0.6 V vs. Ag/AgCl/KCl (3M); tip-sample distance: 10 µm, potential range 0 – 0.5 vs. Ag/AgCl/KCl (3M); scan rate 25 mV/s. The inset shows the different length of times between the time of introducing the acidic 0.1M *NaCl into the electrochemical cell and the time of recording of the marked CV.*

Fig. 41 shows the limiting tip current plotted versus time of exposure in acidic solution. A progressive decrease in the magnitude of the tip current with time can be seen. This also proves the occurrence of the self-healing process that results in the decrease of the tip current by hindering the regeneration of the mediator. The results of the CV experiments show that about 85 min is the time required for the formation of a compact passive film on the Nitinol surface immersed in acidic 0.1 M NaCl. The plot of decreasing current values shown in **Fig.** 41 can be approximated with two linear segments with different slopes. The first segment is from 0 up to 40 min while the other one takes place from 40 to 80 min. Their slopes are -0.039 and -0.019 nA/min respectively. This suggests that the self-healing process of the passive layer on Nitinol surface might be controlled by two different steps. The initial step most likely is a fast-chemical reaction in which the elemental metal cations at the exposed surface react with species being in the electrolyte right at the interface. While the modest slope of the second segment suggests the decelerate outgrowth of the passive film in a process in which diffusion transport might have important role [126].

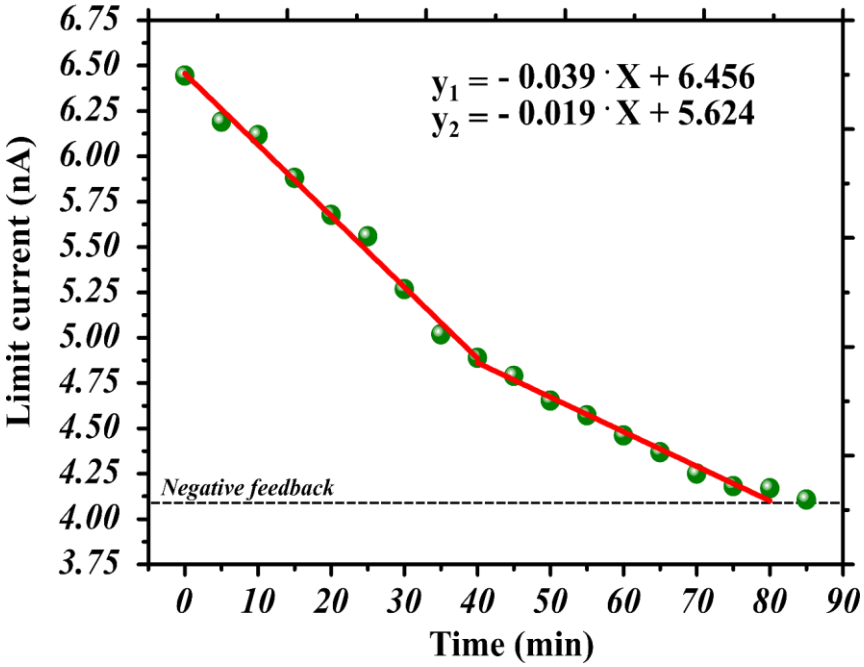

Figure 41: Variation of the limiting current as function of time.

III.4.4. Detection of nickel and titanium releases from Nitinol using AAS

Our experiments carried out to study the effect of exposition of Nitinol surface to corroding media of 0.1M NaCl solution showed an interesting behavior. The surface coated with a spontaneously formed passive layer got activated upon short time acidic exposure. After keeping Nitinol in the same acidic solution however, repassivation of the surface could be observed. In order to get information about the processes involved in this outcome it was interesting to see what changes happened in composition of the corrosive soaking solution. It was anticipated that metal ions could be released when the Nitinol surface is in contact with an acidic aqueous solution. Therefore, the concentration of the ions having roles in these processes was measured with atomic absorption spectroscopy in different times of exposition.

First, Nitinol wire that has a surface area of 0.53 cm^2 was soaked in 10 mL neutral 0.1M NaCl solution for 10 min. It was obtained that the concentrations of titanium and nickel ions in this solution were 15 ppb and 150 ppb, respectively. The high concentration of nickel ions detected is in agreement with expectations and findings [107]. That was suggested to be discharged from the defects. Because of the toxicity nickel ions, extensive research still has been carried on for improving and developing different surface pretreatment procedure that decreases the discharge of nickel ions from Nitinol surface [35]. While the low concentration of titanium ions can be attributed to the formation of pits due to the presence of aggressively corrosive chloride ions [125].

In order to test the stability of Nitinol in acidic media, the sample wire that was exposed before to the neutral solution was soaked sequentially in 10 mL acidic 0.1M NaCl (pH = 3.0) solutions kept in different vials for 10 minutes. **Fig.** 42 illustrates the concentrations of nickel and titanium ions measured in different vials as a function of the total immersion time. Where the blue and red symbols correspond to titanium and nickel respectively. As can be seen, after exposing the Nitinol to acidic NaCl solution for 10 min, concentration of 15 ppb of titanium ions was obtained. The value obtained is almost the same as the one measured in neutral soaking solution. Nevertheless, a high concentration of nickel ions was observed in the same solution. The measured concentration value of 580 ppb is almost four times higher than the one measured for the same time in the neutral solution. For explaining these findings we need to consider that the Nitinol surface is mostly protected by a film composed with TiO_2 and NiO, as reported previously [124]. Taking into account the value of the solubility products (K_{sp}) of $Ti(OH)_4$, which is $7.24 \cdot 10^{-30}$ in aqueous solution [86], the solubility of Ti^{4+} is regarded be smaller than of

Ni^{2+}. Consequently, NiO is suspected to get dissolved in aggressive medium [127]. Hence, the large amount of Ni^{2+} ions observed could be the outcome of dissolution of NiO followed by the release of Ni^{2+} from the nickel content of the Nitinol material through to the following reactions [128]:

$$NiO + 2H^{+} \rightarrow Ni^{2+} + H_2O \quad (23)$$

$$Ni \rightarrow Ni^{2+} + 2e^{-} \quad (24)$$

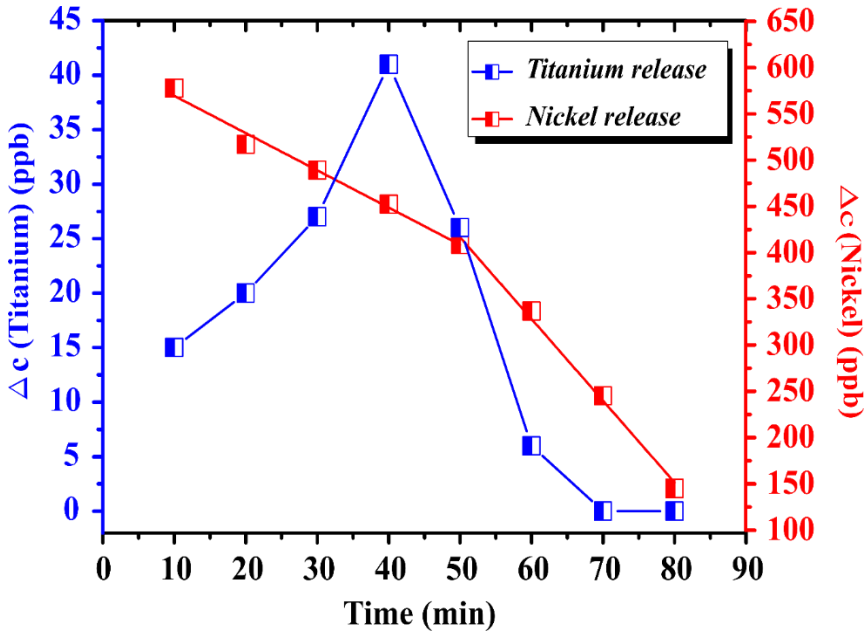

Figure 42: Concentration of nickel (red symbols) and titanium (blue symbols) measured in different vials using AAS. The concentration is plotted against the total exposition time. 10 min considered as the time of immersion at each vial (8 vials).

On the other hand, in consequent vials a progressive decrease in nickel concentration was observed, as it is shown in **Fig.** 42. This suggests that after the initial time the dissolution rate of nickel decreases most likely because of the progress of a passive oxide film formation on the Nitinol surface. Additionally, the rise in titanium concentration with time also supports the development of a passive titanium dioxide layer. As clearly could be seen after 50 min of exposure a drop in the concentration of nickel ions is observed this implies also the formation of a compact passive film.

Based on the experimental findings described above, we can estimate the nature of reactions involved in yielding the unusual changing of surface character that was observed exposing the Nitinol sample to 0.1M, pH=3.0 NaCl solution. After immersing the metal in the solution, the integrity of the surface film that contains mixed oxides of Ti and Ni brakes up. This process is fast and it results in activation of the surface as well as higher amount of Ni and traces of Ti ions release into the solution. As the immersion time increases however, surface repassivation takes place. This reaction is slower, might has two different time constant and during this less Ni and some Ti ions are released into the solution. We can suppose that the newly formed surface layer is compact and is built of TiO_2. The first step in the process can be the oxidation of Ti^0 after the partial dissolution of the native surface film as it is shown by (**Eq.** 25):

$$Ti \rightarrow Ti^{4+} + 4e^- \quad (25)$$

The electrons left the oxidation process (**Eq.** 25) must be consumed by the oxidants present in the electrolyte. Most likely they are oxygen or water, because their reaction with titanium is thermodynamically favored. However, the titanium cation is not steady in an aqueous electrolyte, hydrolysis reaction will take place toward forming the titanium hydroxides, as shown in (**Eqs.** 26-28) [86]. While, the hydrogen ions yielded from the hydrolysis reactions (**Eqs.** 26-28) might lead to a decrease of the pH in the close locality of the Nitinol. Similarly, as it was reported in chapter 1 about the self-healing of the mechanical damaged titanium G4 surface. It can be expected that same reactions might be happening during the repassivation of the Nitinol surface:

$$Ti^{4+} + 2H_2O \rightarrow Ti(OH)_2^{2+} + 2H^+ \quad (26)$$

$$Ti(OH)_2^{2+} + H_2O \rightarrow Ti(OH)_3^{+} + H^+ \quad (27)$$

$$Ti(OH)_3^{+} + H_2O \rightarrow Ti(OH)_4 + H^+ \quad (28)$$

Fovet et al. [86] studied the stability of Ti (IV) in different pH values. Based on their results at pH = 3 the $Ti(OH)_4$ is the stable hydroxide form. Hence, the titanium dioxide film could be formed through the dehydration of $Ti(OH)_4$ via the following reaction:

$$Ti(OH)_4 \rightarrow TiO_2 + 2H_2O \quad (29)$$

These experimental findings obtained with EIS, AAS, and SECM could elucidate the work stated by Huang et al. [111]. In their work, different Nitinol wires were tested in different pH values (2.5, 3.75, 5 and 6.25). They found that at higher pH than 5 there was no release of

titanium, whereas at acidic pH, titanium ions were detected accompanied by a significant release of nickel ions. The nickel ions detected might be mainly the consequence of the dissolution of the native passive film, whereas the titanium ions could be formed during the repassivation of the Nitinol surface film.

Fig. 43 summarizes the corrosion process of the Nitinol surface soaked to neutral and acidic 0.1M NaCl.

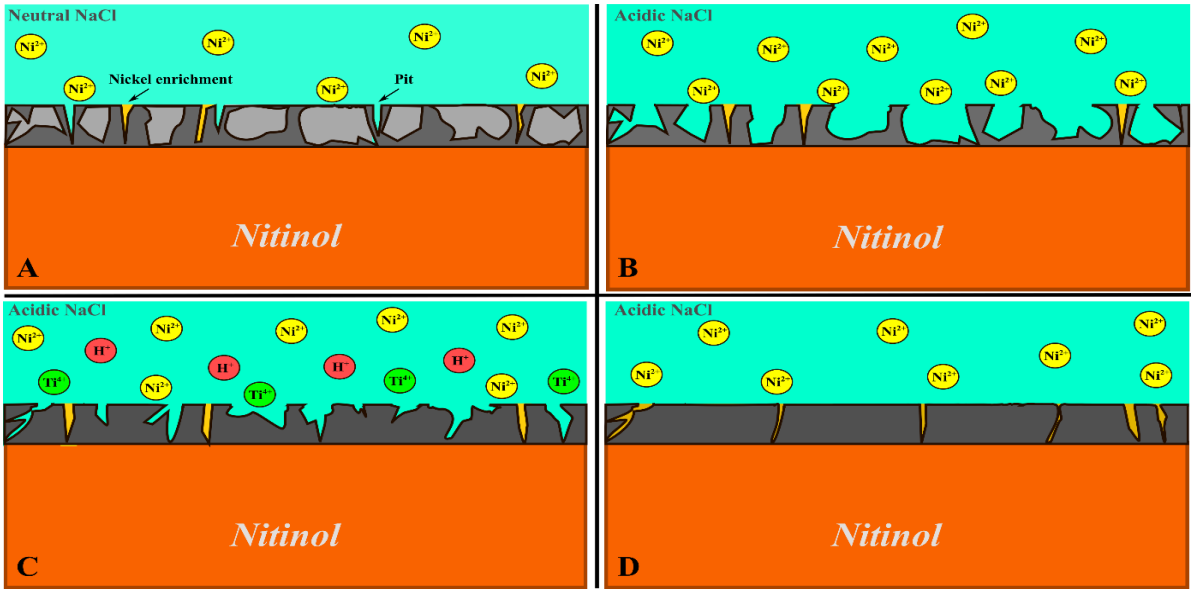

Figure 43: Scheme resume the corrosion process at the Nitinol surface in the neutral and acidic 0.1M *NaCl.* ***A*** *- formation of passive NiO and* TiO_2 ***B*** *- Dissolution of the NiO in the acidic* 0.1M *NaCl* ***C*** *- self-healing of the titanium dioxide in acidic* 0.1M *NaCl* ***D****- Formation of compact passive titanium dioxide layer.*

Thesis points

The work presented in my thesis devoted to the electrochemical characterization of the titanium biomaterials using scanning electrochemical microscopy. Aimed to understand their electrochemical properties and draw attention to new transient events that must be considered for their application. The obtained results are summarized below:

- Thesis point 1:

The mechanical impact on the electrochemical reactivity of the titanium G4 implant surface has been investigated using SECM operated in amperometric mode. It was found that the kinetic of the self-healing of the protective film on the titanium surface is a time dependent process, several minutes needed for the formation of a compact film.

- Thesis point 2:

The corrosion mechanisms of the passive titanium dioxide were studied using the SECM in potentiometric mode. Antimony microprobe was used as SECM probe, while acidification was sensed at the vicinity of the mechanical damaged titanium G4 implant surface. It indicates the discharge of the titanium cations from the implant surface. Therefore, care must be taken for minimizing the time of the self-healing process because longer healing time would enhance the corrosion of the implanted material that causes a discharge of hazardous metal cations. That may lead to reduce the mechanical propertied of the implant.

- Thesis point 3:

Cathodic polarization on the electrochemical properties of the passive film formed on commercial pure titanium has been studied. Using SECM operated in the amperometric mode it was demonstrated that the anticorrosion property of the protective film loses with the increase of the cathodic polarization. That was proved by the occurrence of the electron transfer reaction at the titanium oxide/electrolyte interface. This can arise as a straight forward explanation of the decrease of the viability of the biological cells under cathodic polarization reported in the literature.

- Thesis point 4:

The change of the titanium behavior from passive to conductive under cathodic polarization was explained by the hydrogen intercalation into the titanium oxide film, hydrogen acting as a doping element.

- Thesis point 5:

The corrosion of the anodically treated Nitinol was examined. Using SECM in the amperometric mode, anodic and cathodic sports were visualized. While redox competitive effect was observed in the anodic areas, on the other hand, positive feedback occurs at the cathodic spots. Furthermore, employing antimony as SECM tip acidification and alkalization processes were detected in the anodic and cathodic areas, respectively.

- Thesis point 6:

The effect of acidic medium on the electrochemical properties of the Nitinol surface was investigated. It was demonstrated that at pH close to the normal physiological condition that is about 7, the spontaneously formed passive film on Nitinol stays in passive state. However, at pH-s adjacent to inflammatory condition that is about pH=3, the Nitinol passive film breaks down. It was proved by the occurrence of the electron transfer reaction between Nitinol and the surrounding environment. That is due to the formation of pits on the surface caused by the nickel oxide dissolution. It was confirmed too by the significant discharge of hazardous nickel ions soon after exposure of Nitinol to the acidic solution. Furthermore, it was shown that tens of minutes are required for the total repassivation of the Nitinol upon the acidic attack. Hence, the mitigate of the nickel amount on the Nitinol surface regarded crucial.

References

[1] S. Griza, D.H.G. de Souza Sá, W.W. Batista, J.C.G. de Blas, L.C. Pereira, Microstructure and mechanical properties of hot rolled TiNbSn alloys, Mater. Des. 56 (2014) 200–208.

[2] D.F. Williams, Biocompatibility of clinical implant materials, in: D.F. Williams (Ed.), Biocompatibility of Clinical Impact Materials, vol. 1, CRC Press, Boca Raton, FL, 1981, p. 9.

[3] M. Geetha, A.K. Singh, R. Asokamani, A.K. Gogia, Ti based biomaterials, the ultimate choice for orthopaedic implants – A review, Prog. Mater. Sci. 54 (2009) 397-425.

[4] C. Veiga, J.P.Davim, A.J.R. Loureiro, Properties and applications of titanium alloys: a brief review, Rev. Adv. Mater. Sci, 32 (2012) 14-34.

[5] F.H. Froes, M. Qian. Titaniumin medical and dental applications, p. 3, Woodhead Publishing, United Kingdom (2018).

[6] M.D. Brunette, P.T. engvall, M. Textor, P. Thomsen, Titanium in medicine: material science, surface science, engineering, biological responses, and medical applications. 2001, New York: Springer-Verlag Berlin Heidelberg.

[7] D. F. Williams: 'The Williams dictionary of biomaterials', Liverpool University Press, 1999.

[8] J. Géringer. B. Boyer, K. Kim, Tribocorrosion of Passive Metals and Coatings: Fretting corrosion in biomedical implants, Woodhead Publishing. (2011) 401-423.

[9] Z-S. Tao, W-S. Zhou, X-W. He, W. Liu, B-L. Bai, Q. Zhou, Z-L. Huang, K-K. Tu, H. Li, T. Sun, Y-X. Lv, W. Cui, L. Yan, A comparative study of zinc, magnesium, strontium-incorporated hydroxyapatite-coated titanium implants for osseointegration of osteopenic rats, Mater. Sci. Eng. C 62 (2016) 226-232.

[10] O. Addison, A.J. Davenport, R.J. Newport, S. Kalra, M. Monir, J.F. Mosselmans, D. Proops, R.A. Martin, Do 'passive' medical titanium surfaces deteriorate in service in the absence of wear?, J. R. Soc. Interface. 9 (2012) 3161-3164.

[11] X. Chen, S. Mao, Titanium dioxide Nanomaterials: synthesis, properties, modifications, and applications, Chem. Rev, 107 (2007) 2891-2959.

[12] M.D. Hager, P. Greil, C. Leyens, S. van der Zwaag, U.S. Schubert, Self-healing materials, Adv. Mater. 22 (2010) 5424–5430.

[13] V.M.C.A. Oliveira, C. Aguiar, A.M. Vazquez, A. Robin, M.J.R. Barboza, Improving corrosion resistance of Ti–6Al–4V alloy through plasma-assisted PVD deposited nitride coatings, Corros. Sci. 88 (2014) 317–327.

[14] J. Lu, Y. Zhang, W. Huo, W. Zhang, Y. Zhao, Y. Zhang, Electrochemical corrosion characteristics and biocompatibility of nanostructured titanium for implants, Appl. Surf. Sci. 434 (2018) 63–72.

[15] S. Wang, Y. Liu, C. Zhang, Z. Liao, W. Liu, The improvement of wettability, biotribological behavior and corrosion resistance of titanium alloy pretreated by thermal oxidation, Tribol. Int. 79 (2014) 174–182.

[16] G. Xu, X. Shen, Y. Hu, P. Ma, K. Cai, Fabrication of tantalum oxide layers onto titanium substrates for improved corrosion resistance and cytocompatibility, Surf. Coat. Tech. 272 (2015) 58–65.

[17] M. Niinomi, Recent research and development in titanium alloys for biomedical applications and health care goods, Sci. Technol. Adv. Mater. 4 (2003) 445-454.

[18] G.T. Burstein, R.M. Souto, Observations of localized instability of passive titanium in chloride solution, Electrochim. Acta 40 (1995) 1881.

[19] R.M. Souto, G.T. Burstein, A preliminary investigation into the microscopic depassivation of passive titanium implant materials in vitro, J. Mater. Sci.: Mater. Med. 7 (1996) 337-343.

[20] G.T. Burstein, C. Liu, R.M. Souto, The effect of temperature on the nucleation of corrosion pits on titaniumin Ringer's physiological solution, Biomaterials 26 (2005) 245-256.

[21] A. Sarmiento-González, J.M. Marchante-Gayón, J.M. Tejerina-Lobo, J. Paz-Jiménez, A. Sanz-Medel, High-resolution ICP-MS determination of Ti, V, Cr, Co, Ni, and Mo in human blood and urine of patients implanted with a hip or knee prosthesis, Anal. Bioanal. Chem. 391 (2008) 2583–2589.

[22] Y. Nuevo-Ordónez, M. Montes-Bayón, E. Blanco-González, J. Paz-Aparicio, J.D. Raimundez, J.M. Tejerina, M.A. Peña, A. Sanz-Medel,Titanium release in serum of patients with different bone fixation implants and its interaction with serum biomolecules at physiological levels, Anal. Bioanal. Chem. 401 (2011) 2747–2754.

[23] N. Eliaz. Corrosion of metallic biomaterials: A review. Materials.12 (2019) 407. 1-91.

[24] S.Virtanen, I. Milosev, E. Gomez-Barrena, R.Trebse, J. Salo, Y.T. Konttinen. Special modes of corrosion under physiological and simulated physiological conditions. Acta. Biomater 4 (2008) 468-476.

[25] K.I. Yokoyama, T. Ichikawa, H. Murakami, Y. Miyamoto, K. Asaoka, Fracture mechanisms of retrieved titanium screw thread in dental implant, Biomaterials. 23 (2002) 2459-2465.

[26] J.J. Jacobs, J.L. Gilbert, R.M. Urban, Current concepts review-corrosion of metal orthopaedic implants, J. Bone. Joint. Surg. Am. 80 (1998) 268-282.

[27] W. Jia, M.W. Beatty, R.A. Reinhardt, T.M. Petro, D.M. Cohen, C.R. Maze, E.A. Strom, M. Hoffman, Nickel release from orthodontic arch wires and cellular immune response to various nickel concentrations, J. Biomed. Mater. Res. Part B. 48 (1999) 488-495.

[28] P.H. Gitlitz, F.W. Sunderman Jr, P.J. Goldblatt, Amino acid uria and protein uriain rats after a single intraperitoneal injection of Ni(II), Toxicol. Appl. Pharmacol. 34 (1975) 430–440.

[29] D.J. Wever, A.G. Veldhuizen, J. de Vries, H.J. Busscher, D.R.A. Uges, J.R. van Horn, Electrochemical and surface characterization of a nickel–titanium alloy, Biomaterials 19 (1998) 761–769.

[30] Bhat, S.V. Biomaterials; Narosa Publishing House: New Delhi, India, 2002; pp. 36–38.

[31] B. Aksakal, Ö.S.Yildirim, H. Gul, Metallurgical failure analysis of various implant materials used in orthopedic applications, J. Fail. Anal. Prev. 4 (2004) 17–23.

[32] S. Rao, Y. Okazaki, T. Tateishi, T. Ushida, Y. Ito, Cytocompatibility of new Ti alloy without Al and V by evaluating the relative growth ratios of fibroblasts L929 and osteoblasts MC3T3-E1 cells, Mater. Sci. Eng. C. 4 (1997) 311-314.

[33] S. Piazza, G. Lo Biundo, M.C. Romano, C. Sunseri, F. Di Quatro, In situ characterization of passive films on Al–Ti alloy by photocurrent and impedance, Corros. Sci. 40 (1998) 1087-1108.

[34] G.T. Burstein, C. Liu, R.M. Souto, S.P. Vines, Origins of pitting corrosion, Corr. Eng. Sci. Technol. 39 (2004) 25–30.

[35] S. Shabalovskaya, Surface, corrosion and biocompatibility aspects of Nitinol as an implant material, Biomed. Mater. Eng. 12 (2002) 69-109.

[36] J.P. Collier, V.A. Suprenant, R.E. Jensen, M.B. Mayor. Corrosion at the interface of cobalt-alloy heads on titanium-alloy stems. Clin. Orthop. Relat. Res. 271 (1991) 305-311.

[37] P. Hou, P. Han, C.L. Zhao, H.L.Wu, J.H. Ni, S.X. Zhang, J.Y. Liu, Y.Z. Zhang, H.D. Xu, P.F. Cheng, S. Liu, Y.F. Zheng, X.N. Zhang, Y.M. Chai, Accelerating corrosion of pure magnesium co-implanted with titanium *in vivo*, Sci. Rep. 7 (2017) 41924.1-10.

[38] O. Ige, L.E. Umoru, M.O. Adeoye, A.R. Adetunji, O.E. Olorunniwo, Monitoring, control and prevention practices of biomaterials corrosion – An overview, Trends Biomater. Artif. Organs 23 (2) (2009) 93–104.

[39] M. Traisnel, D. le Maguer, H.F. Hildebrand, A. lost, Corrosion of surgical implants, Clin. Mater. 5 (1990) 309–318.

[40] H.G. Willer, L.G. Broback, G.H. Buchorn, Crevice corrosion of cemented titanium hip implants. Clin. Orthop. 23 (1996) 51-7.

[41] J. Geringer, B. Forest, P. Combrade, Fretting-corrosion of materials used as orthopaedic implants, Wear 259 (2005) 943–951.
[42] J.S. Kawalec, S.A. Brown, J.H. Payer, K. Merritt, Mixed-metal fretting corrosion of Ti6Al4V and wrought cobalt alloy, J. Biomed. Mater. Res. 29 (1995) 867-873.
[43] F. Contu, B. Elsener, H. Bohni, A study of the potentials achieved during mechanical abrasion and the repassivation rate of titanium and Ti6Al4V in inorganic buffer solutions and bovine serum, Electrochim. Acta. 50 (2004) 33–41.
[44] J. Ureña, S. Tsipas, A. M. Pinto, F. Toptan, E. Gordo, A. Jiménez-Morales, Corrosion and tribocorrosion behaviour of β-type Ti-Nb and Ti-Mo surfaces designed by diffusion treatments for biomedical applications, Corros. Sci. 140 (2018) 51-60.
[45] T. Hui, G.W. Kubacki, J.L. Gilbert, Voltage and wear debris from Ti-6Al-4V interact to affect cell viability during in-vitro fretting corrosion, J. Biomed. Mater. Res. B: Appl. Bioma. 106 (2018) 160-167.
[46] A.J. Bard, M.V. Mirkin, Scanning electrochemical microscopy, second edition. CRC Press, New York (2012).
[47] D. Polcari, P. Dauphin-Ducharme, J. Mauzeroll, Scanning Electrochemical Microscopy: A Comprehensive Review of Experimental Parameters from 1989 to 2015, Chem. Rev. 116 (2016) 13234-13278.
[48] S.E. Pust, W. Maier, G. Wittstock, Investigation of localized catalytic and electrocatalytic process and corrosion reactions with scanning electrochemical microscopy (SECM), Z. Phys. Chem. 222 (2008) 1463-1517.
[49] R. Cornut, C. Lefrou, New analytical approximation of feedback approach curves with a microdisk SECM tip and irreversible kinetic reaction at the substrate, J. Electroanal. Chem. 621 (2008) 178-184.
[50] K. Eckhard, X. Chen, F. Turcu, W. Schuhmann, Redox competition mode of scanning electrochemical microscopy (RC-SECM) for visualisation of local catalytic activity, Phys. Chem. Chem. Phys. 8 (2006) 5359–5365.
[51] Y. González-García, S.J. García, A.E. Hughes, J.M.C. Mol, A combined redox-competition and negative-feedback SECM study of self-healing anticorrosive coatings, Electrochem. Commun. 13 (2011) 1094–1097.
[52] N. Aouina, F. Balbaud-Célérier, F. Huet, S. Joiret, H. Perrot, F. Rouillard, V. Vivier, Single pit initiation on 316L austenitic stainless steel using scanning electrochemical microscopy, Electrochim. Acta. 56 (2011) 8589-8596.

[53] Y. Yuan, L. Li, C. Wang, Y. Zhu, Study of the effects of hydrogen on the pitting processes of X70 carbon steel with SECM, Electrochem. Commun. 12 (2010) 1804–1807.

[54] D. Ruhlig, H. Gugel, A. Schulte,W. Schuhmann, Visualization of local electrochemical activity and local nickel ion release on laser-welded NiTi/steel joints using combined alternating current mode and stripping mode SECM, The Analyst 133 (2008) 1700-1706.

[55] D. Ruhlig, W. Schuhmann, Spatial imaging of Cu^{2+} - ion release by combining alternating current and underpotential stripping mode Scanning Electrochemical Microscopy, Electroanalysis. 19 (2007) 191-199.

[56] F. Meng, E. H. Han, J. Wang, Z. Zhang, W. Ke, Localized corrosion behavior of scratches on nickel-base Alloy 690TT, Electrochim. Acta.56 (2011) 1781-1785.

[57] S. Thomas, N. V. Medhekar, G. S. Frankel, N. Birbilis, Corrosion mechanism and hydrogen evolutionon Mg, Curr. Opin.Solid State Mater. Sci., 19, (2015) 85-94.

[58] K. Fushimi, K. A. Lill, H. Habazaki, Heterogeneous hydrogen evolution on corroding Fe–3 at%Si surface observed by scanning electrochemical microscopy, Electrochim. Acta, 52 (2007) 4246 – 4253.

[59] D. Filotás, B.M. Fernández-Pérez, J. Izquierdo, A. Kiss, L. Nagy, G. Nagy, R.M. Souto, Improved potentiometric SECM imaging of galvanic corrosion reactions, Corros. Sci. 129 (2017) 136–145.

[60] D. Filotás, B.M. Fernández-Pérez, J. Izquierdo, L. Nagy, G. Nagy, R.M. Souto, Combined amperometric/potentiometric probes for improved chemical imaging of corroding surfaces using scanning electrochemical microscopy, Electrochim. Acta 221 (2016) 48–55.

[61] J. Izquierdo, A. Kiss, J.J. Santana, L. Nagy, I. Bitter, H.S. Isaacs, G. Nagy, R.M. Souto, Development of Mg^{2+} ion-selective microelectrodes for potentiometric scanning electrochemical microscopy monitoring of galvanic corrosion processes, J. Electrochem. Soc. 160 (2013) C451–C459.

[62] A. Uhl, W. Kestranek, The electrometrictitration of acids and bases with the antimony indicator electrodes, Monatsh. Chem. 44 (1923) 29-34.

[63] B.R. Horrocks, M.V. Mirkin, D.T. Pierce, A.J. Bard, G. Nagy, K. Toth, Scanning electrochemical microscopy. 19. Ion-selective potentiometric microscopy. Analytical Chemistry. 65 (1993) 1213-1224.

[64] N.A. Payne, L.I. Stephens, J. Mauzeroll, The application of scanning electrochemical microscopy to corrosion research, Corrosion. 73 (2017) 759-780.

[65] S.B. Basame, H.S. White, Scanning electrochemical microscopy of native titanium oxide films. Mapping the potential dependence of spatially-localized electrochemical reactions, J. Phys. Chem. 99, 44 (1995) 16430- 16435.

[66] N. Casillas, S. Charlebois, W.H. Smyrl, H.S. White, Pitting corrosion of titanium, J. Electrochem. Soc. 141 (1994) 636–642.

[67] N. Casillas, S.J. Charlebois, W.H. Smyrl, H.S. White, Scanning electrochemical microscopy of precursor sites for pitting corrosion on titanium, J. Electrochem. Soc. 140 (1993) L142–L145.

[68] L.F. Garfias-Mesias, M. Alodan, P.I. James, W.H. Smyrl, Determination of precursor sites for pitting corrosion of polycrystalline titanium by using different technique, J. Electrochem. Soc. 145 (1998) 2005-2010.

[69] K. Fushimi, T. Okawa, K. Azumi, M. Seo, Heterogeneous growth of anodic oxide film on a polycrystalline titanium electrode observed with a scanning electrochemical microscope, J. Electrochem. 147 (2000) 524-529.

[70] R. Zhu, C. Nowierski, Z. Ding, J.J. Noël, D.W. Shoesmith, Insights into grain structures and their reactivity on grade-2 Ti alloy surfaces by scanning electrochemical microscopy, Chem. Mater. 19 (2007) 2533–2543.

[71] R. Zhu, Z. Qin, J.J. Noël, D.W. Shoesmith, Z. Ding, Analyzing the influence of alloying elements and impurities on the localized reactivity of titanium grade-7 by scanning electrochemical microscopy, Anal. Chem. 80 (2008) 1437–1447.

[72] S.E. Pust, D. Scharnweber, C.N. Kirchner, G. Wittstock, Heterogeneous distribution of reactivity on metallic biomaterials: scanning probem microscopy studies of the biphasic Ti alloy Ti6Al4V, Adv. Mater. 19 (2007) 878– 882.

[73] S.E. Pust, D. Scharnweber, S. Baunack, G. Wittstock, Electron transfer kinetics at oxide films on metallic biomaterials – Scanning electrochemical microscopy studies of Ti6Al4V, J. Electrochem. Soc, 154 (2007) C508– C514.

[74] G. Bolat, J. Izquierdo, T. Gloriant, R. Chelariu, D. Mareci, R.M. Souto, Investigation of processing effects on the corrosion resistance of Ti20Mo alloy in saline solutions, Corros. Sci. 98 (2015) 170–179.

[75] R. Chelariu, G. Bolat, J. Izquierdo, D. Mareci, D.M. Gordin, T. Gloriant, R.M. Souto, Meta stable beta Ti–Nb–Mo alloys with improved corrosion resistance in saline solution, Electrochim. Acta. 137 (2014) 280–289.

[76] A. Schulte, S. Belger, M. Etienne, W. Schuhmann, Imaging localised corrosion of NiTi shape memory alloys by means of alternating current scanning electrochemical microscopy (AC-SECM), Mater. Sci. Eng. A 378 (2004) 523–526.

[77] D. Ruhlig, H. Gugel, A. Schulte, W. Theisen, W. Schuhmann, Visualization of local electrochemical activity and local nickel ion release on laser-welded NiTi/steel joints using combined alternating current mode and stripping mode SECM, Analyst 133 (2008) 1700–1706.

[78] J. Izquierdo, M.B. González-Marrero, M. Bozorg, B.M. Fernández-Pérez, H.C. Vasconcelos, J.J. Santana, R.M. Souto, Multiscale electrochemical analysis of the corrosion of titanium and Nitinol for implant applications, Electrochim. Acta 203 (2016) 366-378.

[79] G. Bolat, J. Izquierdo, J.J. Santana, D. Mareci, R.M. Souto, Electrochemical characterization of ZrTi alloys for biomedical applications, Electrochim. Acta 88 (2013) 447–456.

[80] B. Csóka, B. Kovács, G. Nagy, Investigation of concentration profiles inside operating biocatalytic sensors with scanning electrochemical microscopy (SECM), Biosens. Bioelectron. 18 (2003) 141–149.

[81] A. Kiss, G. Nagy, Deconvolution of potentiometric SECM, Electroanalysis. 27 (2015) 587-590.

[82] Y.S. Hedberg, Role of proteins in the degradation of relatively inert alloys in the human body. npj Mater. Degrad. 2 (2018) 26.

[83] J.L. Wang, R.L. Liu, T. Majumdar, S.A. Mantri, V.A. Ravi, R. Banerjee, N. Birbilis. A closer look at the *in vitro* electrochemical characterisation of titanium alloys for biomedical applications using in-situ methods, Acta. Biomater. 54 (2017) 469–478.

[84] S.V. Lamaka, R.M. Souto, M.G.S. Ferreira, In situ visualization of local corrosion by scanning ion-selective electrodetechnique (SIET), in: A. Méndez-Vilas, J. Díaz (Eds.), Microscopy: Science, Technology, Applications and Education, vol. 3, Formatex Research Center, Badajoz (Spain), 2010, 2162–2173.

[85] M. Sakairi, M. Kinjyo, T. Kikuchi, Repassivation behavior of titanium in artificial saliva investigated with a photon rupture method, Electrochim. Acta, 56 (2011) 1786-1791.

[86] Y. Fovet, J.Y. Gal, F. Toumelin-Chemla, Influence of pH and fluoride concentration on titanium passivating layer: stability of titanium dioxide, Talanta 53 (2001) 1053–1063.

[87] J.E. G González, J.C. Mirza-Rosca, Study of the corrosion behavior of titanium and some of its alloys for biomedical and dental implant applications. J. Electroanal. Chem. 471 (1999) 109-115.

[88] B.L. Wang, Y.F. Zheng, L.C. Zhao, Effects of Hf content and immersion time on electrochemical behavior of biomedical Ti–22Nb–xHf alloys in 0.9% NaCl solution, Mater. Corros. 60 (2009) 330–335.

[89] V.A. Alves , R.Q. Reis , I.C.B. Santos, D.G. Souza, T. de F. Gonçalves, M.A. Pereira-da-Silvae, A. Rossi, L.A. da Silva. *In situ* impedance spectroscopy study of the electrochemical corrosion of Ti and Ti–6Al–4V in simulated body fluid at 25 °C and 37 °C, Corros. Sci. 51 (2009) 2473–2482.

[90] J. Lu, Y. Zhang, W. Huo, W. Zhang, Y. Zhao, Y. Zhang, Electrochemical corrosion characteristics and biocompatibility of nanostructure titanium for implants, Appl. Surf. Sci. 434 (2018) 63-72.

[91] A.C. Alves, F. Wenger, P. Ponthiaux, J.P. Celis, A.M. Pinto, L.A. Rocha, J.C.S. Fernandes, Corrosion mechanisms in titanium oxide-based films produced by anodic treatment, Electrochim. Acta. 234 (2017) 16–27. .

[92]. E. Alkhateeb, S. Virtanen, Influence of surface self-modification in Ringer's solution on the passive behavior of titanium, J Biomed. Mater. Res. A. 75 (2005) 934–940.

[93] J. Navarro Laboulais, A. Amigó Mata, V. Amigó Borrás, A. Igual Muñoz. Electrochemical characterization and passivation behaviour of new beta-titanium alloys (Ti35Nb10Ta-xFe). Electrochim. Acta. 227 (2017) 410–418.

[94] A.L. Ribeiro, P. Hammer, L.G. Vaz , L.A. Rocha. Are new TiNbZr alloys potential substitutes of the Ti6Al4V alloy for dental applications? An electrochemical corrosion study. Biomed. Mater. 8 (2013) 065005. 1-11.

[95] G. Wang, Y. Wan, T. Wang, Z. Liu. Corrosion behavior of titanium implant with different surface morphologies. Procedia Manuf. 10 (2017), 363–370.

[96] A. Balamurugan, S. Rajeswari, G. Balossier, A.H.S. Rebelo, J.M.F. Ferreira, Corrosion aspects of metallic implants – An overview, Mater. Corros. 59 (2008) 855-869.

[97] J.L. Gilbert, L. Zarka, E. Chang, C.H. Thomas. he reduction half cell in biomaterials corrosion: oxygen diffusion profiles near and cell response to polarized titanium surfaces, J Biomed. Mater. Res. 42 (1998) 321–330.

[98] M.T. Ehrensberger, S. Sivan, J.L. Gilbert, Titanium is not “the most biocompatible metal” under cathodic potential: The relationship between voltage and MC3T3 preosteoblast behavior on electrically polarized cpTi surfaces, J. Biomed. Mater. Res. Part A, 93 (2010), 1500-1509.

[99] S. Sivan, S. Kaul, J.L. Gilbert. The effect of cathodic electrochemical potential of Ti-6Al-4V on cell viability: voltage threshold and time dependence. J. Biomed. Mater. Res. B. 101 (2013) 1489–1497.

[100] E. Brooks, M. Tobias, K. Krautsak, M. Ehrensberger. The influence of cathodic polarization and simulated inflammation on titanium electrochemistry. J. Biomed. Mater. Res. B. Appl. Biomater. 102 (2010) 1445-1553.

[101] G. Bolat, J. Izquierdo, D. Mareci, D. Sutiman, R.M. Souto, Electrochemical characterization of ZrTi alloys for biomedical applications. Part 2: The effect of thermal oxidation. Electrochim. Acta, 106 (2013) 432-439.

[102] R.M. Torresi, O.R. Cámara, C.P. De Pauli, Influence of the hydrogen evolution reaction on the anodic titanium oxide film properties, Electrochim. Acta. 32 (1987) 1357-1363.

[103] T. Ohtsuka, M. Masuda, N. Sato, Cathodic reduction of anodic oxide films formed on titanium, J. Electrochem. Soc. 134 (1987) 2406-2410.

[104] A. Fujishima, X. T. Zhang and D. A. Tryk, TiO2 photocatalysis and related surface phenomen, Surf. Sci. Rep. 63 (2008) 515–582.

[105] J. Zhou, Y. Zu, A.J. Bard, Scanning electrochemical microscopy Part 39. The proton/hydrogen mediator system and its application to the study of the electrocatalysis of hydrogen oxidation, J. Electroanal. Chem. 491 (2000) 22-29.

[106] Y. Zeng, J.J. Noël, P.R. Norton, D.W. Shoesmith. Hydrogen transport through thin titanium oxides, J. Electroanal. Chem. 649 (2010) 277-285.

[107] S. Shabalovskaya, J. Anderegg, J. Van Humbeeck, Critical overview of Nitinol surfaces and their modifications for medical applications, Acta. Biomater. 4 (2008) 447–467.

[108] A. Wadood, Brief overview on Nitinol as biomaterial, ADV MATER SCI ENG 4 (2016) 1-9.

[109] S.J.L. Sullivan, D. Madamba, S. Sivan, K. Miyashiro, M.L. Dreher, C. Trépanier, S. Nagaraja, The effects of surface processing on in-vivo corrosion of Nitinol stents in a porcine model, Acta. Biomater. 62 (2017) 385–396.

[110] V.A.R. Barao, M.T. Mathew, W.G. Assuncao, J.C.C. Yuan, M.A. Wimmer, C. Sukotjo, Stability of cp-Ti and Ti-6l-4V alloy for dental implants as a function of saliva pH – an electrochemical study, Clin. Oral Impl. Res. 23 (2012) 1055–1062.

[111] H.H. Huang, Y.H. Chiu, T.H. Lee, S.C. Wu, H.W. Yang, K.H. Su, C.C Hsu. Ion release from NiTi orthodontic wires in artificial saliva with various acidities. Biomaterials. 24 (2003), 3585–3592.

[112] M.C. Pereira, M.L. Pereira, J.P. Sousa, Evaluation of nickel toxicity onliver, spleen, and kidney of mice after administration of high-dose metal ion, J. Biomed. Mater. Res. 40 (1998) 40–47.

[113] I. Milošev, B. Kapun, The corrosion resistance of Nitinol alloy in simulated physiological solutions: Part 1: The effect of surface preparation, Mater. Sci. Eng. C, 32 (2012) 1087–1096.
[114] D. Wagman, W. Evans, V. Parker, R. Schumm, I. Halow, S. Bailey. The NBS tables of chemical thermodynamic properties. J Phys Chem Ref Data 1982;11(Suppl. 2).
[115] M. Mirjalili, M. Momeni, N. Ebrahimi, M.H. Moayed, Comparative study on corrosion behaviour of Nitinol and stainless-steel orthodontic wires in simulated saliva solution in presence of fluoride ions, Mater. Sci. Eng. C, 33 (2013) 2084–2093.
[116] M. Alishahi, F. Mahboubi, S.M. Mousavi Khoie, M. Aparicio, E. Lopez-Elvira, J. Mendez, R. Gago, Structural properties and corrosion resistance of tantalum nitride coatings produced by reactive DC magnetron sputtering, RSC Adv. 6 (2016) 89061-89072.
[117] A.P. Romano, M.G. Olivier, Investigation by electrochemical impedance spectroscopy of filiform corrosion of electrocoated steel substrates, Prog. Org. Coat. 89 (2015) 1–7.
[118] C. Wei, A.J. Bard, Scanning electrochemical microscopy XXIX .In situ monitoring of thickness changes of thin films on electrodes, J. Electrochem. Soc. 142 (1995) 2523-2527.
[119] P. Dauphin-Ducharme, C. Kuss, D. Rossouw, N.A. Payne, L. Danis, G.A. Botton, J. Mauzeroll, Corrosion product formation monitored using the feedback mode of scanning electrochemical microscopy with carbon microelectrodes, J. Electrochem. Soc. 162 (2015) C677-C683.
[120] A. Mazzarolo, M. Curioni, A. Vicenzo, P. Skeldon, G.E. Thompson, Anodic growth of titanium oxide: Electrochemical behaviour and morphological evolution, Electrochim. Acta 75 (2012) 288–295.
[121] M. Pourbaix (Ed.), Atlas of electrochemical equilibria in aqueous solutions, Pergamon Press, Oxford, 1966.
[122] W. M. Haynes, D.R. Lide, T.J. Bruno, (2016). CRC handbook of chemistry and physics.
[123] D. Trihn, P. Dauphin Ducharme, U.M. Tefashe, J.R. Kish, J. Mauzeroll, Influence of edge effects on local corrosion rate of magnesium alloy/mild steel galvanic couple, Anal. Chem. 84 (2012) 9899–9906.
[124] R. Ding, J.X. Shang, F.H. Wang, Y. Chen, Electrochemical Pourbaix diagrams of Ni-Ti alloys from first-principles calculations and experimental aqueous states, Comput. Mater. Sci. 143 (2018) 431e438.
[125] G.S. Frankel, Pitting corrosion of metals: A review of the critical factors, J. Electrochem. Soc. 145 (1998) 2186–2198.

[126] D.S. Kong, W.H. Lu, Y.Y. Feng, Z.Y. Yu, J.X. Wu, W.J. Fan, H.Y. Liu, Studying on the point-defect-conductive property of the semiconducting anodic oxide films on titanium, J. Electrochem. Soc. 156 (2009) C39-C44.

[127] L.F. Huang, M.J. Hutchison, R.J. Santucci, J.R. Scully, J. M. Rondinelli, Improved electrochemical phase diagrams fromt heory and experiment: the Ni–water system and itscomplexcompounds. J. Phys. Chem. C. 121 (2017) 9782–9789.

[128] S.E. Ziemniak, M.E. Jones, K.E.S. Combs, Solubility and phase behavior of nickel oxide inaqueous sodium phosphate solution satelevated temperatures, J. Solution. Chem. 18 (1989) 1133–1152.